



fatigue damage, or both. Modeling results show competing interactions between void size and location, that results in a non-monotonic relationship between void size and durability. It also suggests that voids in general are not detrimental to reliability except when a large portion of the damage propagation path is covered with either a large void or with many small voids.

In addition, this dissertation also addresses several fundamental issues in solder fatigue damage modeling. One objective is to use experimental data to identify the correct fatigue constants to be used when explicitly modeling fatigue damage propagation in Pb-free solders. Explicit modeling of damage propagation improves modeling accuracy across solder joints of vastly different architectures, since the joint geometry may have a strong influence on the ratio of initiation-life to propagation-life. Most solder fatigue models in the literature do not provide this capability since they predict failure based only on the damage accumulation rates during the first few cycles in the undamaged joint.

Another objective is to incorporate into cyclic damage propagation models, the effect of material softening caused by cyclic micro-structural damage accumulation in Pb-free solder materials. In other words the model constants of the solder viscoplastic constitutive model are continuously updated with the help of experimental data, to include this cyclic softening effect as damage accumulates during the damage-propagation phase. The ability to model this damage evolution process increases the accuracy of durability predictions, and is not available in most current solder fatigue models reported in the literature. This mechanism-based microstructural damage evolution model, called the Energy Partitioning Damage Evolution (EPDE) model is

developed and implemented in Finite Element Analysis of solder joints with the successive initiation technique and the results are provided here. Experimental results are used as guidance to calibrate the Energy Partitioning fatigue model constants, for use in successive initiation modeling with and without damage evolution.

FEA results show 15% difference between the life predicted by averaging technique and successive initiation. This difference could significantly increase in the case of long joints such as thermal pads or die-attach, hence validating the use of successive initiation in these cases. The difference between using successive initiation with and without damage evolution is about 10%. Considering the small amount of effort that has to be made to update the constitutive properties for progressive degradation, it is recommended that softening be included whenever damage propagation needs to be explicitly modeled. However the damage evolution exponents and the corresponding E-P model constants obtained in this study, using successive initiation with damage evolution, are partially dependent on the specimen geometry. Hence, these constants may have to be re-calibrated for other geometries.

DAMAGE INITIATION AND EVOLUTION IN VOIDED AND UNVOIDED  
LEAD FREE SOLDER JOINTS UNDER CYCLIC THERMO-MECHANICAL  
LOADING

By

Leila Jannesari Ladani

Dissertation submitted to the Faculty of the Graduate School of the  
University of Maryland, College Park, in partial fulfillment  
of the requirements for the degree of  
Doctor of Philosophy  
2006

Advisory Committee:  
Professor Abhijit Dasgupta, Chair and Advisor  
Professor Avram Bar-Cohen  
Professor Bongtae Han  
Professor Hugh Bruck  
Professor Patrick McCluskey  
Professor Lourdes G. Salamanca-Riba

© Copyright by  
Leila Jannesari Ladani  
2006

## Dedication

To my mother, my husband, and my son, three generations who stood beside me  
patiently

## Acknowledgements

Most of all I would like to express my sincere thanks to my advisor Prof. Dasgupta for his valuable guidance and his warm support during my graduate studies. I sincerely appreciate his patience, understanding and encouragements. He has been an excellent mentor and role model which will forever inspire me for good quality work. It was a privilege for me to study and research in his care.

I am especially thankful to Prof. Bar-Cohen for his excellent advice and guidance during my graduate studies. I am grateful to him for his goodwill, care and support toward me and my family and his patience in listening to my problems.

I would like to thank Prof. McCluskey who has often advised me kindly and helped me in my research. I enjoyed his classes as well as collaborating with him in research.

I would like to acknowledge Prof. Han, and his help in my research and his valuable comments.

I would like to thank Prof. Bruck, who has advised me in my research and career in several occasions.

In particular I would like to thank Prof. Riba, for evaluating my dissertation and serving in my committee as Dean's representative. She has been a good friend and support for me.

My special thanks go to my husband Jafar Razmi for all his patience during my graduate study and his help with my experiment. I also would like to acknowledge and appreciate my son Soroush, whom I live for, for giving me the inspiration and hope. My forever thanks goes to my mother whose life was dedicated to me.

I would like to thank Dr. Juscelino Okura (currently at Microsoft) and Tommie Reinikainen, from INdT for sponsoring the project and Idelcio Cardoso, and Eduardo Monlevade from INdT, for their help in running the experiment and characterizing the specimens.

I would like to thank Dr Osterman and Snehaunshu Chowdhury for providing the test results.

I would like to thank my lab mates. In particular I would like to thank Roman Ottmar Kuehner, German exchange student for his help in cross sectioning.

# Table of Contents

Dedication.....	ii
Acknowledgements.....	iii
Table of Contents.....	v
List of Tables.....	viii
List of Figures.....	ix
List of Figures.....	ix
1. Chapter 1: Introduction and background.....	1
1.1. Objectives and problem statement.....	2
1.2. Background and motivation for studying voids.....	4
1.2.1. Manufacturing process.....	5
1.2.1.1. Printing process.....	5
1.2.1.2. Reflow Process.....	7
1.2.1.3. Manufacturing Variabilities.....	11
1.2.2. Defects Introduced in Printing and Reflow.....	12
1.2.2.1. Voids.....	2
1.2.2.2. Types of process induced voids.....	3
1.2.2.3. Industry Standards.....	7
1.2.3. Literature Review.....	8
1.2.3.1. Effect of manufacturing variation on voids formation.....	8
1.2.3.2. Effect of Process Induced Voids on Durability of Joints.....	10
1.2.4. Gaps in Literature.....	14
1.2.4.1. Effect of manufacturing variation on void formation.....	15
1.2.4.2. Effect of voids on durability of interconnects.....	16
1.3. Durability modeling.....	19
1.3.1. Modeling approaches.....	19
1.3.1.1. Stress based approaches.....	21
1.3.1.2. Strain based approaches.....	21
1.3.1.3. Energy based approaches.....	23
1.3.1.4. Energy Partitioning damage model.....	24
1.4. Damage evolution caused by cyclic loading in solders.....	27
1.4.1. Literature review for Pb-free solder materials.....	32
1.4.2. Gaps in the literature.....	33
1.5. Scope and overview of approach.....	34
2. Chapter 2: Thermo-mechanical durability experiments.....	36
2.1. Study 1.....	36
2.1.1. Background and introduction.....	36
2.1.2. Design of Experiment.....	38
2.1.3. Specimen design.....	41
2.1.4. Void Analysis.....	44
2.1.5. Statistical analysis of voids as response variable.....	46
2.1.6. Test design.....	47
2.1.7. Accelerated thermal cycling test results.....	48
2.1.8. Micro-structural failure analysis.....	51

2.1.9.	Statistical analysis of durability as response variable.....	53
2.1.10.	Summary and conclusion of Study 1 .....	54
2.2.	Study 2 .....	55
2.2.1.	Test condition.....	55
2.2.2.	Test specimen.....	56
2.2.3.	X-ray Analysis .....	57
2.2.4.	Destructive failure analysis.....	58
2.2.5.	Summary and Conclusions of Study 2.....	60
2.3.	Summary and Conclusions .....	60
3.	Chapter 3: Durability modeling: effect of voids on durability .....	61
3.1.	Investigating effect of voids on thermo-mechanical durability .....	61
3.1.1.	Investigating durability of voided joints using averaging techniques	63
3.1.2.	Durability of voided joints using successive initiation technique .....	64
3.1.3.	Implementation of successive initiation approach: Case studies .....	68
3.1.4.	Solder joint material properties.....	69
3.1.5.	Global modeling for BGA256 (Study 2 specimen) .....	74
3.1.6.	Local modeling of voided solder balls.....	79
3.1.6.1.	Case 1: void in the middle with partial crack .....	83
3.1.6.2.	Case 2: void close to initiation site .....	84
3.1.6.3.	Case 3: full crack with void far away from damage path .....	85
3.1.6.4.	Case 4: small void in crack path .....	86
3.1.6.5.	Case 5: no void, partial crack.....	87
3.1.7.	Results of successive initiation technique.....	88
3.1.8.	Result of case Studies: qualitative comparison.....	90
3.2.	Summary and conclusion.....	97
4.	Chapter 4: Parametric study of voids.....	98
4.1.	Global modeling of CTBGA132 (Study 1 specimen).....	98
4.2.	Local modeling of solder balls.....	102
4.2.1.	FEA model analysis using averaging technique .....	104
4.2.2.	Effect of multiple voids .....	113
4.2.3.	Investigating voids using successive initiation .....	116
4.3.	Summary and conclusions .....	122
5.	Chapter 5: Damage evolution due to cyclic loading.....	124
5.1.	Problem statement.....	124
5.2.	Energy Partitioning Damage Evolution (EPDE) method .....	126
5.2.1.	Experimental Approach .....	129
5.2.2.	Analysis of Result of Experiment.....	131
5.2.3.	Implementation of damage evolution approach.....	137
5.3.	Summary and conclusions .....	141
6.	Chapter 6: Calibrating Energy Partitioning Constants.....	143
6.1.	Calibration of E-P constants for successive initiation .....	143
6.2.	Calibrating E-P constants for successive initiation including damage evolution .....	147
6.3.	Summary and Conclusions .....	148
7.	Chapter 7: Summary, contribution and future work .....	149
7.1.	Contribution of the dissertation .....	151

7.2.	Suggestions for future work.....	154
8.	Appendices.....	158
8.1.	Appendix I: Pre-test micro-structural analysis .....	158
8.2.	Appendix II: Accelerated thermal cycling test results.....	161
9.	References.....	167

## List of Tables

Table 1-1: Lead-free reflow profile recommendations [J-STD-020C], [ALTERA Corporation, 2004], and [ZiLOG Inc., 2003].....	9
Table 1-2: Peak reflow temperature ( $T_p$ ) for lead-free process [J-STD-020C], [ALTERA Corporation, 2004].....	10
Table 1-3: IPC classification for Voids inside BGA ball [IPC-7095]. .....	7
Table 2-1: DOE matrix, L18 [Taguchi, 1993].....	40
Table 2-2: Variable and levels of variables selected for this study .....	41
Table 2-3: Test board stack up and material [JESD22-B111] .....	42
Table 2-4: Void percentage averaged for BGA specimens observed in different DoE runs.....	45
Table 2-5: Durability averaged over BGAs of each board for different DoE runs.....	49
Table 2-6: Summary of the Weibull parameters for CTBGAs .....	50
Table 2-7: Test Matrix used in long term Pb-free consortium project [Osterman et al., 2006] .....	55
Table 3-1: Solder creep and plastic properties [Zhang, 2004].....	74
Table 3-2: Dimension of the package in microns .....	75
Table 3-3: Material properties used in FEA modeling [Zhang, 2004] .....	77
Table 3-4: Thermo-mechanical Energy Partitioning damage model constants for Sn3.8Ag0.7 solder [Zhang, et al. 2003].....	78
Table 3-5: Thermo-mechanical Energy Partitioning damage model constants for Sn3.8Ag0.7 solder [Zhang et al., 2003].....	90
Table 4-1: Dimension of the package in microns .....	98
Table 4-2: Material properties used in FEA modeling .....	101
Table 4-3: Nomenclature of geometric configuration .....	104
Table 4-4: Thermo-mechanical Energy Partitioning damage model constants for Sn3.8Ag0.7 solder [Zhang et al., 2003].....	105
Table 5-1: Isothermal-mechanical constants for Sn3.9Ag0.6Cu.....	135
Table 6-1: Thermo-mechanical Energy Partitioning damage model constants for Sn3.8Ag0.7 solder [Zhang et al., 2004].....	144
Table 6-2: E-P creep constants calibrated for successive initiation.....	146
Table 6-3: E-P creep constants calibrated for successive initiation with damage evolution .....	147
Table 8-1: Summary of the Weibull parameters for CTBGAs .....	163
Table 8-2: Summary of the Weibull parameters for MLFs .....	164
Table 8-3: Summary of the Weibull parameters for LCRs.....	164

## List of Figures

Figure 1-1: The SMA process flowchart .....	5
Figure 1-2: Schematic of stencil printing process 17.....	6
Figure 1-3: A typical reflow profile consists of preheat, soak, reflow and cool down sub-steps.....	8
Figure 1-4: IR/convection reflow profile J-STD-020, used in ALTERA and ZiLOG [J-STD-020C], [ALTERA Corporation, 2004].....	9
Figure 1-5: Typical Ramp-Soak-Spike profile [www.TKB-4U.COM].....	11
Figure 1-6: Typical Ramp-To-Spike profile[www.TKB-4U.COM] .....	11
Figure 1-7: Fish bone diagram for manufacturing defects of solder joints.....	12
Figure 1-8: Manufacturing Defects in Pb- Free Solders Voids[Willies, 2005] .....	2
Figure 1-9: Two examples of macro voids (a) void inside BGA ball (b) Void inside through hole [Aspandiar, 2005].....	3
Figure 1-10: planar micro voids at the interface of solder and PCB pad [Aspandiar, 2005] .....	4
Figure 1-11: Shrink-hole voids in solder, (a) in solder joint, (b) in fillet [Aspandiar, 2005]. .....	5
Figure 1-12: Examples of microvia voids (a) when the solder has not wet the inside copper pads of microvia and (b) when the solder has wet the inside copper pads of microvias [Aspandiar, 2005].....	5
Figure 1-13: Pin holes in the copper pad in PCB land [Aspandiar, 2005].....	6
Figure 1-14: Kirkendall voids observed in Texas Instrument by aging at 125° C for 10 days [Aspandiar, 2005].....	7
Figure 1-15: Outline of solder ball and void inspected by Xray from top view .....	8
Figure 1-16: Finite element mesh of voids 40 .....	12
Figure 1-17: BCC solder joints with various void size, location and percentage [Lau and Erasmus, 2002].....	12
Figure 1-18: Weibull plot of failures on 256 I/O 1 mm PBGA [Yunus et al., 2003].	17
Figure 1-19: Weibull plots of failures on 48 I/O flex CSP [Yunus et al., 2003] .....	18
Figure 1-20: Procedure for Energy Partitioning Damage Model.....	26
Figure 1-21: Microstructure of flip chip joint of Sn4.7Ag1.7Cu as reflowed condition (a) and after 200 and 1200 Thermal cycles (b and c respectively) [Datta, 2003].....	29
Figure 1-22: Hysteresis loop of Pb-free solder alloys at strain amplitude of 0.8% [Qiu, 2005] .....	29
Figure 1-23: comparison of stress-strain hysteresis loop for damaged and undamaged material under constant stress .....	30
Figure 1-24: Comparison of stress-strain hysteresis loop for damaged and undamaged material under constant strain .....	31
Figure 1-25: Approach used to investigate the effect of voids as well as cyclic softening and damage evolution .....	35
Figure 2-1: Fishbone diagram of variables affecting the solder interconnects quality and reliability .....	39
Figure 2-2: Typical Ramp-to-Spike profile .....	41
Figure 2-3: ball view daisy chain map for CTBGA 132.....	43
Figure 2-4: Schematic picture of BGA .....	43

Figure 2-5: Schematic picture of MLF component.....	43
Figure 2-6: Specimen used in accelerated temperature cycle loading.....	44
Figure 2-7: X-ray analysis of voids .....	45
Figure 2-8: Factor effect analysis for void as response variable .....	46
Figure 2-9: Chamber characterization; temperature profile observed on boards .....	47
Figure 2-10: Typical example of BGA resistance during thermal cycling test .....	48
Figure 2-11: 3-P Weibull plots for main population of failures of CTBGAs.....	50
Figure 2-12: Probability density function for main population of failures for CTBGA .....	51
Figure 2-13: Crack in intermetallic due to insufficient intermetallic formation in board A1.....	52
Figure 2-14: Damage moved to the bulk of the solder in main population .....	52
Figure 2-15: Damage moved to the component side for the most durable specimens .....	53
Figure 2-16: factor effect plots for different variables for durability as response variable.....	53
Figure 2-17: Temperature cycle used in long term Pb-free solder consortium project .....	56
Figure 2-18: test board used for thermal cycling test for long term Pb-free consortium project [Osterman et al., 2006] .....	57
Figure 2-19: Example of X-ray analysis for Im-Sn surface finish.....	58
Figure 2-20: Relatively big voids located in the middle of damage path .....	59
Figure 2-21: Small void located close to damage initiation site.....	59
Figure 2-22: Relatively big void located close to initiation site .....	60
Figure 3-1: Global – local modeling approach .....	62
Figure 3-2: Damage propagation using successive initiation .....	67
Figure 3-3: Map of the balls of one quarter of the package and cases studies in detail .....	69
Figure 3-4: Typical constant load creep deformation.....	71
Figure 3-5: Schematic of a log-log plot of the shear secondary creep strain Vs. shear stress [Zhang, 2005, Schubert et al., 2001].....	72
Figure 3-6: Dimension of the package.....	74
Figure 3-7 Global FEA model for BGA256 .....	76
Figure 3-8: Global FEA model for PBGA256, with applied boundary conditions ....	77
Figure 3-9: Temperature profile used in FEA modeling .....	78
Figure 3-10: Contour plot of cyclic fatigue damage calculated based on E-P model. ....	79
Figure 3-11: Normalized damage with respect to critical ball.....	81
Figure 3-12: 3-D local model.....	82
Figure 3-13: Contour plot of cyclic fatigue damage.....	83
Figure 3-14: Case 1: Solder ball with relatively big void in the middle near the component.....	84
Figure 3-15: Case 2: big void located close to damage initiation site .....	85
Figure 3-16: Full crack with small void close to PWA bond pad.....	86
Figure 3-17: Small void close to damage initiation site .....	87
Figure 3-18: Case 5, solder ball with no void and partial crack .....	88
Figure 3-19: Example of displacement history at one node at top of the joint.....	89

Figure 3-20: Example of damage starting circumferentially from the top and bottom of the ball for un-voided joint .....	91
Figure 3-21: Contour plot of damage in solder ball with a void in the middle.....	92
Figure 3-22: Comparison between Case 1 and 5 solder ball with big void in the middle and solder ball without void.....	93
Figure 3-23: Comparison between the initiation time for case 1, 2 and 5 .....	94
Figure 3-24: Initiation site in Case 4, solder ball with void far from crack and Case 3, solder ball with small void on the crack path .....	95
Figure 3-25: Damage propagation length normalized with respect to total path length .....	96
Figure 3-26: Damage propagated in second step of successive initiation, when it reached the void .....	96
Figure 3-27: Damage propagated in third step of successive initiation, stopped by void locally.....	97
Figure 4-1 Global FEA model for CTBAG132 and the critical ball at the outer corner .....	99
Figure 4-2: Global FEA model for CTBAG132, with applied boundary conditions	100
Figure 4-3: Contour plot of equivalent stress in balls.....	101
Figure 4-4: Temperature profile used in FEA modeling .....	102
Figure 4-5: Local modeling of the ball (a) without and (b) with voids .....	103
Figure 4-6: Cases studied.....	103
Figure 4-7: Example of void with area fraction of 49% located in the middle of the ball, figure courtesy of Brizoux et al. 2005. ....	104
Figure 4-8: Contour plots of (a) damage calculated based on E-P model, (b) damage calculated based on Strain based model at a diagonal diametric cross-section of a critical ball without voids.....	106
Figure 4-9: E-P damage contour plot in critical solder ball, for small void located at inner corner, towards the component bond pad (a) front view (b) Isometric view ..	107
Figure 4-10: Contour plot of damage based on E-P model for ball with different void sizes at the outer corner close to component interface .....	109
Figure 4-11: Life estimate using E-P model and Strain based model, normalized with respect to un-voided joint with different void $A_F$ (a) 1%. (b) 3.2% (c) 9% (d) 14.4% .....	109
Figure 4-12: Normalized durability for voided joints with different void area fractions; Comparison between E-P and strain based method.....	110
Figure 4-13: Effect of void location on durability .....	111
Figure 4-14: Effect of Void Size on durability .....	112
Figure 4-15: Hypothesis of effects of competing factors.....	112
Figure 4-16: Interaction effect between void size and location.....	113
Figure 4-17: Meshed ball with multiple voids on damage path.....	114
Figure 4-18: Contour plots of damage calculated using E-P damage model in the ball with multiple voids: (a) concentration in the neck, (b) Distribution over the surface and between the voids.....	115
Figure 4-19: Cases studied using Successive Initiation Method .....	116
Figure 4-20: Damage initiation life, normalized with respect to results for a void-free joint .....	117

Figure 4-21: Damage propagation life, normalized with respect to results for a void-free joint.....	118
Figure 4-22: Growth of damaged zone with temperature cycling.....	119
Figure 4-23: Total life normalized with respect to a void-free joint.....	120
Figure 4-24: Different cases of solder ball modeled with void in different location on damage path.....	121
Figure 4-25: Total life for different cases with small void located in different distances from initiation site on damage path.....	122
Figure 5-1: Extrusion and damage observed for Sn3.5Ag after 350 thermal cycles	82
.....	125
Figure 5-2: Extrusion and damage observed in Sn3.9Ag0.7Cu after 290 thermal cycles	82.....
.....	125
Figure 5-3: Post test ESEM micrograph of Sn3.9Ag0.6Cu solder joint (high creep cyclic conditions 125°C, 7.9 % inelastic strain range control 4.5 E-4 S <sup>-1</sup> shear strain rate, 55% total load drop) [Zhang, 2004].....	125
Figure 5-4: Plot of D Vs. w for different values for $\eta$ .....	127
Figure 5-5: TMM specimen schematic [Zhang, 2004].....	130
Figure 5-6: TMM test frame [Zhang, 2004].....	130
Figure 5-7: Tex Matrix used in Zhang Studies [Zhang, 2004].....	131
Figure 5-8: Example of Hysteresis loops at 25°, strain rate of 0.05 s <sup>-1</sup> and inelastic strain range of 0.04.....	132
Figure 5-9: Typical load drop observed in cyclic loading.....	133
Figure 5-10: Logarithmic plot of damage versus number of cycles to failure.....	134
Figure 5-11: Schematic of Analytical model used in TMM test.....	136
Figure 5-12: Plot of $\eta_c$ for different values of inelastic strain ranges.....	137
Figure 5-13: Comparison of damage propagation calculated using successive initiation with and without damage evolution.....	140
Figure 5-14: Hysteresis loop predicted by FEA for undamaged and damaged material (Damage is averaged over the entire joint).....	141
Figure 6-1: Selected ball from BGA256 model in local modeling for calibration purposes.....	145
Figure 6-2: comparison of damage propagation calculated using successive initiation and calibrated successive initiation.....	147
Figure 8-1: Specimens reflowed in three different levels of reflow variables (A1: all reflow variables at the lowest level, A2: all reflow variables at middle level, A3: all reflow variables at highest level).....	160
Figure 8-2: Number of grains as function of distance from board pad.....	160
Figure 8-3: 2-P Competing failure modes Weibull diagram for CTBGA failures ...	164
Figure 8-4: 3-P Weibull plots for premature failures and main population of failures of CTBGAs.....	165
Figure 8-5: Probability density function for early and main population failures for CTBGA.....	166



## **1. Chapter 1: Introduction and background**

The electronics industry is driven by component miniaturization and by an increasing demand for smaller, cheaper and more capable devices. Large number of small electronic components can be built-in into the same device, this increasing functionality and decreasing the cost of assembly. Many small components that previously were considered difficult to assemble are now the most commonly used components, such as, chip scale packages (CSP), micro ball grid arrays ( $\mu$ BGA) and small capacitors. As the number of components per board increases and components shrink the probability of manufacturing defects on the board increases. These defects affect the quality and durability of solder joint interconnects. Voids are one type of process induced defects that have not been understood completely.

Voids are one of several types of defects that may be introduced during the manufacturing processes. Voids are defined as cavities formed in the solder joint [Nurmi, 2003]. Manufacturing voids in solders are relatively large and are caused by entrapped air during reflow and out-gassing from either the PWB laminates or the solder flux [Lau et al., 2002]. Voids can cause quality and reliability issues. Very large voids may cause starved joints and premature failures. Voids may also pose reliability issues depending on the geometry of the joint, void size, location and frequency. Void may change the damage initiation time and propagation depending on their location and size. These issues are not fully understood and require future studies.

Another important issue that has not been very well addressed in literature is the impact of cyclic loading on damage evolution of Pb-free solders joint materials. This issue could be very important in cases that explicit modeling of damage initiation is used. Damage

caused by cyclic loading can potentially change the constitutive properties of material. These changes have to be considered and updated in modeling damage initiation and propagation in order to accurately predict durability using successive methods.

### **1.1.Objectives and problem statement**

Manufacturing defects can affect the in-service durability of miniature components that are becoming increasingly popular because of the demand for small hand-held products such as cell phones, personal organizers, and other smaller devices. The majority of defects in the assembly of SMT electronics assembly is introduced during the reflow and printing processes. Studies have shown that about 60% of defects identified after reflow originated during the solder paste printing process [Peck, 1998].

Manufacturing defects and their effects on durability are reasonably well understood for Sn37Pb solder joints because of their relative maturity in the electronics industry. The assembly processes have been optimized to improve the quality of the process and the durability of products made with Sn37Pb solders. The manufacturing process for Pb-free solders has not yet undergone the same level of scrutiny for quality issues. Due to different melting temperature and wettability, Pb-free solder joints are more prone to some types of defects, than Sn37Pb solder joints. Difference in wettability can cause certain kinds of manufacturing defects such as voids, reduced spread on copper and wicking, in assemblies with Pb-finished surfaces. Higher melting temperature causes other kinds of defects such as secondary reflow effect, fillet lifting, intermetallic growth, increased oxidation, and popcorned components. Therefore, the optimal processes of solder paste deposition and reflow in Pb-free solders are different from those for Sn-Pb solders.

Voids are one of the major categories of manufacturing defects in solder joints of electronic assemblies. They can potentially degrade the reliability of interconnects. Process-induced voids can be considered to be a quality issue, and many researchers have addressed the potential of these large voids to reduce interconnect reliability. However the effect of voids is not fully understood and requires future studies.

The issue of voids intensifies with the introduction of Pb-free solders. Pb-free solders are more prone to voids due to less wettability, increased level of flux and higher reflow temperature [Lee, 2002, Huang et al., 2004, Harrison et al, 2001, Li et al., 2001, Dasgupta et al, 2004]. The level of flux is increased to prevent oxidation due to higher reflow temperature. Higher reflow temperature also increases out-gassing of laminates [Lee, 2002].

Existence of microvias also aggravates voiding by introducing dead corners for adequate solder paste filling and wetting. Solder often tents the microvia during the printing. During reflow, air expands inside these tents and creates voids. One solution to this problem is to filled microvias usually with copper. Many factors in printing and reflow affect the creation of voids. Unfortunately, many of these factors have not yet been investigated. Additionally, some of the factors that have been investigated are only in the context of SnPb solders and in some cases, literature review shows conflicting results. the electronic industry needs a clear understanding of how these manufacturing factors affect the creation of voids and how these voids affect the durability of the Pb-free solder joints.

Another objective of this dissertation is to investigate damage initiation and propagation in voided solder joints. This is proposed to be done by separating damage

initiation and propagation using a technique called successive initiation. Separating damage initiation from propagation raises the question of how the change in material properties due to cyclic loading would affect the durability and damage propagation.

Cyclic loading deteriorates material and causes micro-crack / micro-voids to initiate, coalescent and propagate. This is manifested in decrease in load bearing capacity of the material. Studies have shown that constitutive properties of material change during the cyclic loading. These changes have not been conventionally included in FEA modeling of solder material. This study addresses this issue. The objective in this part of study was to develop a damage evolution model that predicts the change in constitutive properties of solder as function of number of cycles. Another objective of this part of study is to observe the change in FEA predictions in case where the damage evolution is taken into consideration for successive prediction of life.

## **1.2. Background and motivation for studying voids**

This section contains subsections which provide information pertaining to: SMT manufacturing process, effect of process variabilities on defect generation specially voids, the different types of voids; standards introduced by IPC and other known manufacturing sources for voids; literature review for manufacturing variables that have been investigated for both tin-lead and Pb-free solders; and the effect the variables on creation of voids, as well as effect of voids on mechanical and thermo-mechanical durability of solder joints.

It also provides background about continuum damage techniques used in literature to predict the damage evolution in materials. The gaps in the literature and shortcomings of existing approaches are explained.

### 1.2.1. Manufacturing process

Surface Mount Technology is the practice and methodology of attaching leaded and non-leaded active and passive electrical components on to the surface of a conductive pattern on a PWB without utilizing leads in feed through holes. The Surface Mount Assembly (SMA) process is divided into four separate, but interconnected process operations; stencil printing, component placement, reflow, and cleaning. A very simplified schematic flowchart of the SMA process is shown in Figure 1-1. However, not all the steps of the SMA process are intended to be studied in this dissertation. The only steps that will be covered are printing and reflow processes. The following section provides brief descriptions for these two steps.

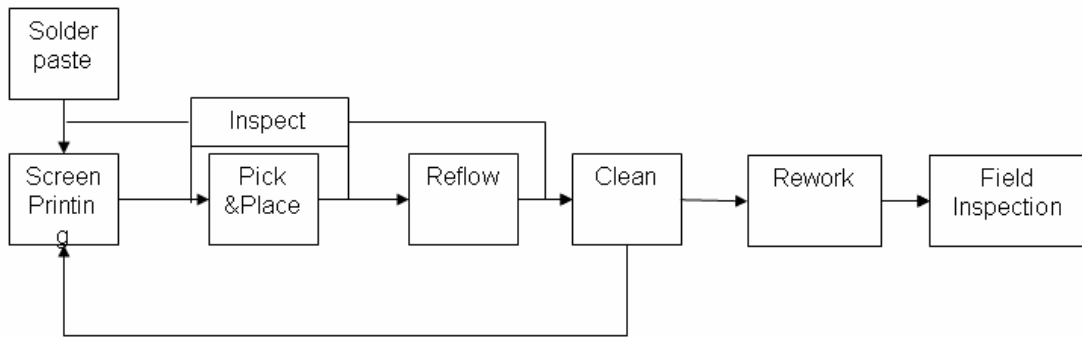


Figure 1-1: The SMA process flowchart

#### 1.2.1.1. Printing process

The paste deposition process involves the printing of solder paste on the substrate (printed wiring board) [Lee, 2002]. Solder pastes typically consist of solder alloy powder, flux, viscosity control agents, and solvent systems. The most commonly used solder paste deposition process is the stencil printing process. In this process, solder paste rolls in front of a squeegee blade, filling in stencil apertures some distance ahead of the squeegee Figure 1-2. A 60 degree blade angle relative to the stencil surface is commonly used in

most printing applications, though an angle of 45 degrees is also used in some instances [Durairaj et al., 2002]. The apertures of a stencil are fully opened and do not obstruct the flow of solder paste. The paste flows through these apertures which are precisely aligned with the PCB joint pads. The squeegee shears off the excess paste above the apertures as it moves over head. Once the print stroke is completed, the PCB is separated mechanically from the stencil leaving free standing deposits on the joint pads.

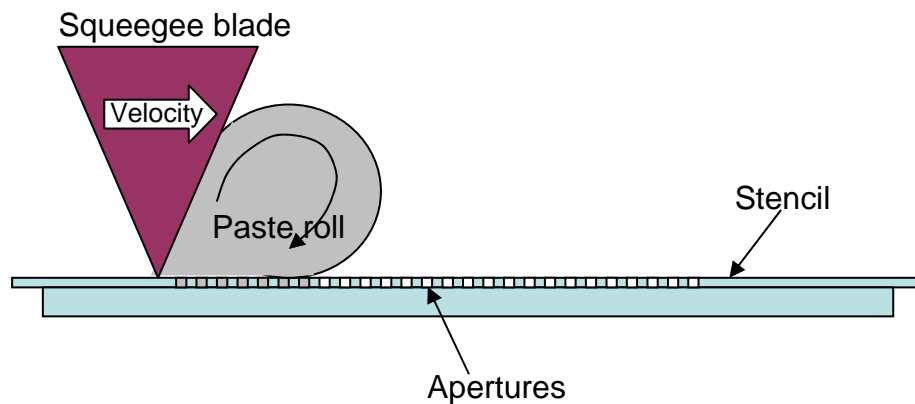


Figure 1-2: Schematic of stencil printing process 17

Consistent deposition of sufficient solder volume is an essential factor in the paste deposition process, in order to achieve high quality joints. Uniform solder paste deposition presents a considerable challenge in ultra-fine pitch applications such as Flip chips.

A variety of defects can be introduced during the printing process, including paste insufficiency, paste skip, excessive paste, excessive slump, alignment problems, bridging of paste deposits between pads, stencil smearing and blockage. Other than these defects, parameters such as paste height, volume, consistency and uniformity are important factors in determining the quality of the joints that will be formed after the reflow process.

Accurate in-line monitoring and control of the printing process is possible with sophisticated machine vision and process control tools. Solder paste inspection systems are classified into two types. One system is based on image processing system (2-D and 3-D) while the other type is based on laser scanning (3-D) [Okura et al., 1995]. 2-D digital video cameras can be used to carry out inspection and measurement of 2-D characteristics such as paste area and position. 3-D laser triangulation (profilometers) can be used to determine 3-D paste characteristics such as height and volume. These 3-D systems often use lasers as light sources. Consequently, they vary considerably in speed and accuracy. Hybrid systems are also possible measurement tool which takes advantage of speed and simplicity of 2-D video for measuring 2-D paste characteristic and use 3-D sensors to collect height and volume information at selected sites to ensure product quality and to provide data for process control [Owen et al., 2000]. Studies have shown that 60% of defects identified after reflow originated during the solder paste printing process [Rajewski, 1995].

#### **1.2.1.2. Reflow Process**

Another important step in the SMA process is Reflow. Reflow heating is commonly done using different methods, such as infrared reflow, forced convection reflow, and in-line conduction reflow [Lee, 2002]. In reflow the temperature of the solder paste is increased until it melts and forms the joint. Then it is slowly decreased to the room temperature. An inert gas such as nitrogen ( $N_2$ ) is sometimes used to prevent solder and pad oxidation. A typical reflow profile for a multi stage reflow oven is shown in Figure 1-3.

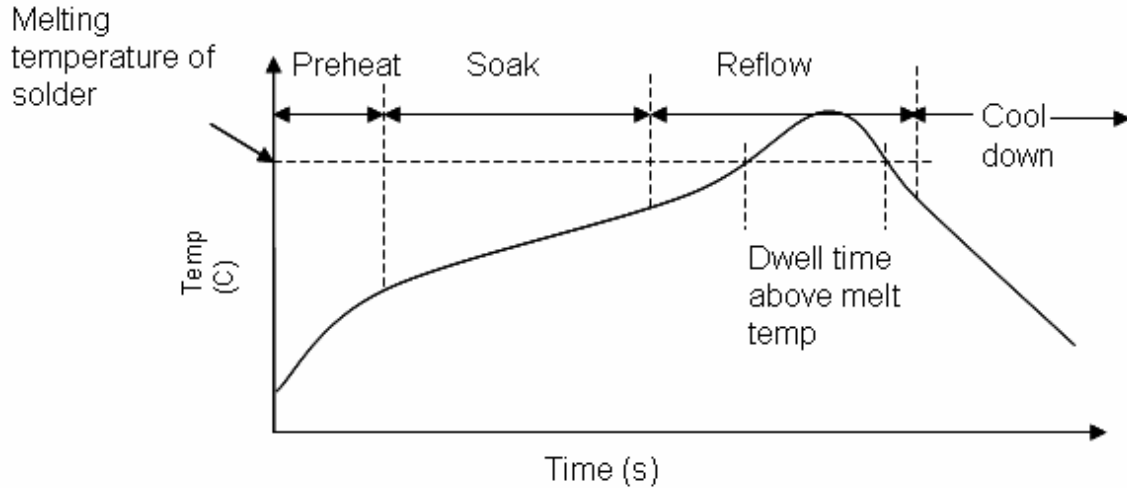


Figure 1-3: A typical reflow profile consists of preheat, soak, reflow and cool down sub-steps

Reflow process consists of several sub-steps. The first sub-step is preheat. The purpose of preheat is to raise the temperature uniformly on the board and alleviate excessive temperature gradients. Preheat temperature for SAC solders is about 150 °C and time for preheat is about 60 to 180 seconds.

After preheat there is a soak. The goal of this step is to evaporate solvents and activate the flux. It also helps to further equilibrate the temperature across the printed circuit board before entering the reflow zone. Essentially having a significant temperature gradient across the board may cause tombstoning, or walking parts due to uneven wetting behavior at the two ends of the chip. However, soaking the PCB for too long may cause excessive powder oxidation and flux vaporization, thereby poor wetting 45.

The third sub-step is reflow. Reflow temperatures vary according to the melting temperature of the solder, solder paste composition, type of the oven used and also it depends on the manufacturer. In reflow, the temperature of the solder is increased until it melts. Additionally, solder is kept in a molten state for sometimes to assure complete wetting and IMC formation. Each company has its own mostly confidential profile.

Figure 1-4 shows profile used for Pb-free solders based on JEDEC/IPC standard (J-STD-020) in ALTERA, and ZiLOG Corporation. Characteristics of this profile are shown in Figure 1-4, Table 1-1 and Table 1-2.

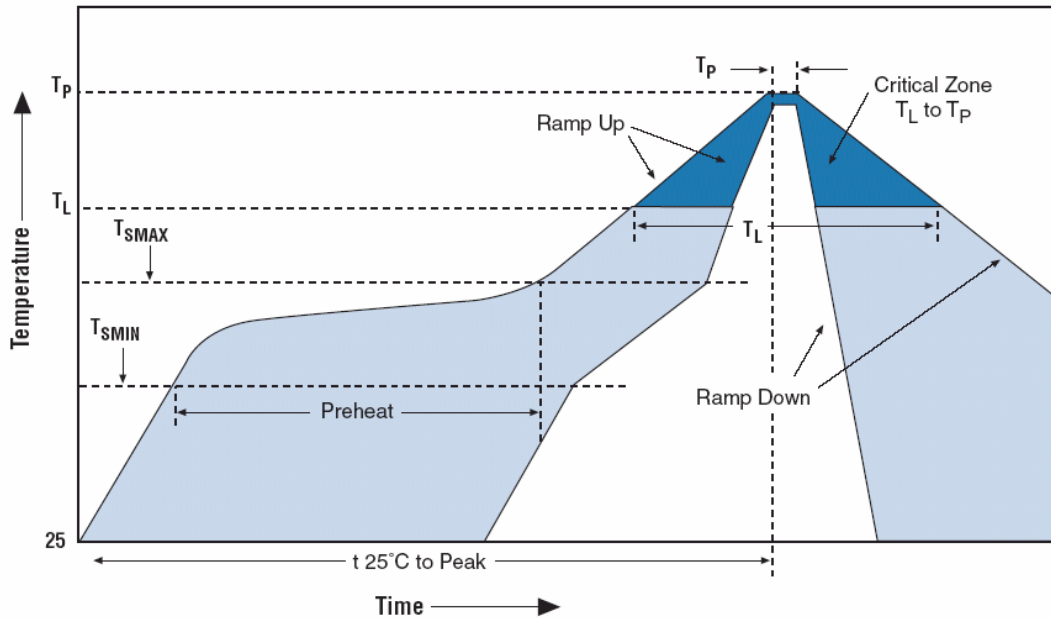


Figure 1-4: IR/convection reflow profile J-STD-020, used in ALTERA and ZiLOG [J-STD-020C], [ALTERA Corporation, 2004].

Table 1-1: Lead-free reflow profile recommendations [J-STD-020C], [ALTERA Corporation, 2004], and [ZiLOG Inc., 2003]

Reflow Parameter	Lead-free assembly
Minimum Preheat temperature ( $T_{SMIN}$ )	150°C
Maximum preheat temperature ( $T_{SMAX}$ )	200°C
Preheat time	60 – 180 second
Ramp rate ( $T_{SMAX}$ to $T_L$ )	3°C/second maximum
Time above melting temperature $T_L$ ( $t_L$ )	217°C (60 to 120) second
Peak temperature $T_P$	See table 1-3
Time from 25°C to peak temperature	6 minutes maximum
Time within 5°C of peak temperature	10 – 20 second
Ramp down rate	4°C/second maximum

Table 1-2: Peak reflow temperature ( $T_p$ ) for lead-free process [J-STD-020C], [ALTERA Corporation, 2004]

Package thickness	Volume mm <sup>3</sup> < 350	Volume mm <sup>3</sup> 350 - 2000	Volume mm <sup>3</sup> > 2000
< 1.6 mm	260°C	260°C	260°C
1.6mm – 2.55 mm	260°C	250°C	250°C
> 2.5 mm	250°C	245°C	245°C

The final step in the reflow process is cooling. It is observed that higher cooling rate results in finer grain and therefore shinier joints. However, a cooling ramp less than 4°C/second is not recommended due to thermal shock.

Currently two different reflow profiles are used in industry; ramp-soak-spike (RSS) and ramp-to-spike (RTS) also known as Soak and Tent profiles [Apell, 2003]. Figure 1-5 and Figure 1-6 represent typical RSS and RTS profiles. In the RTS profile, soaking is eliminated and the temperature is increased uniformly until the peak temperature is achieved. In efficient ovens, where the temperature is in virtual equilibrium, soak becomes an unnecessary step. Solders show better wettability with the RTS profile. Therefore RTS profile is appropriate for lead-free solder since the wettability of lead-free solder is less than that of Tin-Lead solders. Generally, it is shown that RTS results in shinier, brighter and better quality joints. Additionally, since the ramp rate is constant through the whole heating up process, it is much easier to control the temperature, and therefore RTS results in less defects due to thermal shock.

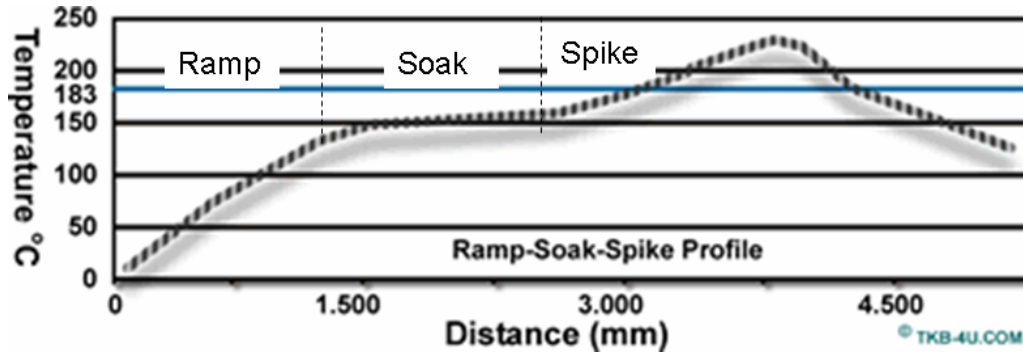


Figure 1-5: Typical Ramp-Soak-Spike profile [www.TKB-4U.COM]

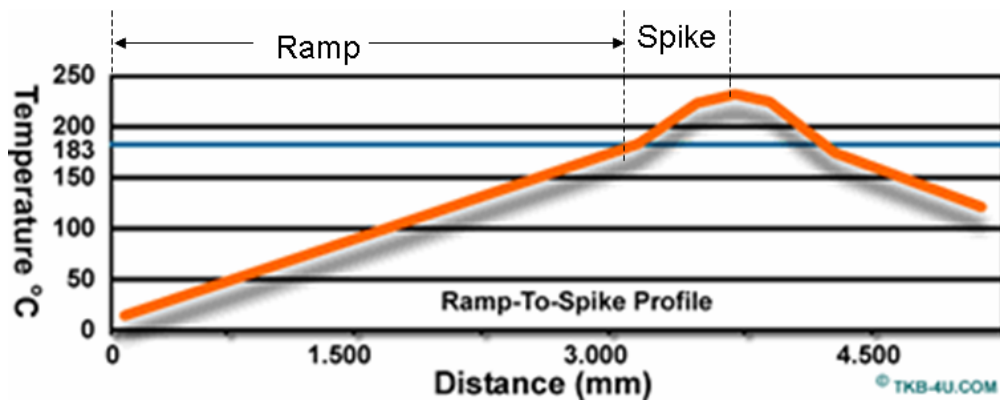


Figure 1-6: Typical Ramp-To-Spike profile[www.TKB-4U.COM]

### 1.2.1.3. Manufacturing Variabilities

Many variables affect the quality and reliability of solder joints. Manufacturing variables that may cause defects in solder joints are represented in the form of a fish-bone diagram (see Figure 1-7). For this study, only variables in the printing and reflow processes are investigated. These variables are marked in the fishbone diagram with boxes. Several variables affect printing and reflow behavior of the solder such as, temperature, humidity, stencil opening area, waiting time before/during print, peak temperature of the reflow and so on. Manufacturing defects can be controlled by choosing optimum value for the paste deposition and reflow processes variables.

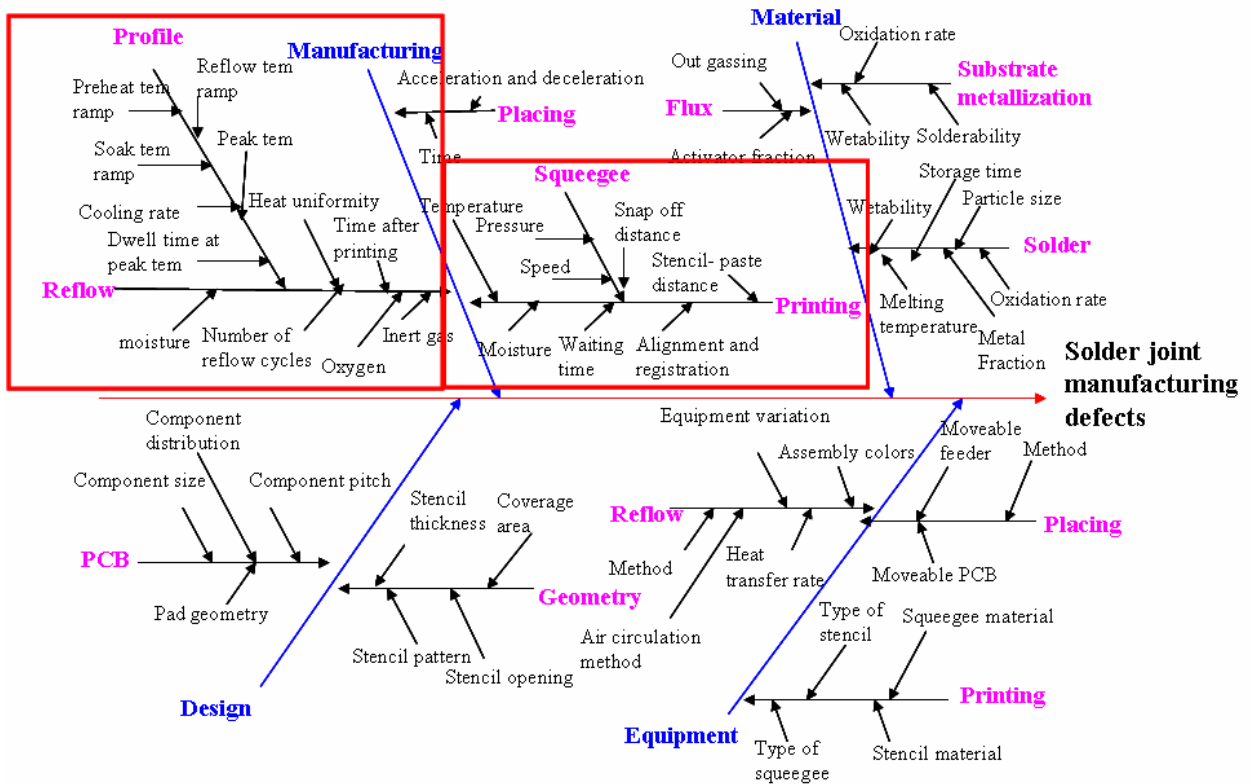


Figure 1-7: Fish bone diagram for manufacturing defects of solder joints

### 1.2.2. Defects Introduced in Printing and Reflow

Defects that are introduced during the printing and reflow can be classified into fatal defects and latent defects. Defects that cause devices to malfunction or dysfunction immediately after assembly are called fatal defects. These defects cause quality issues. Some defects, however, do not cause the device failure immediately after assembly, but cause infant mortalities and reliability issues. These defects are called latent defects.

A list of solder joint defects is provided below.

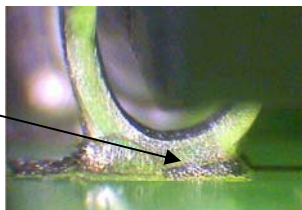
- Cold joints
- Non-wetted joints
- De-wetted joints
- Leaching
- Skipped joints
- Intermetallics

- Tombstoned components
- Wicked up solder
- Starved joints
- Open joints
- Bridge
- Solder balls
- Insufficient Intermetallic growth
- Skewed components
- Solder beads
- Spattered joints
- Misalignment
- Void

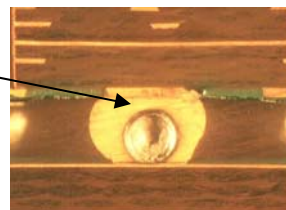
Different manufacturing steps that might contribute in creation of these defects are paste deposition process, component placements and reflow process.

Due to various melting temperatures and wettabilities, Pb-free solders are prone to different kinds of defects than tin-lead solders. Wettability differences cause certain kinds of manufacturing defects such as voids, reduced spread on copper and wicking in assemblies with Pb finished surfaces. Higher melting temperatures result in defects such as secondary reflow effect, fillet lifting, and damaged components. Some of these defects are presented in Figure 1-8. Therefore, the standard processes of solder paste deposition and reflow must be changed to be compatible with Pb-free solders.

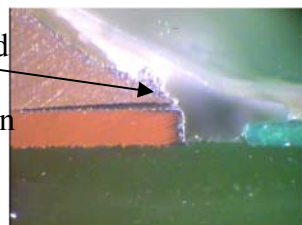
Incomplete lead wetting because of short reflow process



Voids caused by out gassing or trapped gas.



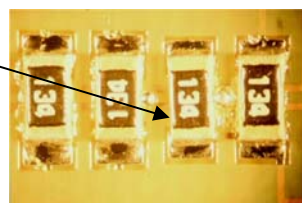
Fillet lifting caused by differences in solder solidification



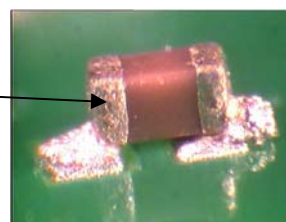
Wicking as a result of high solderability of the component.



Solder beading due to presence of solder paste under the component



Incomplete reflow due to not uniform heat flux



Pb-free solders investigated: Sn3.8Ag0.7Cu, Sn3Ag0.5Cu, Sn0.7Cu

Figure 1-8: Manufacturing Defects in Pb- Free Solders Voids[Willies, 2005]

The focus of this study is on voids which are one major category of manufacturing defects in solder joints of electronic assemblies, because they can potentially degrade the reliability of the interconnects.

### 1.2.2.1. Voids

Process-induced voids can be considered to be a quality issue, and many researchers have addressed the potential of these large voids to reduce interconnect reliability. As will be discussed later, many of these studies came up with inconclusive or contradictory conclusions, and there is no definitive quantitative answer yet about the influence of process induced voids on reliability. Investigators agree that the severity of the effect will depend on the solder properties, the geometry and location of the voids and geometry of the joint, and the type of loading (thermal vs mechanical loading).

### 1.2.2.2. Types of process induced voids

Voids originating during the manufacturing process can be divided into the following groups [Aspandiar, 2005]; Macro voids, planar micro voids, shrinkage voids, microvia voids, pin-hole voids, Kirkendall voids.

Macro voids are voids generated by volatile ingredients found in solder joints and solder paste. The size of these voids is relatively large. In this study we categorize voids larger than 30 microns in diameter to be in this group. These voids can be found in both Pb-free and Sn-Pb solders. They can be found anywhere inside the solder or at the interface between the solder and the board or components. Macro voids can occur anywhere, even in through holes. Figure 1-9 shows two examples of this type of void in a BGA solder ball and inside a plated through hole (courtesy of Intel).

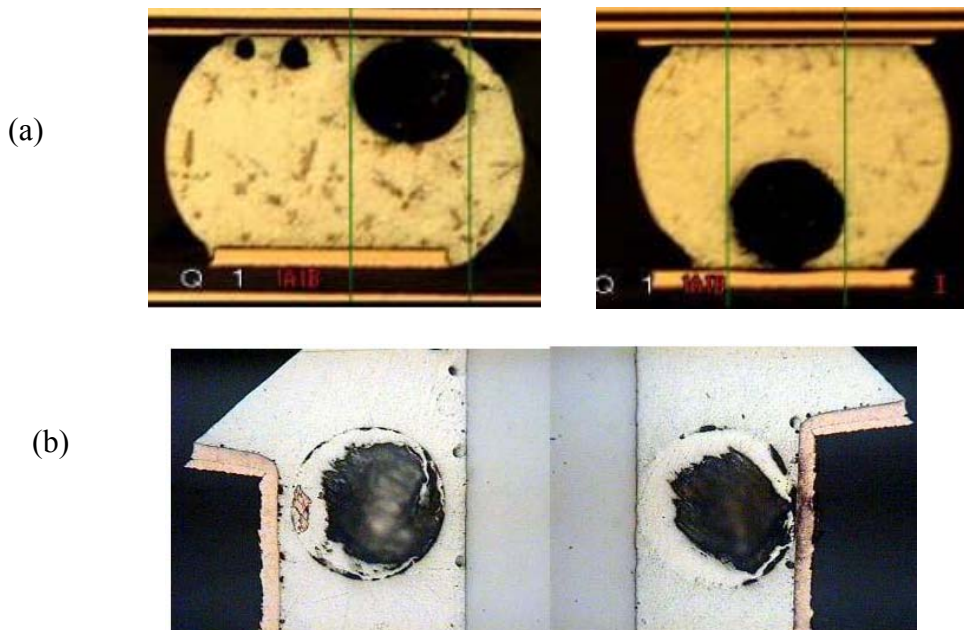


Figure 1-9: Two examples of macro voids (a) void inside BGA ball (b) Void inside through hole [Aspandiar, 2005]

Planar micro voids are voids smaller than 30 microns in diameter. There are usually several of them located at a plane right above the intermetallic layer and at the interface

of the solder with PCB. This type of void has been reported with different surface finishes, such as immersion silver (ImAg), electroless nickel immersion gold (ENIG) and organic solderability preservative (OSP). These voids are more common in solder mask defined lands [Aspandiar, 2005]. Figure 1-10 shows an example of a planar micro-void at the interface of the solder and a PCB pad. The precise causing of the planar micro voids is not very well understood. Some studies have shown that surface finish might have affect on the creation of planar micro-voids [Joint Intel, Enthone Inc. Study, 2006]

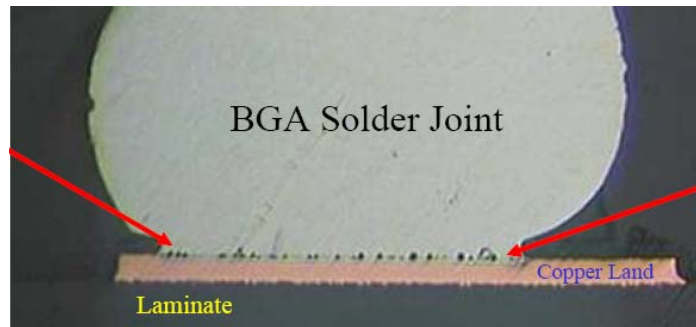


Figure 1-10: planar micro voids at the interface of solder and PCB pad [Aspandiar, 2005]

Shrink-hole voids, also called sink holes and hot tears, are elongated voids with rough, dendretic edges emanating from the surface of the solder joint. These voids are seen in all different joints such as BGA, as well as through holes. They are more common in Sn-rich Pb-free solders (eg. SAC) and are believed to be caused by the slow cooling of Sn in solder joints. Interestingly these voids do not appear to cause reliability problems and do not grow during the life cycle [Aspandiar, 2005].

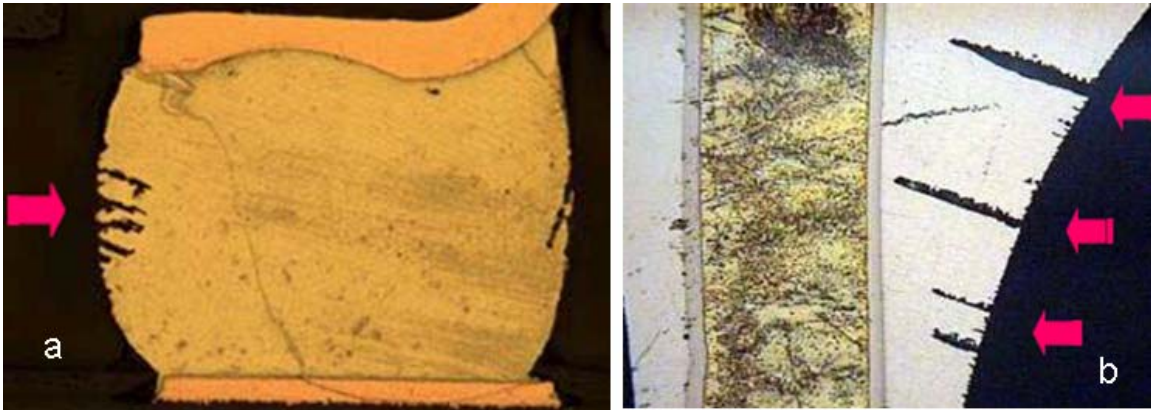


Figure 1-11: Shrink-hole voids in solder, (a) in solder joint, (b) in fillet [Aspandiar, 2005].

Microvia voids are voids similar in size of macro voids. They are generated due to the presence of microvias under the solder. There are ways to reduce the size and number of microvia voids, such as double printing, increasing the diameter of the microvia or plating the microvia shut. The microvia voids are exempt from the IPC A-610 standard. This standard will be reviewed in the next section.

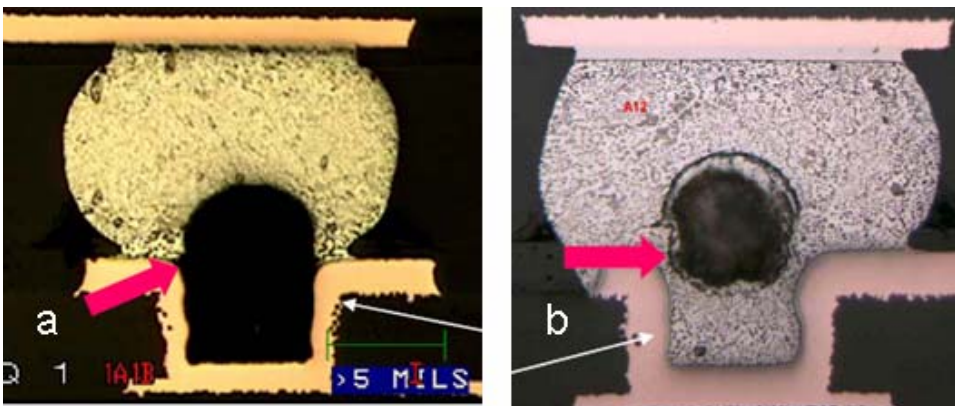


Figure 1-12 shows two examples of microvia voids. Figure 1-12 (a) shows how the solder has not wet the copper pad inside the microvia. In Figure 1-12 (b) the solder has wet the copper pad and left a void above it. Void that form in or above a microvia, sometimes detach from the via during the reflow and float up into the solder ball.

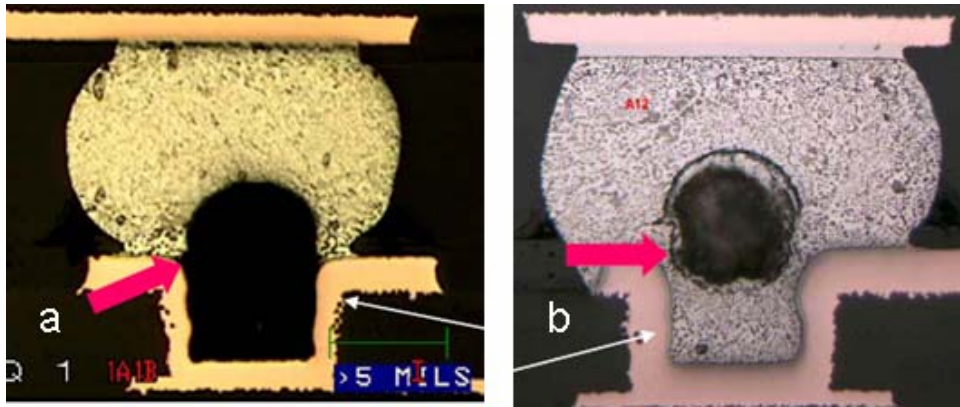


Figure 1-12: Examples of microvia voids (a) when the solder has not wet the inside copper pads of microvia and (b) when the solder has wet the inside copper pads of microvias [Aspandiar, 2005]

Pin holes are holes that exist in the PCB land before the board goes through the reflow process. They are caused by copper plating issues in board manufacturing and are located in or right above the IMC. Pin holes pose serious reliability issues, since cracks can propagate through them. Figure 1-13 shows different magnifications of pin holes observed under the solder and on PCB pads.

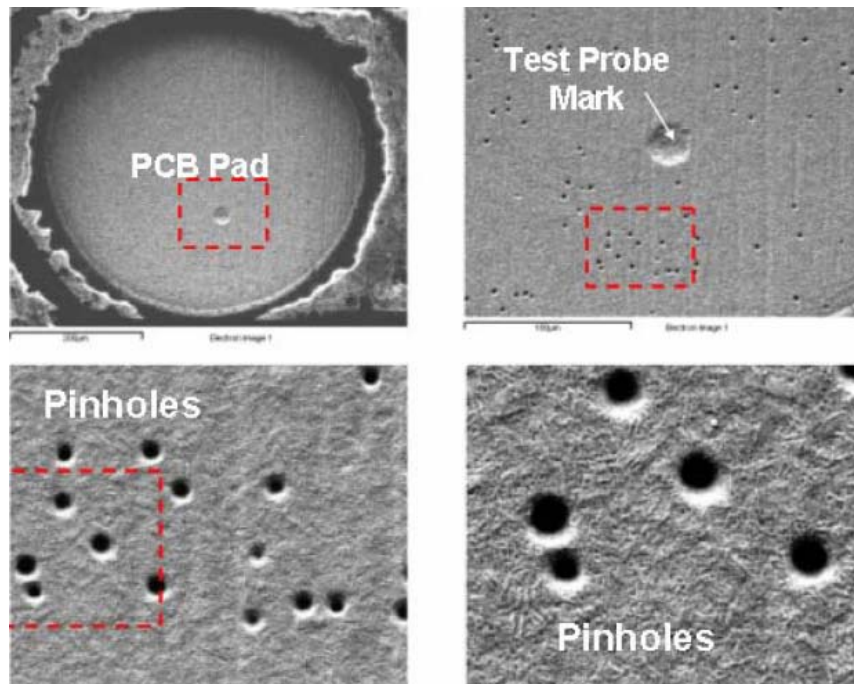


Figure 1-13: Pin holes in the copper pad in PCB land [Aspandiar, 2005].

Kirkendall voids are formed when two metals of different inter diffusion rates within each other are in contact across an interface. Tin-copper (Sn-Cu) is one such example. Because copper diffuses much faster in tin than tin does in copper, atomic vacancies and depletion sites are left behind in the copper layer. These vacancies coalesce and form Kirkendall voids inside the IMC. These voids worsen during thermal aging due to increase in IMC growth rate and are independent of surface finish as long as there is Cu-Sn diffusion couple. Figure 1-14 shows an example of kirkendall voids in Pb-free solders.

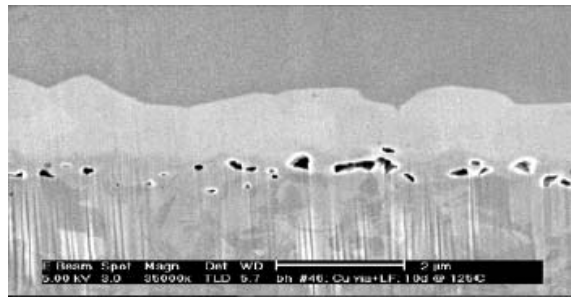


Figure 1-14: Kirkendall voids observed in Texas Instrument by aging at 125° C for 10 days [Aspandiar, 2005]

### 1.2.2.3. Industry Standards

The most common standards currently used in the electronics industry are the IPC standards. IPC was founded in 1957 as the institute for printed circuits. IPC provides standards for electronic manufacturing and for quality and reliability inspections. Criteria for void acceptance and rejection criteria for BGAs are provided in IPC-A-610.

Void inspection criteria are based on the size of the void (relative to size of the ball), as well as the location of void inside the BGA ball. The IPC standard divides voids into three major categories; voids within the ball, voids at the package interface and voids at the mounting surface interface [IPC-7095]. Among these three categories, the IPC A-610 subdivides voids further into size groups. Table 1-3 shows IPC classification of voids

based on Figure 1-15. Thus depending on the percentage of voids (if multiple voids, total percentage) present and their location, IPC has recommends corrective actions.

Table 1-3: IPC classification for Voids inside BGA ball [IPC-7095].

Location of the void	Class I	Class II	Class III
In ball % dia, %area	60% dia = 36% area	45% dia = 20.25% area	30% dia = 9% area
At interface of ball and substrate	50% dia = 25% area	35% dia = 12.25% area	20% dia = 4% area

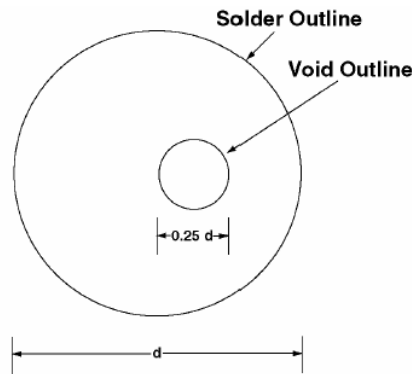


Figure 1-15: Outline of solder ball and void inspected by Xray from top view

### 1.2.3. Literature Review

The literature review is categorized into two sections. The first section focuses on researches that address the creation of voids and other manufacturing defects during the reflow and printing processes. The second section focuses on studies that have been conducted to examine the effect of voids on the durability of solders. Durability is defined as number of cycles that a solder joint interconnect can stand thermo-mechanical cycling.

#### 1.2.3.1. Effect of manufacturing variation on voids formation

Li et al. [Li et al., 2001] studied the variables of the reflow window. They conducted experiments on the effect of peak reflow temperatures and time above liquid on bump characteristics of flip chips. They selected Sn3.5Ag, SnAg3.8Cu0.7 and Sn0.7Cu solders.

All solders were found to have significant void formation during solder bump reflow. They observed that reflow at low peak temperature resulted in fewer and smaller voids in the solder bump than at high peak temperatures. Furthermore, voiding increased with time above liquidus temperature. They also concluded that larger bond pads resulted in larger and more numerous voids than smaller bond pads.

Nurmi [Nurmi, 2003] studied the effect of multiple reflow cycles on solder joint voids and the reliability of solder joints for pure as well as mixed metal systems. Pure metal systems consisted of Pb-free solder paste and Pb-free PBGA components. Mixed metal systems consisted of Sn-Pb solder paste and Sn-Pb-Ag PBGA components, and Pb-free solder paste with Sn-Pb-Ag PBGA components. The effect of voids on solder joint reliability was tested using a temperature cycling test.

The reflow profile was repeated on different sample groups up to 3 times. Two different profiles were used, during the reflow; a SnPb temperature profile for the test boards with SnPb solder paste and lead containing PBGA components and a Pb-free profile for the test boards with Pb-free solder paste.

The voids on the fracture surface of the solder were counted and they were grouped into three categories; sizes less than 10% of fracture surface area, sizes between 10% and 50% of fracture surface area and sizes larger than 50% percent of fracture surface area.

Cracks mostly occurred at the interface between the solder joint and component and only the voids on the crack path were counted. They concluded that the effect of voids close to PCB was negligible.

In pure Pb-free solder joints the voids were scattered more evenly in proportion to the number of reflow cycles. It was also observed that the number of voids decreased

while their size increased, as time being above the molten state increased. This confirms Li's studies that concluded that void percentage increased as the time above liquid increased. They concluded that this was due to coalescence of small voids. Ultimately, reliability of joints created by both Pb-free solder and Sn-Pb-Ag PBGA was seriously decreased due to the increased number and size of the voids.

Harison and Vincent [Harisson, 2001] conducted a three year study to develop a Pb-free soldering solution. Their studies showed that Sn<sub>3.8</sub>Ag<sub>0.7</sub>Cu was best candidate. For this solder differences in alloy density, melting point, and surface tension relative to conventional solders were found to give higher levels of internal voids, reduced spread on copper and duller joints with rougher surfaces.

Echeverria and Santos [Echeverria et al, 2004] conducted a study to investigate the creation of voids in mixed and pure Pb-free systems. Their results showed that overall Pb-free assemblies performed better since the voids created in them were generally class III of IPC standard, which includes voids with area fractions between 0 to 9%. Mixed assemblies showed voids in class II between 9% to 20.25% of area fraction. They also investigate the effect of surface finishes and concluded that ENIG produces less voiding than OSP or immersion tin. Comparison of two different reflow profiles showed that Ramp-Soak-Spike profiles produces less voids than Ramp-to-Spike profiles.

### **1.2.3.2. Effect of Process Induced Voids on Durability of Joints**

Nurmi et al. [Nurmi et al., 2003] studied the effect of voids on the durability (number of cycles to failure) of PBGA joints under temperature cycling. They conducted a thermo-mechanical durability testing on boards created under different manufacturing conditions. Specimens were assembled with Sn-Pb solder as well Pb-free solder and mix of both Sn-

Pb and Pb-free solders. This study revealed that large voids significantly reduce the characteristic life of the joints. Failure analysis of the failed specimen under temperature cycling test revealed that crack was located at top side of the ball close to the component bond pad. This also showed that multiple small voids on the component side (crack propagation path) accelerate the failure as the crack tends to link up between the voids.

Kim et al, 2004 [Kim et al., 2004] conducted experiments and modeling of BGAs with voids under mechanical cycling. Solder balls with different void sizes and locations were modeled under mechanical loading for Pb-free solders. A mechanical cycling test was conducted for specimens with different void sizes that were created using Sn-Pb and Pb-free solders. They concluded that shear strain and equivalent plastic strain in balls with voids are not always bigger than those without voids. This study also revealed that the mean fatigue strength of sample lots with and without voids did not differ significantly. Mechanical test results showed that the fatigue strength of solder joints is not affected by voids and voids do not participate in damage initiation and propagation. They concluded that the effect of void formation on fatigue strength of solder joints is so small that that it may be neglected.

One shortcoming of the Kim study is that the solder materials were modeled elastic-plastic and not viscoplastic materials, hence their modeling conclusions may not directly apply to thermal cycling. Furthermore they only modeled voids up to 5% volume fraction of the solder balls (voids up to 20% of volume have been observed in Zhu's study [Zhu et al, 2003]). Figure 1-16 shows an example of a void modeled by Kim and co-authors [Kim et al., 2004].

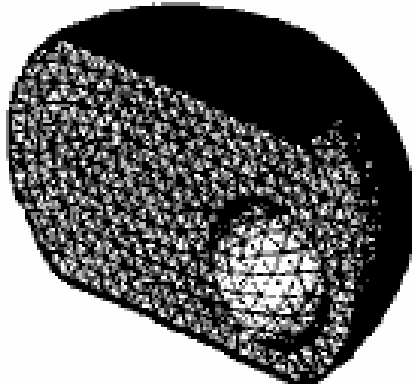


Figure 1-16: Finite element mesh of voids 40

John and Erasmus [Lau, and Erasmus, 2002] studied the effect of void size, location and volume fraction on the reliability of Sn-Pb solders for Bump Chip Carriers (BCC++) under thermal cyclic loading using two-dimensional finite element analysis. They modeled crack propagation using a fracture mechanics approach (J integral). Figure 1-17 shows examples of the various cases that they studied.

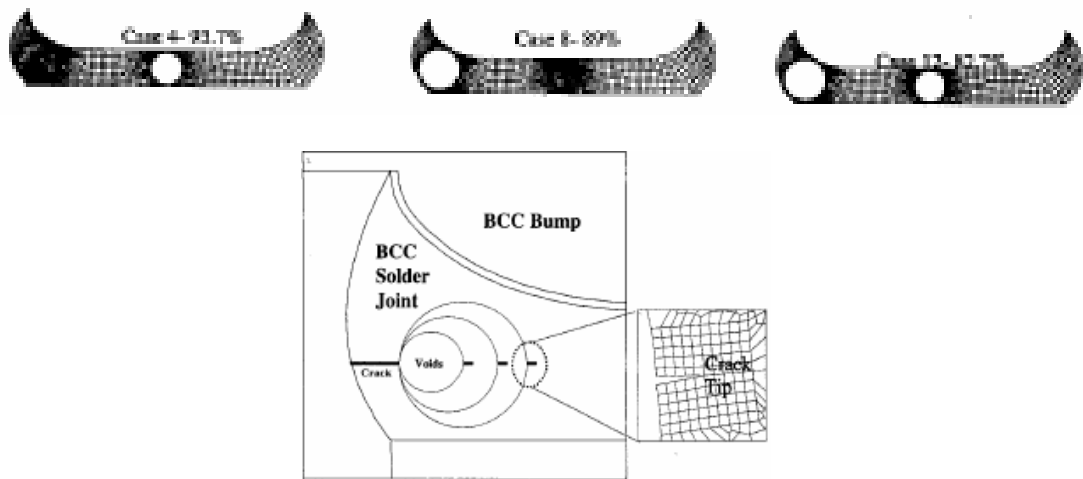


Figure 1-17: BCC solder joints with various void size, location and percentage [Lau and Erasmus, 2002]

The Lau's approach was to calculate the J integral around the tip of the crack when there was no void and compare the result with the cases where there were voids of

different sizes. Their result showed that voids can slow down the crack propagation rate. They concluded that voids up to 20% were no threat to reliability.

Yunus et al [Yunus et al., 2003] created samples with three different solder pastes reflowed in air and Nitrogen. They observed excessive amount of voids in all assemblies. Voids were observed in all three pastes and in assemblies reflowed in both air and Nitrogen. However, the void volumes were different for each solder paste. Thermo-mechanical cycling fatigue tests were also conducted. Characteristic life for the specimens with small, big and no voids were obtained from a Weibull distributions of the failure data. The characteristic life ( $\eta$ ) which is defined as time to failure for 62.3% of population for failures with no voids, small voids and big voids were 1457, 1443, 1278 cycles. Samples with big voids failed considerably earlier than of those with either small voids or no voids (Figure 1-19). Additionally failure analysis of the joints revealed that small voids (Void area less than 50% of the joint area) do not significantly change the characteristic life of interconnect. However the frequency and location of small voids plays a critical role. They concluded that the exact nature of failure depends on the location, size and the frequency of voids and that with increasing void size the probability of failure increases.

Zhu et al [Zhu et al., 2003] conducted modeling and thermal cycling of Sn-Pb BGA interconnects. Their study showed that if the area percentage of void is larger than 20% of joint area, characteristic life of the device decreases significantly. They conducted a 3D slice finite element analysis and used Anand's Viscoplastic constitutive model. Fatigue life was estimated by Darveaux's model [Darveaux et al., 1995]. They concluded that voids act negatively on solder joint reliability. A simple estimation method was

suggested that assumes fatigue life reduction is proportional to the ratio of the void size to solder resist opening (SRO) size.

#### **1.2.4. Gaps in Literature**

Voids in solder joints have the potential to aggravate the reliability of electronic products. They can degrade thermal, mechanical and electrical characteristics of the joints. Formation of voids, their size, location and volume fraction are a function of many manufacturing variabilities. Problems with voids can be more intensified in Pb-free products.

Many researchers have addressed the potential of large voids to reduce interconnect reliability. As will be discussed later, many of these studies came up with inconclusive or contradictory conclusions, and there is no definitive quantitative answer yet about the influence of manufacturing voids on durability. Investigators agree that the severity of the effect will depend on the solder properties, the geometry and location of the voids and the joint, and the type of loading (thermal vs mechanical loading).

Many of the process variables have not yet been investigated for Pb-free solder. For those variables that have been investigated, the results are contradictory. This section consists of two parts. The first section identifies the variabilities of manufacturing processes that have not been investigated, as well as, studies that have resulted in conflicting conclusion. Additionally, the first section rationalizes areas for additional investigation. The second section compares studies that have investigated the effects of voids on durability, as well as, identifying the shortcomings and conflicts between these studies and provides justification for further investigation.

#### **1.2.4.1. Effect of manufacturing variation on void formation**

Many factors affect void content in solders, such as, solder composition and rheology, flux content, surface finishes, pad dimensions, reflow variables and printing variables. This study and literature review focuses only on reflow and printing variables. Reflow process parameters that affect void formation are divided into two groups;

Factors that have been investigated and proved to have an effect:

- Peak temperature [Li et al., 2001, Maattanen et al., 2001, Nurmi et al, 2003]
- Time above peak temperature [Li et al., 2001, Maattanen et al., 2001, Nurmi et al, 2003]
- Number of reflow cycles [Nurmi et al., 2003]
- Inert gas [Melton, 1993]

Factors that have not been investigated but are believed to have an effect [Lee, 2002]:

- Moisture
- Soak ramp rate
- Cooling rate
- Reflow ramp rate
- Temperature uniformity
- Preheat ramp rate

The effect of these six variables has not been investigated in the studies listed above. Thus the effects that these variables have on voids formation are still unknown. Additionally, responses functions were considered to be linear, so variables were mostly considered at two levels in the design of experiment. However, linearity of factor effects

has not been proven and there is still need for more sophisticated DoEs with a higher number of levels for each variable.

#### **1.2.4.2. Effect of voids on durability of interconnects**

Comparison of studies in the literature shows that there are inconsistencies between modeling and experimental data. Lau [Lau and Erasmus, 2002] concluded that voids with 20% volume fraction are no threat to reliability, but Zhu's [Zhu et al., 2003] experimental result showed that voids with 20% area fraction reduce the life of joints significantly.

Yunus et al [Yunus et al., 2003], conducted thermo-mechanical cycling tests for PBGAs with 256 I/O's that showed specimens with big voids failed significantly earlier than specimens without voids. In this case the Weibull  $\eta$  (characteristic life) is affected by voids and decreases significantly in the presence of large voids. These results are shown in Figure 1-18.

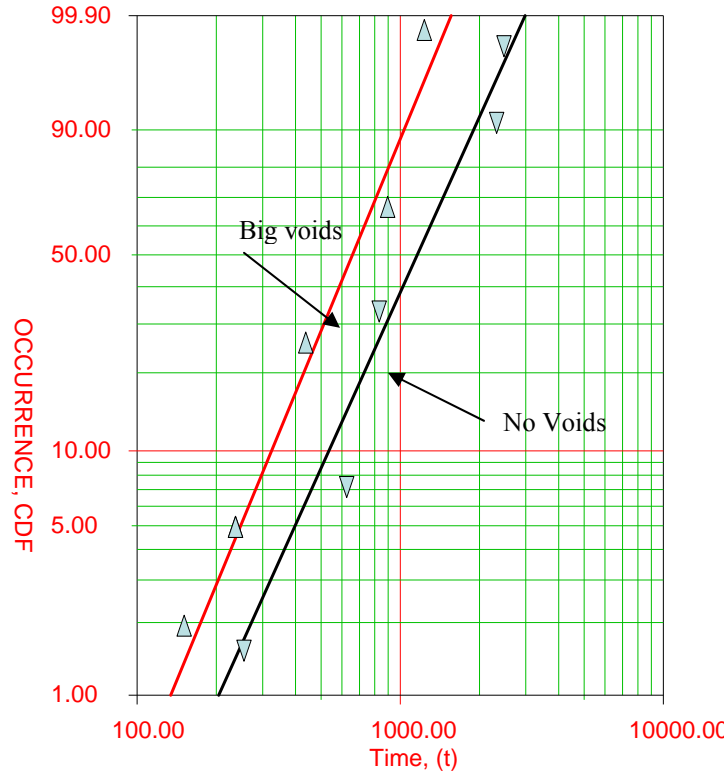


Figure 1-18: Weibull plot of failures on 256 I/O 1 mm PBGA [Yunus et al., 2003]

Figure 1-19 shows Yunus' results for flex CSP with 48 I/O's. In this case the characteristic life ( $\eta$ ) is not affected by the void size, but the shape parameter ( $\beta$ ), which shows the distribution width, is affected by void size.  $\beta$  is small in the presence of large voids, but increases when there are small or no voids. Thus the failure free operating period (FFOP) is much shorter when there are large voids. Samples with small voids have a much smaller variance (larger  $\beta$ ). Based on this observation we can conclude that lots with large voids are not as reliable as lots with small or no voids. The causes of difference between these two cases (Flex CSP vs PBGA) in terms of  $\eta$  and  $\beta$  have not been discussed in this paper, and the causes are unknown.

There is some controversy about whether small voids improve or reduce the reliability of joints [Lau and Erasmus, 2002, Yunus et al., 2003]. Researchers such as Lau

[Lau and Erasmus, 2002], and Yunus [Yunus et al., 2003] reported that small voids can improve reliability by arresting crack propagation. However, there is no specific or quantitative definition in these studies about the size of detrimental voids.

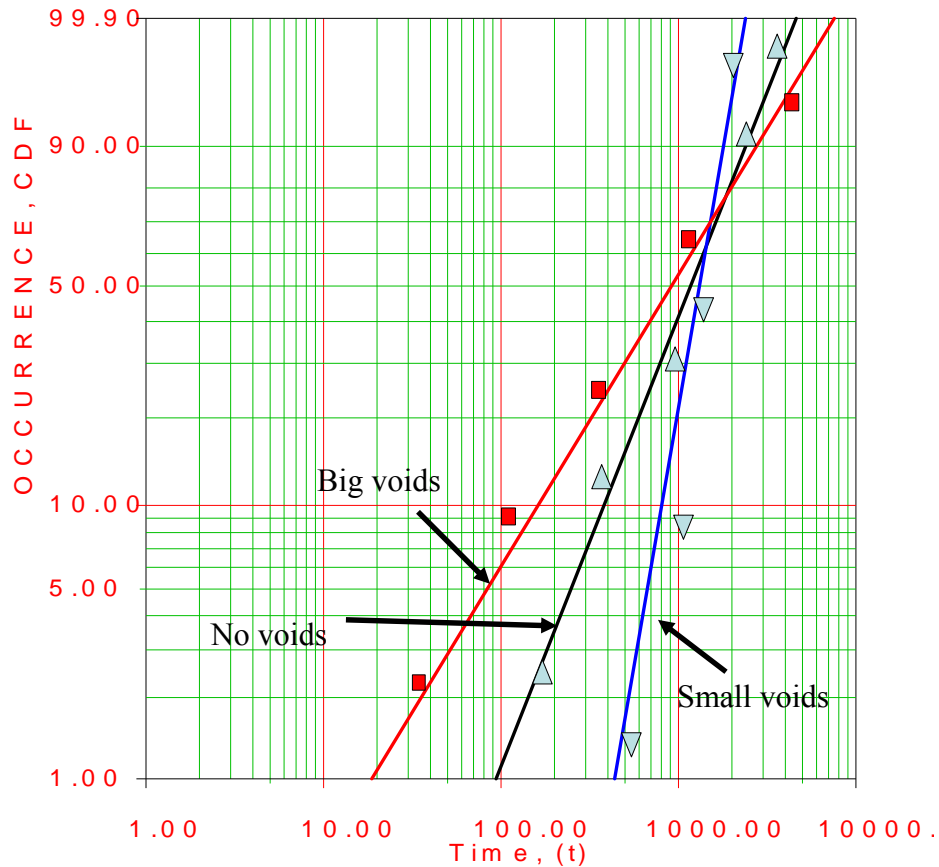


Figure 1-19: Weibull plots of failures on 48 I/O flex CSP [Yunus et al., 2003]

Another aspect requiring investigation is the modeling approach. Fracture mechanics [Lau, Erasmus, 2002] considers propagation of a single dominant crack through an otherwise undamaged material. However, the damage mechanism in solder is different. In solder, damage is propagated by growth, coalescence and the interconnection of micro-cracks and voids distributed all over the stress regions of the joint. Therefore, use of a continuum damage model is more appropriate. In addition, the change of constitutive

properties of the material caused by progressive damage accumulation has been ignored in the literature.

### **1.3. Durability modeling**

Fatigue is defined as a process by which the material is weakened by cyclic loading. The resulting stress may be below the ultimate tensile stress or even the yield stress of material yet still cause catastrophic failure<sup>101</sup>. Fatigue is a phenomenon that is very hard to test for due to the long times that are necessary for cracks to initiate and propagate under real environmental condition. Therefore many durability models have been proposed for predicting material life of the material. These methods are mostly based on material deformation (stress-strain behavior) and the work done on the material during one cycle of loading. Most models that address fatigue need cyclic history of strain and/or stress in order to predict life [Lee et al., 2000]. Stress strain histories could be obtained both experimentally as well as using Finite Element Analysis.

Due to difficulty in obtaining stress-strain histories through testing for some structures, such as electronic packages, Finite Element analysis has become one of the practical paths for obtaining cyclic histories of stress and strain in these cases. This chapter provides a brief background about different durability schemes reported in the literature and provides a brief comparison and a justification for the model used in this study.

#### **1.3.1. Modeling approaches**

Fatigue behavior of material is usually classified into two regimes, low cycle fatigue and high cycle fatigue. Low cycle fatigue occurs when the cyclic deformations are so large that they are predominantly inelastic. If the cyclic deformations are small enough to be predominately elastic, the fatigue is called high cycle fatigue. A common example of

high cycle fatigue is failure in solder material due to vibration at moderately low temperature. As the temperature and excitation level increases the probability of plasticity increases due to the low melting temperature and low yield stress of solder. Therefore, higher temperatures increase the probability of getting low cycle fatigue. When the loading rates are smaller (e.g. mechanical cycling of the solder in low strain rates or thermo-mechanical cycling of solder) the solder material experiences both plastic and creep deformations at common application temperatures because of its low melt temperatures. In this study plastic refers to rate-independent mechanical deformation and creep refers to rate-dependent mechanical deformation. Therefore, thermal cycling of solder can produce low cycle fatigue with the inelastic strains containing both plastic and creep deformation.

There are several different approaches that have been used in the literature to predict the life of solder joints. The type of approach used depends on many factors, such as, type of material, types of deformation, regime and mode of cyclic loading. One example is fracture mechanics approach. Fracture mechanics considers propagation of a single dominant crack through an otherwise undamaged material. However, the damage mechanism in solder is different. In solder, damage in thermo-mechanical cycling is propagated by growth, coalescence and the interconnection of micro-cracks and voids distributed all over the stresses region of ball. Therefore, use of a continuum damage model is more appropriate. Continuum damage approach is another common approach that will be explained in detail in later sections. Other basic life prediction methods that are neither fracture mechanics based nor continuum damage based have been classified

into the following groups in this context; stress based approach, strain based approach, and energy based approach.

### **1.3.1.1. Stress based approaches**

The stress based approach to life prediction is the oldest method used in fatigue modeling [Frear, 1991]. In this method the fatigue life of solder is expressed as function of a strength parameter. Basquin proposed the following equation:

$$\sigma_a = \sigma'_f (2N_f)^b \quad \text{Equation (1-1)}$$

In which,  $\sigma_a$  is the stress amplitude,  $\sigma'_f$  is called the fatigue strength coefficient and b is the fatigue strength exponent. For solder material long hold times under stress control create large and unstable creep strains. So there is not a lot of data available for solder joint material using this approach.

### **1.3.1.2. Strain based approaches**

The strain based approach to fatigue modeling is one of the most widely used approaches for predicting the life of solder joints. It is especially useful in the case of low cycle fatigue of solder joint material used in electronic products. The solder goes under controlled shear strain due to the CTE mismatch between the component and board in these applications. Therefore low cycle fatigue could be considered a strain control phenomena. If only plastic strain is considered, the function that correlates the number of cycles to plastic strain is called the Coffin –Manson [Coffin, 1954, Manson 1965] relation and is as follow:

$$\frac{\Delta \varepsilon_p}{2} = \varepsilon'_f (2N_f)^c \quad \text{Equation (1-2)}$$

Where  $\varepsilon'_f$  fatigue ductility coefficient and c is the fatigue ductility exponent. Sometimes the Basquin equation is combined with the Coffin-Manson equation to obtain a generalized fatigue model based on total strain as follows [Kilinski et al, 1991]:

$$\frac{\Delta \varepsilon_t}{2} = \frac{\sigma'_f}{E} (2N_f)^b + \varepsilon'_f (2N_f)^c \quad \text{Equation (1-3)}$$

The Coffin- Manson equation shows good correlation with experiment. However, in real life environment the loading is not always constant amplitude sinusoidal. The total life could be broken into subsets of cycles with different amplitudes, means and frequencies. The coffin-Manson equation was modified to include the effect of frequency and is available in [Coffin, 1973, 1983]

Because there is no practical method to separate plastic shear strain from total shear strain during typical accelerated testing, Engelmaier [Engelmaier, 1983] proposed a new formula based on Coffin- Manson equation using total shear strain rather than plastic shear strain using the following formula:

$$N_f = \frac{1}{2} \left( \frac{\Delta \gamma}{2\varepsilon'_f} \right)^{1/c} \quad \text{Equation (1-4)}$$

Where  $\varepsilon'_f$  is fatigue ductility coefficient,  $N_f$  is mean cycles to failure, and c is fatigue ductility exponent. Fatigue ductility exponent includes both effect of temperature and frequency. A Linear temperature correlation and a logarithmic frequency correlation have seemed to describe the relation best.

Manson and Halford [Manson, and Halford, 1992] were motivated to develop a more sophisticated strain based approach due to various shortcomings of available approaches.

Their model is called strain-range partitioning approach. In this model the total inelastic strain is broken into two parts consisting of plastic and creep strain components. In the case of axial tension and compression loading, the two possible inelastic components allow for a maximum of four permutation in basic cycle types: pp (plastic in tension and compression), cp (creep in tension and plastic in compression), pc (plastic in strain tension and creep in compression), cc(creep in tension and compression). To apply the strain range partitioning method, an interactive damage rule is used that relates the four separate strain range to life relationships.

$$\frac{1}{N_f} = \frac{F_{pp}}{N_{pp}} + \frac{F_{cc}}{N_{cc}} + \frac{F_{cp}}{N_{cp}} + \frac{F_{pc}}{N_{pc}} \quad \text{Equation (1-5)}$$

Where  $N_f$  is predicted cycles to failure for the given complex hysteresis loop,  $N_{ij}$  is cycles to failure for a given partitioned strain range of type ij (pp, cc, pc, or cp), and  $F_{ij}$  is fraction of total inelastic strain range that is actually of type ij. This method has been applied widely for many alloys and often resulted in very good correlation with experimental data. This method also was modified by Solomon [Solomon, 1986] for the cyclic frequency of the load. His frequency dependent model showed that a family of parallel Coffin-Manson fatigue curves should exist, one for each frequency.

### **1.3.1.3. Energy based approaches**

Energy based models are the largest group of fatigue models [Lee et al, 2000]. Cyclic hysteresis energy is believed to be a comprehensive metric of cyclic fatigue damage as it includes both stress and strain hysteresis. Energy based models can be used to predict fatigue failure based on hysteresis loops. These models are divided into two groups; unified and partitioned energy. Several researchers have reported different unified models for solder material. One of the most widely used models is Darvaeux Model [Darvaeux,

1995] which uses the accumulated inelastic strain energy density per thermal cycle and correlate crack initiation time and crack growth to the average energy as follows:

$$N_0 = K_1 (\Delta W_{avg})^{K_2} \quad \text{Equation (1-6)}$$

$$\frac{da}{dN} = K_3 (\Delta W_{avg})^{K_4} \quad \text{Equation (1-7)}$$

Where  $N_0$  is the number of cycles to initiation and  $K_1$ ,  $K_2$ ,  $K_3$ , and  $K_4$  are crack constants.  $\Delta W_{avg}$  is volume-weight average of total inelastic work density accumulated per thermal cycle. For more details about this method please refer to Darveaux et al, 1995.

Another example is Akay's model which was proposed based on total energy [Akay, 1997]1.

$$N_f = \left( \frac{\Delta W_{Total}}{W_0} \right)^{\frac{1}{k}} \quad \text{Equation (1-8)}$$

In which the  $\Delta W_{Total}$  is the total strain energy and  $N_f$  is mean cycles to failure and  $W_0$  and  $K$  are fatigue coefficients.

#### **1.3.1.4. Energy Partitioning damage model**

In this context cyclic creep-fatigue damage under thermal cycling will be modeled using an Energy Partitioning (E-P) model. Inspired the point that plastic and creep deformation result in different types of material damage as seen in various partitioned damage models such as, Strain Range Partitioning [Manson, and Halford, 1992] a mechanism based damage model was proposed by Dasgupta and Oyan [Dasgupta, and Oyan, 1992]. This

model assumes that cyclic fatigue damage is due to a combination of creep deformation mechanisms, plastic deformation mechanisms, and elastic deformation mechanisms. In the context of this paper, the term ‘plastic’ refers to rate-independent inelastic deformation, while ‘creep’ refers to rate-dependent anelastic and inelastic deformations. This model predicts cyclic creep fatigue damage based on deviatoric energy densities:  $U_e$  (elastic),  $W_p$  (plastic), and  $W_c$  (creep) for a typical load cycle. The damage due to each of these deformation mechanisms is determined by using a power law as provided in Equation (2-7) to (2-9)

$$U_e = U_{e0} N_{fe}^b \quad \text{Equation (1-9)}$$

$$W_p = W_{p0} N_{fp}^c \quad \text{Equation (1-10)}$$

$$W_c = W_{c0} N_{fc}^d \quad \text{Equation (1-11)}$$

The total energy is obtained by superposition of these contributions.

$$\text{Total Energy} = U_e + W_p + W_c = U_{e0} N_{fe}^b + W_{p0} N_{fp}^c + W_{c0} N_{fc}^d \quad \text{Equation (1-12)}$$

where  $U_{e0}$ ,  $W_{p0}$ , and  $W_{c0}$  represent the intercept of the elastic plastic and creep energy density plots versus cycles to failure, on a log-log plot; while the exponents b, c, and d are their corresponding slopes. These constants are material properties. The variables  $N_{fe}$ ,  $N_{fp}$ , and  $N_{fc}$  represent the cycles to failure due to elastic, plastic, and creep damage respectively. Subscripts e, p and c refer to elastic, plastic and creep damage, respectively. The total number of cycles to failure  $N_f$  is then calculated from Equation (2-12), by estimating the total cyclic damage as a superposition of the three individual damage mechanisms (elastic, plastic and creep):

$$D_{total} = D_e + D_p + D_c$$

Equation (1-13)

$$1/N_f = 1/N_{fe} + 1/N_{fp} + 1/N_{fc}$$

Equation (1-14)

Where, D is cyclic fatigue damage. The overall procedure for damage estimation using E-P model is shown in Figure 1-20.

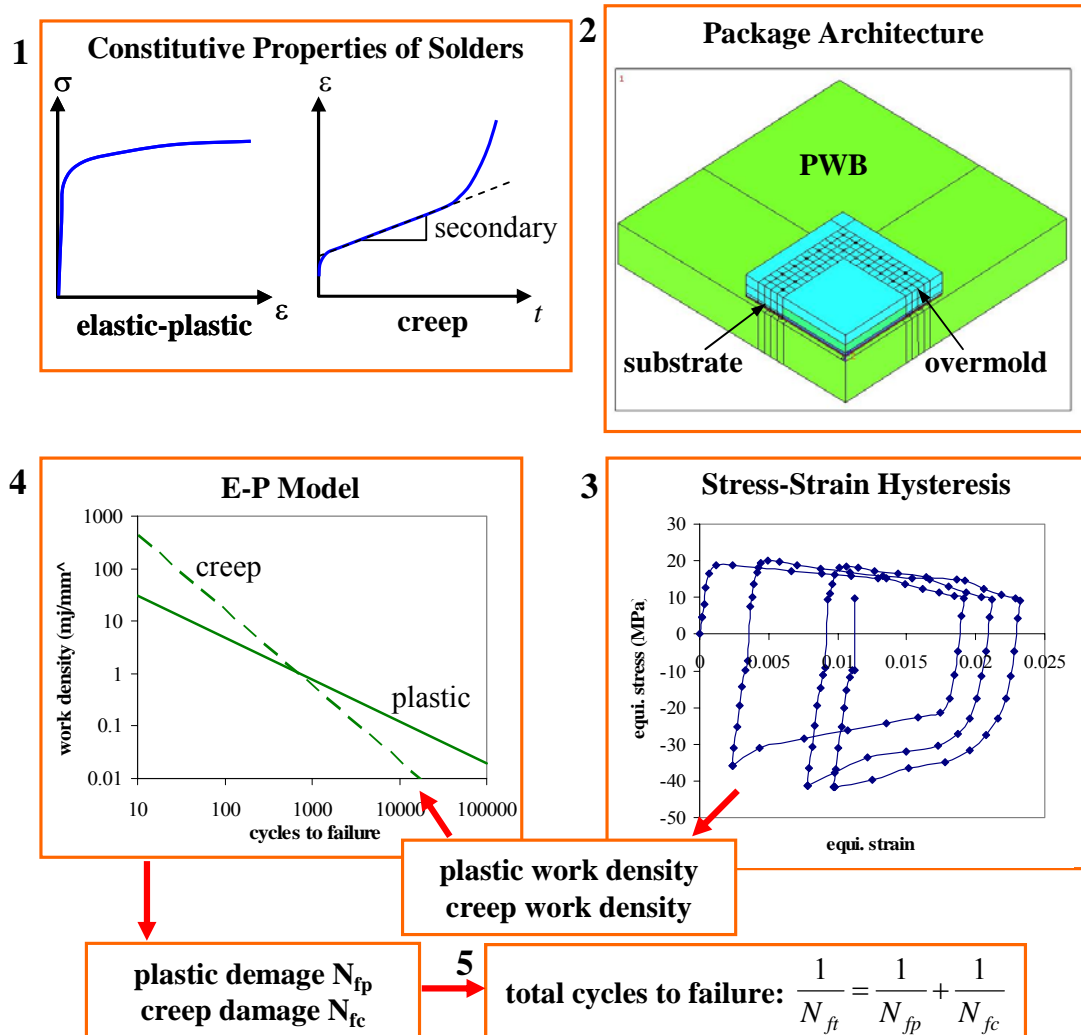


Figure 1-20: Procedure for Energy Partitioning Damage Model

Elastic-plastic and creep constitutive properties of the solder are obtained from literature [Zhang, Dagupta, and Haswell, 2003]. Then the package is modeled on the board under thermal cycling load. Since the test is performed under accelerated condition, modeling is

also conducted for accelerated temperature cycle. The energy work densities are calculated in the solder and averaged over a local neighborhood around the damage initiation site. The plastic and creep work densities then are used obtain the  $N_{fc}$  and  $N_{fp}$  using the fatigue plot in part 4 of Figure 1-20. The total life can be calculated using Equation (2-12)

$$1/N_f = 1/N_{fe} + 1/N_{fp} + 1/N_{fc} \quad \text{Equation (1-14)}$$

Plastic and creep average energy densities are estimated by cycling the model until a stable hysteresis loop is obtained. This usually occurs by the third cycle in most configurations. In this method, damage caused during initiation and during propagation has usually not been considered separately.

#### **1.4. Damage evolution caused by cyclic loading in solders**

When the solder undergoes cyclic loading the microstructure of the solder evolves in different ways. One of the changes in microstructure is solder coarsening. It is seen in the literature [Dutta, 2003], [Ubachs et al., 2004] that Sn-Pb and Pb-free solders undergo significant coarsening during thermo-mechanical cycling. Figure 1-21 shows an example of coarsening due to thermal cycling in lead free solders. Cycling also deteriorates material due to damage accumulation which causes material softening. As seen in Figure 1-22, as number of mechanical or thermo-mechanical cycles increase the solder material load bearing capacity decrease [Zhang, 2004].

The material damage is caused by the presence of micro-cracks/voids which initiate, coalesce and grow. As solder undergoes cycling either thermo-mechanical or isothermal mechanical, plastic and creep deformation occur. The mechanisms of inelastic (creep and

plastic) deformations are different in different solder material. Plastic mechanism in Sn-Pb solders is dislocation slide. Creep mechanism in Sn-Pb solder is mostly diffusion, grain boundary sliding and void nucleation and growth [Sharma, 2000]. However, inelastic deformation both plastic and creep are mostly caused by dislocation motion and diffusion in SAC solders. Grain boundary sliding is not a common mechanism for creep in Pb-free solders due to presence of intermetallic particles between the grains that pin the grain and prevent sliding. Dislocation slide is a fairly fast process thus mechanism for plastic deformation. As soon as the dislocations hit an obstacle the dislocation is stuck and need a lot of energy to climb the obstacle. The dislocations keep piling up behind the obstacle. This causes a compressive field around the dislocation and causes the dislocation to climb around the obstacle. Dislocation climb is a relatively slower process with respect to dislocation slide and needs lots of energy and thus mechanism for creep deformation. As the dislocations reach the grain boundaries and pile up at the boundaries, the energy of the dislocations increases as much as to overcome Gibbs free surface energy and then causing micro-crack to initiate. Another mechanism in creep deformation of SAC solders is diffusion that is movement of material from one point to another point. Diffusion is a time dependent phenomena and thus a mechanism for creep.

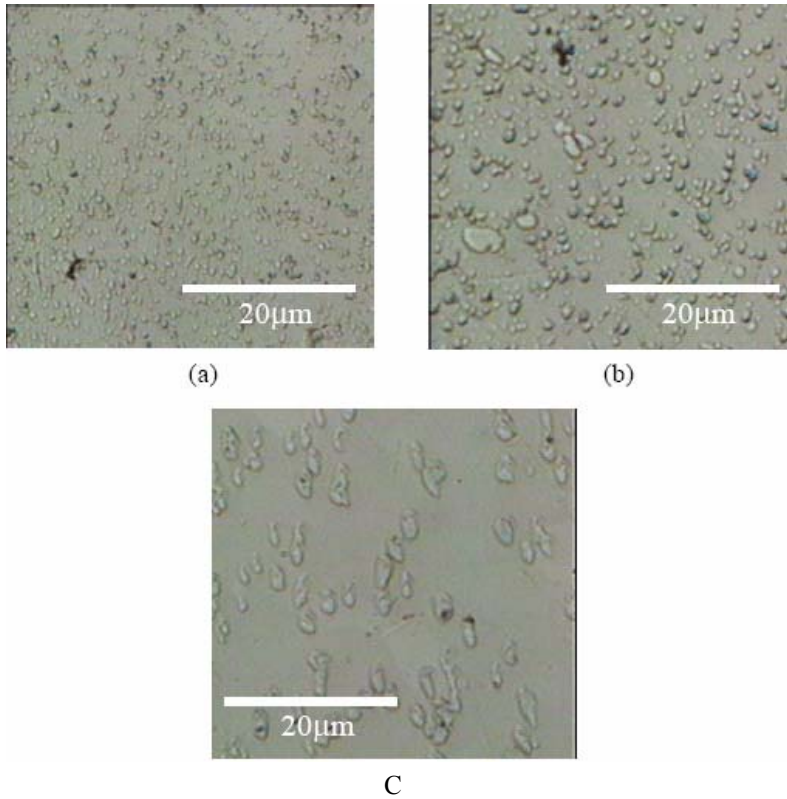


Figure 1-21: Microstructure of flip chip joint of Sn4.7Ag1.7Cu as reflowed condition (a) and after 200 and 1200 Thermal cycles (b and c respectively) [Datta, 2003].

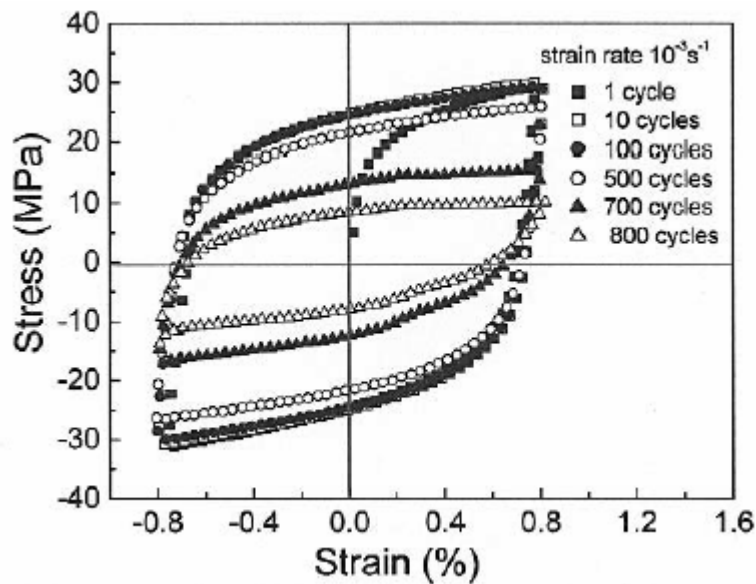


Figure 1-22: Hysteresis loop of Pb-free solder alloys at strain amplitude of 0.8% [Qiu, 2005]

The accumulation of damage is manifested as reduction in the effective load bearing area of the material, causing eventually micro crack initiation and failure.

Suppose we have a piece of undamaged material. When the material undergoes cycling it degrades and load bearing area decreases. If we keep the stress constant, due to decrease in area, true stress increases locally which causes the material to deform more as shown in Figure 1-23. But this is not what happens in most electronic applications. Electronic applications are mostly strain controlled. Thus in most experiments the strain is kept constant and the stress is measured. In strain controlled environment, due to softening happened during cycling loading the load or stress drops as shown in Figure 1-24.

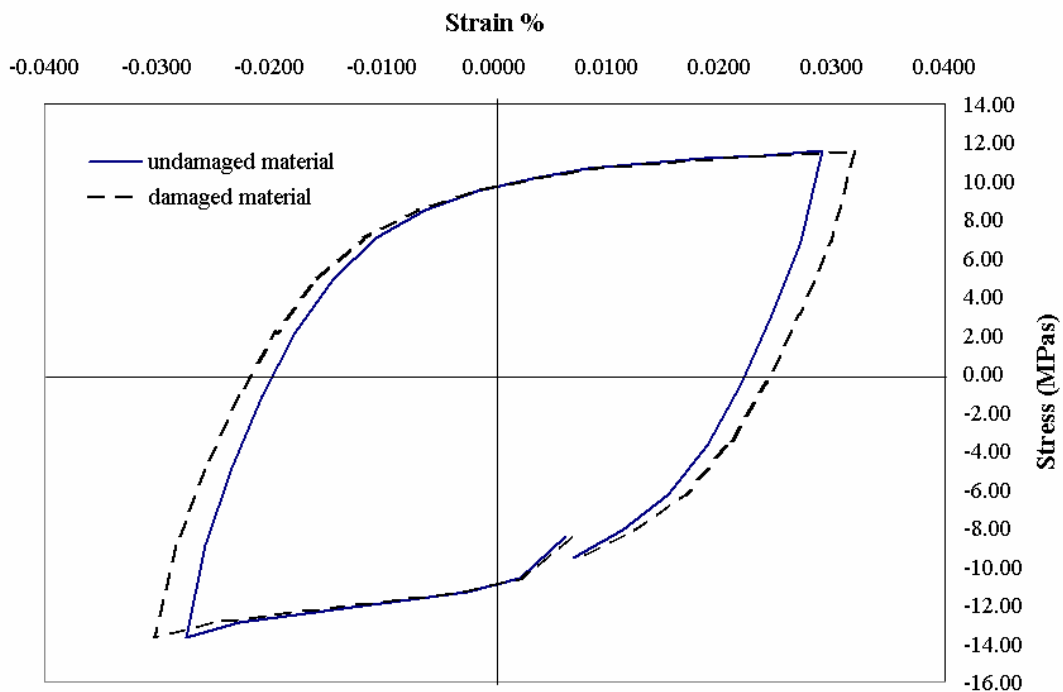


Figure 1-23: comparison of stress-strain hysteresis loop for damaged and undamaged material under constant stress

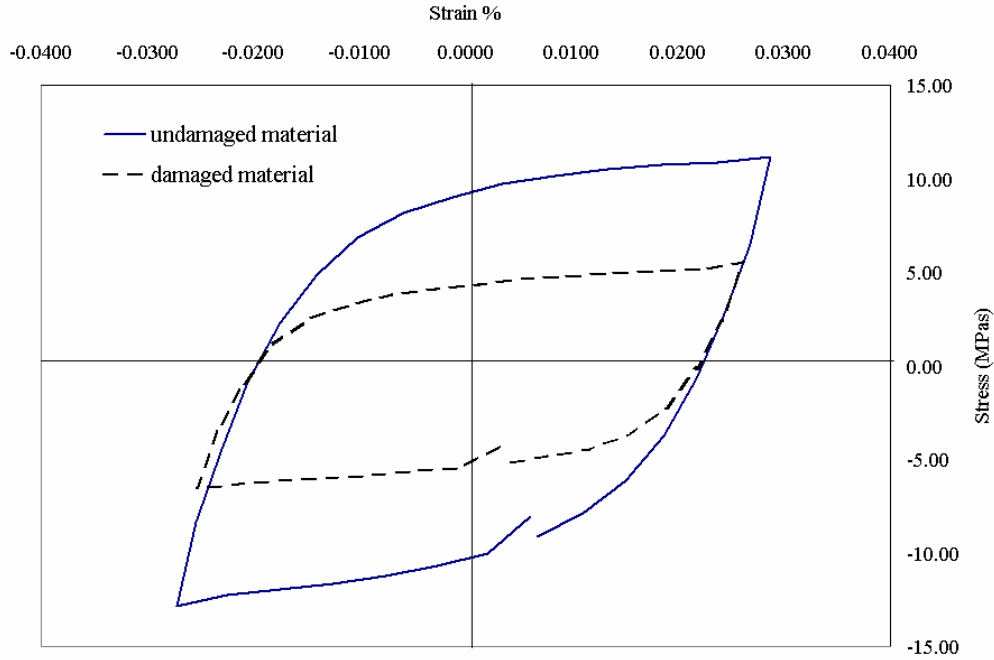


Figure 1-24: Comparison of stress-strain hysteresis loop for damaged and undamaged material under constant strain

Kachanov 40[Kachanov, 1986] introduced the concept of actual stress and its relation to damage and nominal stress. Let  $A_0$  be the initial area of undamaged section. As a result of damage a certain part of the section is lost. If we denote the lost area by  $A$ , the area left is  $A_0 - A$ . we assume that we have isotropic damage, in which the cracks and voids are equally distributed in all directions. Then the damage variable is considered as a scalar and defined as:

$$D = \frac{A}{A_0} \quad \text{Equation (1-15)}$$

$D$  is a positive monotonically increasing function. Kachanov introduced a field variable  $\psi$ , called continuity [Kachanov, 1986], 5 which is considered by many as the starting point of continuum damage mechanics (CDM). Over the years  $D = (1-\psi)$  has become accepted as damage representative for the material.  $D = 0$  identifies the

undamaged state and  $D = 1$  is used to identify total failure. None of these two states happen in reality. Most materials and structures have initial micro-cracks and flaws and they always fail before  $D$  even reaches 1. If we assume that  $\sigma$  is the stress related to the undamaged material or nominal stress, then actual stress is obtained through the following equation:

$$\sigma_a = \frac{P}{(A_0 - A)} = \frac{P}{A_0(1 - D)} = \frac{P}{A_0\psi} = \frac{\sigma}{\psi} \quad \text{Equation (1-16)}$$

$$\psi = 1 - D \quad \text{Equation (1-17)}$$

So the stress-strain behavior of the damaged material can be represented by the constitutive equation of the undamaged material with the stress in it replaced by the actual stress. Several investigations were carried out to examine the effect of damage on the behavior of solder alloys.

#### **1.4.1. Literature review for Pb-free solder materials**

Wen and Keer investigated the change in constitutive properties of Pb-free solders using unified creep plasticity (UCP) approach [Wen et al., 2001]91. They used McDowell's [McDowell, 1992] equation in which the thermodynamic restrictions have been verified. Their damage model is based on Mura and Nakasone [Mura and Nakasone, 1990] dislocation model for fatigue under cyclic loading. The issue with their damage model is that it is based on dislocation motion and only applicable for plastic deformation. In reality, damage caused by creep deformation is not negligible due to very low melting temperature of solder and high amount of creep deformation. So damage cannot be merely modeled based on change in dislocation density and crack initiation due to dislocation pile up. This issue is very well represented in Sn-Pb solder where Sharma and

Dasgupta [Sharma and Dasgupta, 2002]<sup>78</sup> investigated creep fatigue damage in solders due to thermal cycling using a micro-macro stress transition model. They considered cyclic softening, grain coarsening and void nucleation and growth.

Basaran and Yan [Basaran and Yan, 1998] proposed a thermodynamic approach to investigate damage evolution due to cycling for SnPb solder materials.

Chaw, Lau, Vianco and Fang [Chaw et al., 2004] investigated behavior and damage evolution in Lead-free solders under thermo-mechanical loading. They defined two damage scalars called  $D$  and  $\mu$  and damage state variable called  $c$ . There were two issues that prevent this study to use their approach. First they used a unified damage model which is not used in our study. Second the study was verified for very limited range of strain and strain rates. Huang, et al, [Huang et al., 1992], studied damage evolution for Sn-Pb solders. Their approach also is only dislocation motion based mechanism and does not include creep. In addition their study was conducted for Sn-Pb solders and thus their constants cannot be used for Pb-free solders. Erinc, et al [Enric et al., 2004] , investigated the micro structural evolution using a nano-indentation technique. He developed a model to predict damage initiation and propagation using interfacial de-bonding models. In their approach degradation through the cycling process is accounted by an interfacial damage evolution.

#### **1.4.2. Gaps in the literature**

In order to accurately predict the life of joints in the package, the degradation of material also has to be considered in modeling especially when a successive process is used. Due to the following reasons the approaches proposed in literature and mentioned in literature review section is not applicable to this study:

- The approach was proposed for Sn-Pb solders and constants derived not applicable for Pb-free solders such as Basaran and Huang approaches.
- The approach only modeled dislocation motion and thus only modeled damage caused by plastic deformation such as micro-mechanic approach used by Keer et al, and Huang, et al.
- The approach was not a mechanistic approach, was for a very limited strain range and rate, or it was coupled in a unified damage model such as keer, et al., Chaw, et al., and Ernic et al.

There is still need for a simple experimental approach that is convenient and can be used for broader range of applications.

An experimental approach is proposed here to estimate the degradation in material and change in constitutive properties of solder due to thermo- mechanical cycling. An Energy Partitioning Damage Evolution Method (EPDE) is proposed to be coupled into energy partitioning damage model and predict the material degradation using plastic and creep work densities dissipated in the first few cycles of cyclic loading. Next section explains this method in more details.

### **1.5.Scope and overview of approach**

There are two major objectives in this dissertation: first is to investigate the effect of voids on thermo-mechanical durability and second is to assess the influence of cyclic loading on damage evolution and softening of Pb-free solder material. The approach is shown in Figure 1-25. the first step in the process is to fabricate voided specimens. Next chapter provides the detail of experiments conducted to fabricate voided specimens,

characterize specimens for void and to qualitatively evaluate the effect of voids on thermo-mechanical durability.

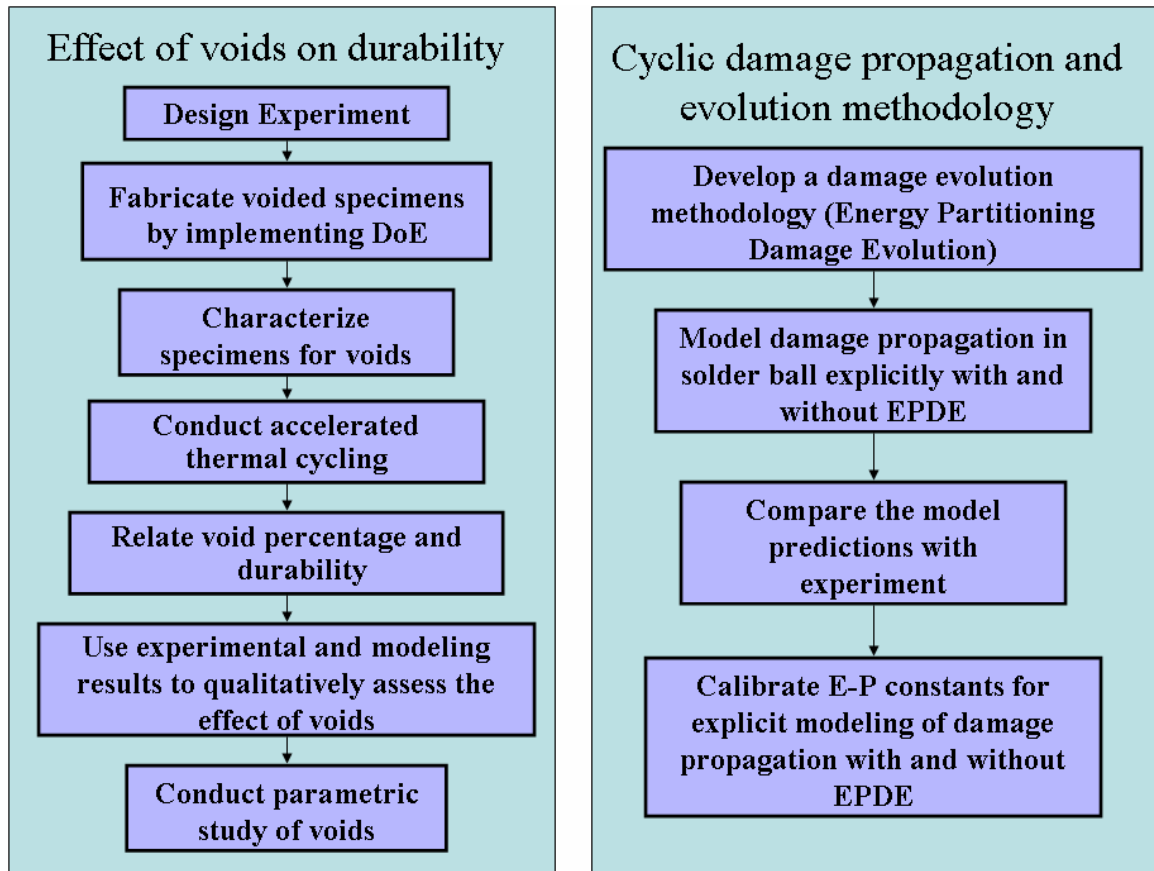


Figure 1-25: Approach used to investigate the effect of voids as well as cyclic softening and damage evolution

## **2. Thermo-mechanical durability experiments**

This chapter provides detail information about the experiments conducted and to fabricate voided specimens and to evaluate the effect of voids on durability.

Two different experiments were conducted; which are called Study 1 and Study 2. Study one was conducted and the results were analyzed by the author. The durability test for Study 2 was conducted by Osterman et al. [Osterman et al., 2006]. Author only conducted the failure analysis and evaluation of the results. The following sections explain these two sets of experiment and discuss the result of these experiments.

### **2.1.Study 1**

DOE experiment was designed to systematically vary the reflow and printing process variables, in order to fabricate voided specimens. The voided samples were then inspected visually and with x-ray, to identify different types of defects, especially voids, and tested for electrical performance. The specimens were subjected to accelerated thermal cycling test to characterize the durability of specimens and to study the effect of each manufacturing variable on the durability of solder joints. The response variable for the design of experiments is void percentage and thermal cycling durability of the solder joints.

#### **2.1.1. Background and introduction**

Manufacturing defects can affect the in-service durability of miniature components that are becoming increasingly popular because of the demand for small hand-held products such as cell phones, personal organizers, and other smaller devices. The majority of defects in the process of SMT electronics assembly is introduced during the reflow and printing processes. Studies have shown that about 60% of defects identified

after reflow originated during the solder paste printing process [Nguty et al., 2001]. Voids are one type of defects that form during manufacturing process.

Voids are one of the major categories of manufacturing defects in solder joints of electronic assemblies. They can potentially degrade the reliability of interconnects. Process-induced voids can be considered to be a quality issue, and many researchers have addressed the potential of these large voids to reduce interconnect reliability. However the effect of voids is not fully understood and requires future studies.

The issue of voids intensifies with the introduction of Pb-free solders. Pb-free solders are more prone to voids due to less wettability, increased level of flux and higher reflow temperature [Lee, 2002, Huang et al., 2004, Harrison et al, 2001, Li et al., 2001, Dasgupta et al, 2004]. The level of flux is increased to prevent oxidation due to higher reflow temperature. Higher reflow temperature also increases out-gassing of laminates [Lee, 2002].

Many variables affect the void formation in solder joints. Some of these variables have been investigated in the past. Nurmi et al [Nurmi, 2003] studied the effect of multiple reflow cycles on solder joint voids for Pb-free BGAs. Their study showed that longer time in molten state caused bigger voids. The percentage of voids also increased as the number of reflow cycles increased. Other researchers have also investigated the effect of manufacturing variables on void formation in Pb-free solder joints such as Melton [Melton et al., 1993], Maattanen et al [Maattanen et al., 2001], Jackson et al [Jackson et al., 2002], Li et al [Li et al., 2001], and Ryan et al [Ryan et al., 2004]. All the researchers mentioned above show sensitivity of void formation during manufacturing process of joints to reflow and printing variables. The shortcomings of most of these

studies are that in most cases the process variables are considered to have linear effect on durability, and hence only two-level experiments have been designed and conducted [Ryan et al., 2004] for factorial effect analysis. In some cases the result are conflicting [Harrison et al., 2001] and [Li et al., 2001] and some variables have not been investigated at all. A comprehensive matrix of variables and a 3-level DoE is proposed in this study, to systematically explore the nonlinear effects of selected process variables on void formation thermal cycling durability.

### **2.1.2. Design of Experiment**

As explained in chapter 1, many factors in the printing and reflow processes affect the void formation in solder joints. Many of these factors are shown in the fishbone diagram shown in Figure 2-1. Studying all of these variables requires a huge test matrix, especially when the nonlinearities in the response necessitate more than 2 levels for each variable. Due to limitations in resources, a total of 6 variables (2 from print process and 4 from reflow process) have been selected in this study. The variables chosen in the print process include: stencil thickness ( $\delta$ ) and waiting time ( $t_p$ ). The reflow process in this specific application uses a Ramp-to-Spike profile (Figure 2-2) and the variables chosen in the reflow process include: heating ramp rate ( $\alpha_h$ ), peak temperature ( $T_p$ ), time above melt temperature ( $t_m$ ) and cooling ramp rate ( $\alpha_c$ ) ( refer to table Table 2-2). Responses are considered to be nonlinear, except for stencil thickness, since the paste volume is expected to be a linear function of stencil thickness. Therefore the stencil thickness is studied at two levels, while all other variables are studied at three levels.

Since the test matrix for a conventional factorial or fractional factorial DoE is very large for such a study, a Taguchi orthogonal array [Taguchi, 1993] is selected. Taguchi

arrays allow the use of smaller test matrices, but the penalty is that obtaining interaction effects is very difficult, because many of the interaction effects are confounded into main factor effects and cannot be separated.

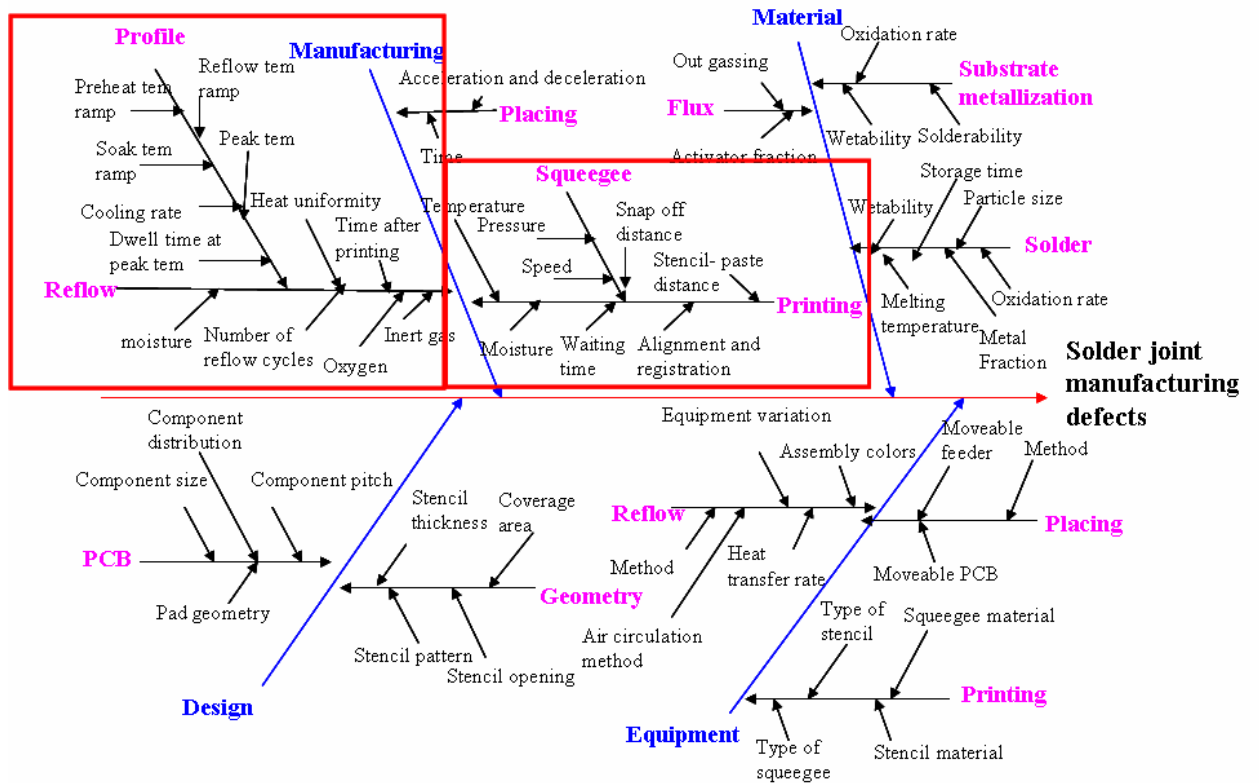


Figure 2-1: Fishbone diagram of variables affecting the solder interconnects quality and reliability

A mixed L18 orthogonal array, which can handle one two-level variable (variable A) and up to 7 three-level variables (variables B to H), is selected. The L18 test matrix is shown in Table 2-1. The first column in Table 2-1 shows the run number and the DoE variables are placed in the subsequent columns. “1” refers to the “low” level of each variable, “2” represents the “intermediate” or “nominal” level and “3” refers to the “high” level. The only interaction effect that can be identified correctly in this L18 array is that between variables A and B. Based on the terminology presented here, variable A

represents stencil thickness and variable B represents the waiting time during printing. Thus, their interaction effect can also be assessed. The variables and levels for each variable are shown in Table 2-2. The response variables in this study are thermal-cycling durability under the accelerated test condition which will be discussed in the next section and void area percentage.

Table 2-1: DOE matrix, L18 [Taguchi, 1993]

Column Run #	A	B	C	D	E	F	G	H
1	1	1	1	1	1	1	1	1
2	1	1	2	2	2	2	2	2
3	1	1	3	3	3	3	3	3
4	1	2	1	1	2	2	3	3
5	1	2	2	2	3	3	1	1
6	1	2	3	3	1	1	2	2
7	1	3	1	2	1	3	2	3
8	1	3	2	3	2	1	3	1
9	1	3	3	1	3	2	1	2
10	2	1	1	3	3	2	2	1
11	2	1	2	1	1	3	3	2
12	2	1	3	2	2	1	1	3
13	2	2	1	2	3	1	3	2
14	2	2	2	3	1	2	1	3
15	2	2	3	1	2	3	2	1
16	2	3	1	3	2	3	1	2
17	2	3	2	1	3	1	2	3
18	2	3	3	2	1	2	3	1

Table 2-2: Variable and levels of variables selected for this study

Process	Variable	Sign	Variation	Levels	Minimum level (1)	Nominal level (2)	Maximum level (3)
Print	Stencil Thickness ( $\delta$ )	A	Linear	2	4mils		5mils
	Waiting time after print ( $t_p$ )	B	Non linear	3	8h	36h	72h
Reflow	Heating ramp ( $\alpha_h$ )	C	Non linear	3	0.8°C/sec	0.9°C/sec	1.0°C/sec
	Peak temperature ( $T_p$ )	D	Non linear	3	235	245	255
	Time above melt tem ( $t_d$ )	E	Non linear	3	30 sec	40 sec	50 sec
	Cooling rate ( $\alpha_c$ )	F	Non linear	3	-3°C/sec	-4°C/sec	-5°C/sec

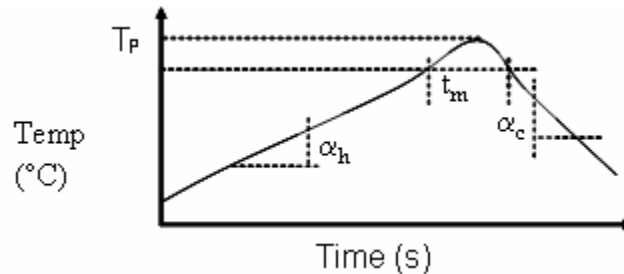


Figure 2-2: Typical Ramp-to-Spike profile

### 2.1.3. Specimen design

Miniature components are used in cell-phones and other hand held electronic products. The size of boards and component is shrinking everyday and manufacturers of cell-phone are using components with pitch size smaller than 0.5 mm. Since this study is conducted for small electronic products, the specimen was designed to represent this group of products. An 8 layer board with size of 132mm to 77mm and thickness of 1mm was designed based on JEDEC standard for drop testing [JESD22-B111]. The standard represents the test board construction, dimensions and material that is representative of those used in hand held electronic products. Table 2-3 provides the thickness, copper coverage and material for each layer. The surface finish for PCB is Organic Solderability Preservatives (OSP) to avoid any surface oxidation before component mounting.

Different kinds of components were used to represent various geometries. Components are selected based on their availability for lead free solders as well as dimension and size and price. Three different components were selected for this study. CTBGA 132, which is a partially arrayed BGA with 132 balls that are arranged in 3 rows around the component, was selected. This component size is 8mm\* 8 mm and has a silicon die inside. The balls are daisy chained and all the balls are in one net. The ball view daisy chain map for this component is provided in Figure 2-3. The ball pitch is 0.5 mm. A schematic picture of CTBAG is shown in Figure 2-4. Two more components also were selected: MLF and ceramic chip resistors (LCR)(1210), components. The MLF size is 10mm \*10mm and has 68 leads and pitch of 0.5 mm (Figure 2-5).

Table 2-3: Test board stack up and material [JESD22-B111]

<b>Board layer</b>	<b>Thickness (microns)</b>	<b>Copper coverage (%)</b>	<b>Material</b>
Solder mask	20		LPI
Layer 1	35	Pads + traces	Copper
Dielectric1-2	65		RCC
Layer 2	35	40% including daisy chain links	Copper
Dielectric 2-3	130		FR4
Layer 3	18	70%	Copper
Dielectric 3-4	130		FR4
Layer 4	18	70%	Copper
Dielectric 4-5	130		FR4
Layer 5	18	70%	Copper
Dielectric 5-6	130		FR4
Layer 6	18	70%	Copper
Dielectric 6-7	130		FR4
Layer 7	35	40%	Copper
Dielectric 7-8	65		RCC
Layer 8	35	Pads + traces + daisy chain links	Copper
Solder mask	20		LPI

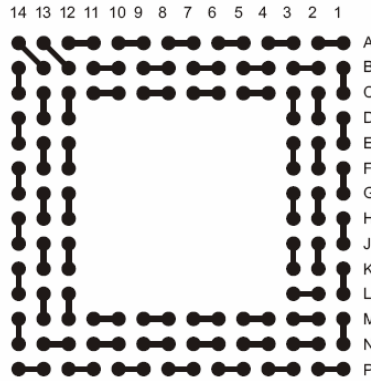


Figure 2-3: ball view daisy chain map for CTBGA 132

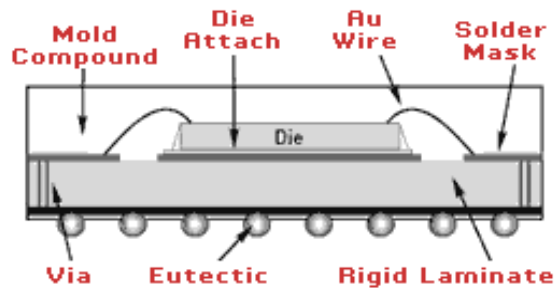


Figure 2-4: Schematic picture of BGA

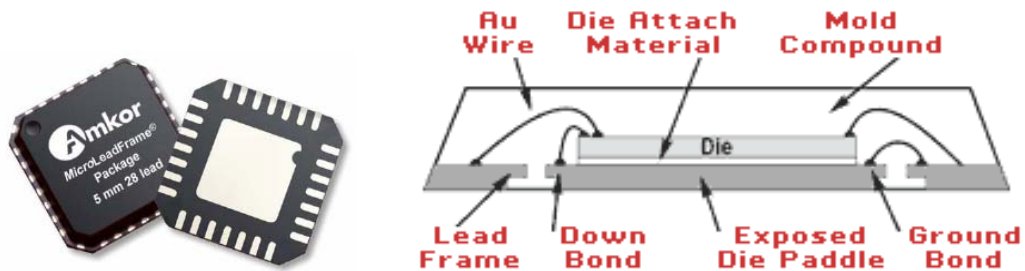


Figure 2-5: Schematic picture of MLF component

The components are mounted on the boards using a lead free paste. There are 6 CTBGAs, 6 MLFs and 18 LCRs on the board. All the components are daisy chained and are monitored during the test. All the balls in the CTBGA are in a single net, but test points are added at the corners so that the resistance of each two ball at the corner can be measured manually after failure. Adding test points at the corner makes it possible to measure the resistance of balls at the outer row at each side and it facilitates failure site

detection. The same strategy is used for MLFs and all leads were put in one net. Every 6th resistors are placed in one net. Manual test points are added between the chip resistors so that resistance of each chip can be measured manually. The thermal test board is configured for singulation of each MLF & CTBGA, for immediate removal & physical analysis of each failed component. The board specimens are shown in Figure 2-6.

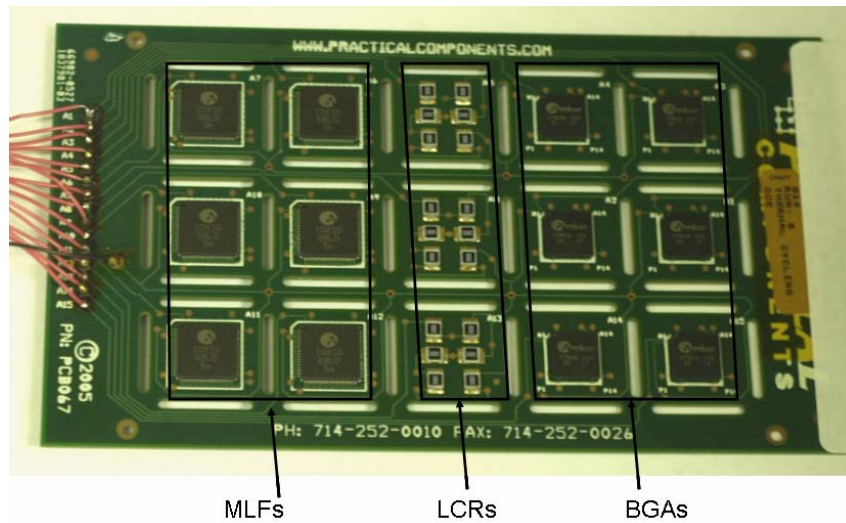


Figure 2-6: Specimen used in accelerated temperature cycle loading

#### 2.1.4. Void Analysis

To evaluate the void area percentage in specimens fabricated under different DoE runs, 2-D Xray analysis was conducted for the BGA specimens using MicroRTB X-ray imaging system. An internal BGA module was used in the Xray instrument to calculate void percentage for solder balls. One example of x-ray pictures and void calculation is shown in Figure 2-7. The void percentage was averaged over all the components on PWA in each specific DOE run.

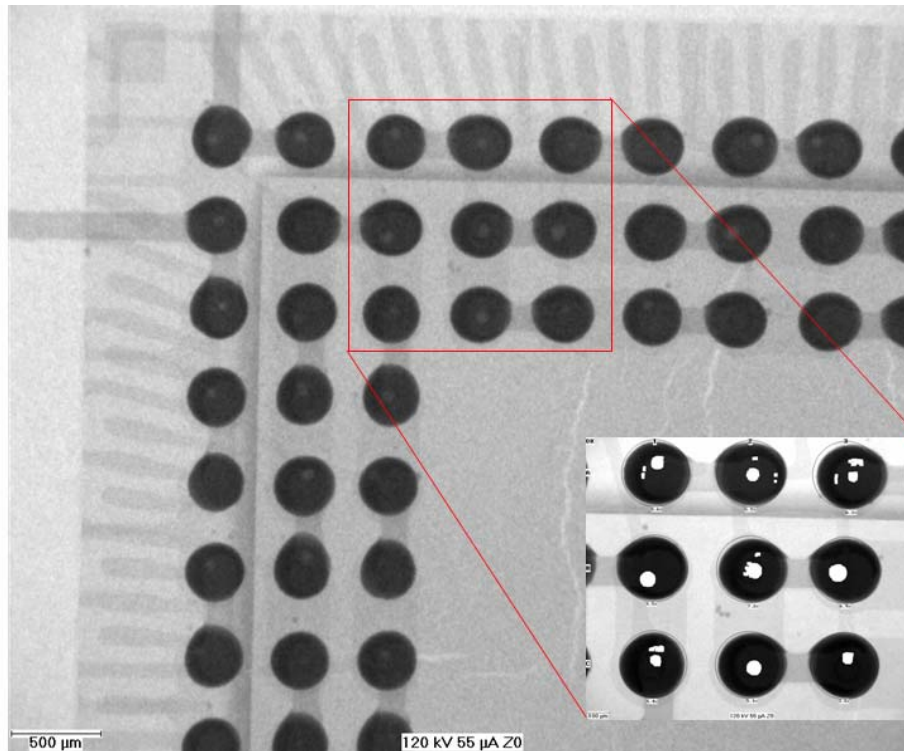


Figure 2-7: X-ray analysis of voids

Table 2-4: Void percentage averaged for BGA specimens observed in different DoE runs

Run Number	Void area percentage
1	0.47
2	0.5
3	2.5
4	1.4
5	1.39
6	1.02
7	1.09
8	1.22
9	0.78
10	2.8
11	0.4
12	0.73
13	2.1
14	2.08
15	1.2
16	1.8
17	1.8
18	0.57

### 2.1.5. Statistical analysis of voids as response variable

X-ray analysis was conducted to study the effect of reflow and printing variables on the creation of voids. Using commercial software the factor effects for different variables is plotted for average of voids percentage area as response variable. The result for significant factors are shown in Figure 2-8. Analysis of the results shows higher percentage of voids for higher stencil thickness. This is due to higher volume of solder and therefore higher flux content. This analysis also shows that void percentage increases as peak temperature ( $T_p$ ) and time above melt temperature ( $t_m$ ) increases which confirms the study conducted by Nurmi et al [Nurmi et al., 2003]. This can be rationalized by the fact that higher temperature can cause faster volatilization of flux. Furthermore, longer time above melt can cause void due to re-oxidation. cooling rate does not have a strong effect of void creation. The other two factors, waiting time and heating ramp have no significant effect of void generation.

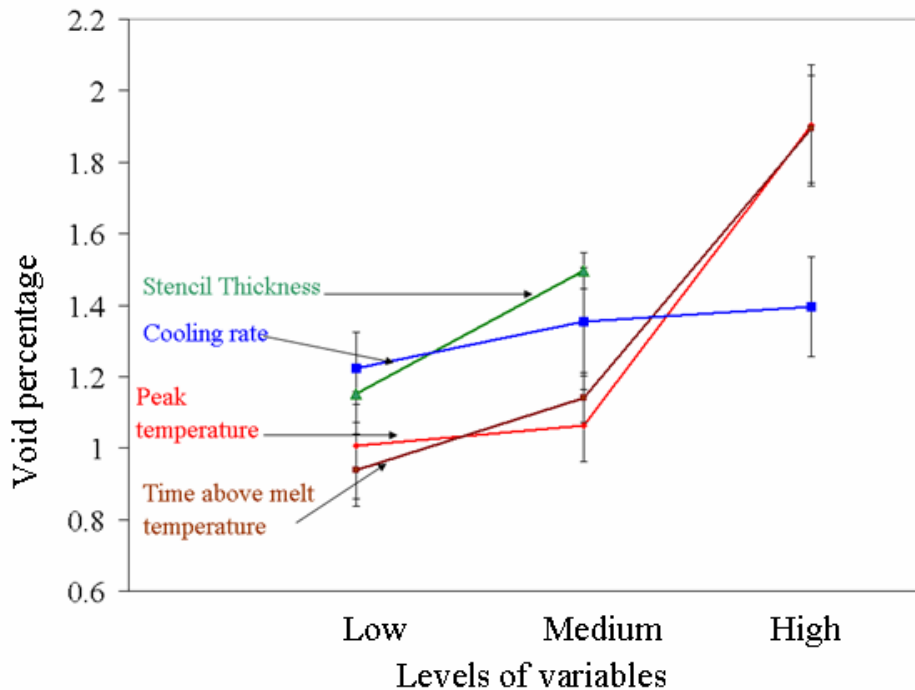


Figure 2-8: Factor effect analysis for void as response variable

### 2.1.6. Test design

After characterizing the specimens for voids, the specimens are tested for durability to correlate the effect of voids to durability. The thermo-mechanical testing is conducted using a thermal chamber. All the channels on the boards were connected through soldered wires to a data logger which monitored the resistance of each channel. Several thermocouples were mounted on several boards inside the chamber and connected to data logger to monitor the temperature inside the chamber.

Since the modeling was done for a temperature profile illustrated in chapter 2, the chamber was also programmed to follow the same temperature profile. The chamber then was characterized to assure the accuracy of the profile. Characterization curve is shown in Figure 2-9.

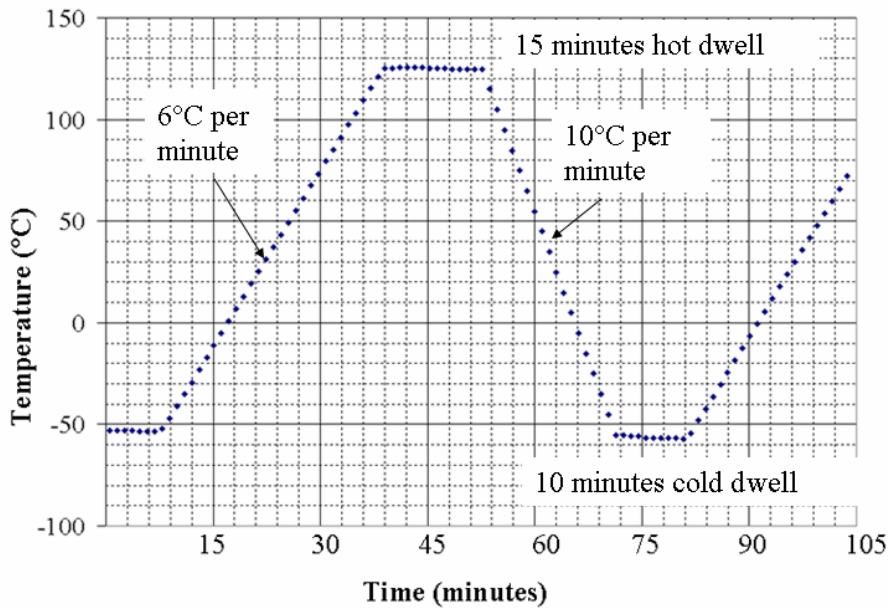


Figure 2-9: Chamber characterization; temperature profile observed on boards

Data acquisition system shows resistance of  $300\Omega$  in regular condition when the channel is connected. If there is disconnect in the channel the resistance shows a sudden increase, “spike”. The spike is usually in magnitude of thousands. Monitoring the

resistance of channels for BGAs shows that resistance increases gradually as the BGA starts to develop damage and fail. After BGA fails, the resistance shows spikes when the crack opens, during bending of board due to temperature cycle. The specimens are considered failed when the electrical resistance measured by data acquisition system spikes, through 10 successive cycles. A typical example of BGA resistance when close to failure is shown in Figure 2-10.

The failure shows up differently in MLFs and LCRs. There is no gradual increase in resistance for these components. The resistance only shows spike in failure.

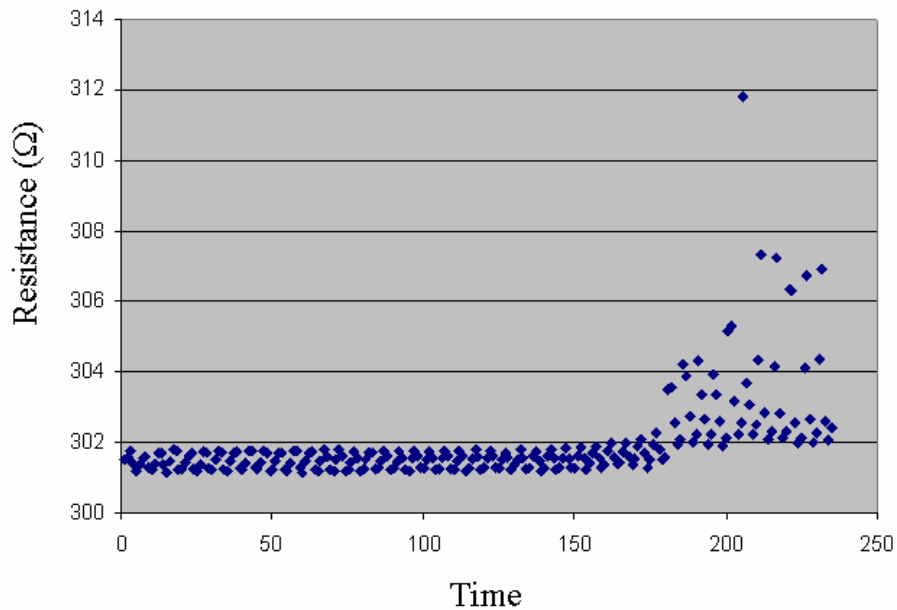


Figure 2-10: Typical example of BGA resistance during thermal cycling test

### 2.1.7. Accelerated thermal cycling test results

Accelerated thermal cycling test was conducted and the cycles to failure were recorded. The specimens are considered to have failed when the electrical resistance measured by the data acquisition system shows a sudden increase, “spike”, (several orders of magnitude relative to initial resistance) consistently through 10 successive

cycles. Result of durability averaged over BGAs on each board for different runs are provided in

Table 2-5: Durability averaged over BGAs of each board for different DoE runs

Run #	Thermo-mechanical durability
1	315
2	555
3	1264
4	728
5	745
6	436
7	568
8	587
9	639
10	328
11	527
12	463
13	713
14	474
15	622
16	503
17	720
18	637

Weibull distributions were fit to the failure data using commercial software. Failures were found to have two distinct Weibull slopes ( $\beta$ ) and were accordingly divided into two populations: premature failure sub-population and main population of failures using a competing failure mode analysis. Further analysis of the failed specimen which is discussed in the later section showed that early failures occurred due to insufficient intermetallic formation and wetting. Further discussions are provided in Appendix II for CTBGA and MLF. The premature population was eliminated from the data to avoid other drivers of failures than voids. The analysis then was conducted for main population of failures. Three-parameter (3-P) Weibull analysis was used to analyze the main failure

populations. The 3-P Weibull plots for the CTBGA are provided in Figure 2-11. A summary of the Weibull parameters and correlation coefficients is provided in Table 2-6,

Table 2-6: Summary of the Weibull parameters for CTBGAs

	$\eta$	$\beta$	$\gamma$	$\rho$
CTBGA 2-P	683	3.51		0.92
CTBGA 3-P	348	1.215	302	0.99

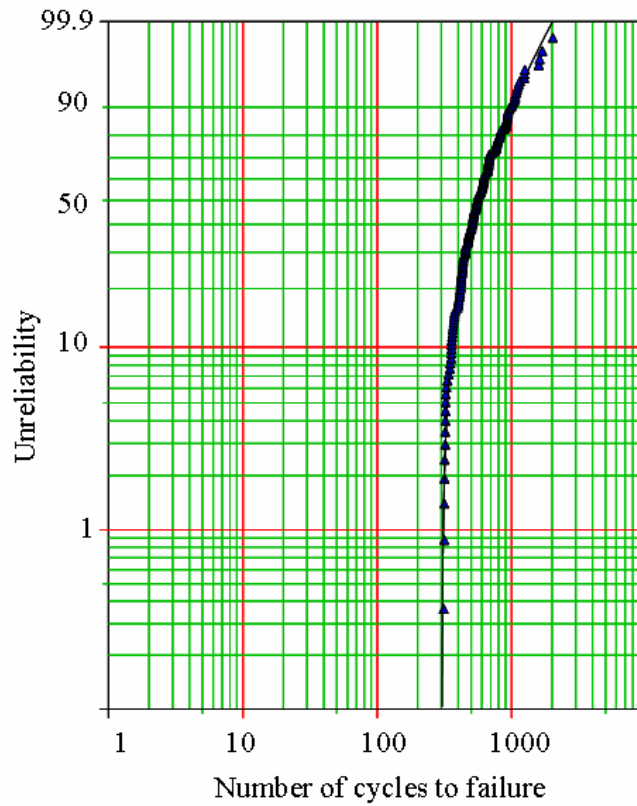


Figure 2-11: 3-P Weibull plots for main population of failures of CTBGAs

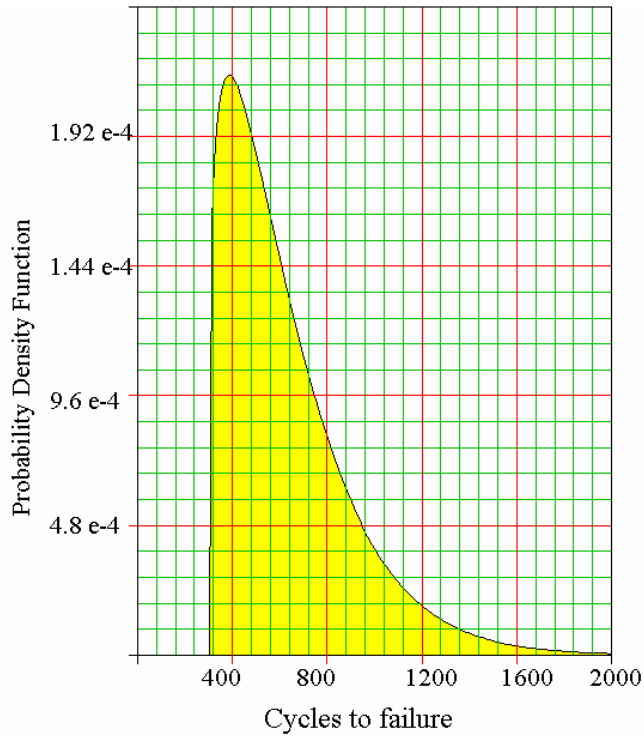


Figure 2-12: Probability density function for main population of failures for CTBGA

### 2.1.8. Micro-structural failure analysis

Most BGAs located on the PWBs that were assembled at the lowest levels of the DOE variables (A1 PWAs) experienced premature failures. Failure analysis of A1 PWAs showed that the cracking mostly occurred between the solder and PWA intermetallic. The failure analysis in Figure 2-13 clearly shows that A1 samples did not have enough time for the solder to melt and create sufficient interfacial intermetallic for a reliable joint.

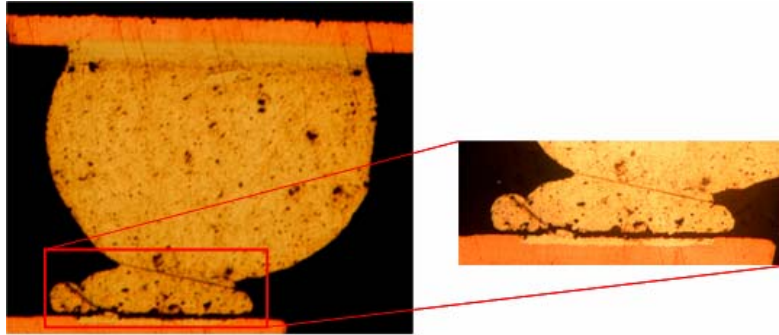


Figure 2-13: Crack in intermetallic due to insufficient intermetallic formation in board A1  
Failure analysis of the specimens reflowed under higher level of peak temperature and time above melt point shows that damage path moves from intermetallic to bulk of the solder for main population of failures. One example is shown in Figure 2-14. One sample selected from the board that was selected from highest levels of variables show that crack has moved to the top of the joint. This is shown in Figure 2-15.

It is observed that other types of defect are coexisting with voids. The impact of other types of defects, such as insufficient intermetallic formation and wetting, seem to be higher relative to voids. To eliminate the impact of other types of defects the early failures were eliminated from the population and statistical analysis was conducted for main population of failures and presented in the next section.



Figure 2-14: Damage moved to the bulk of the solder in main population

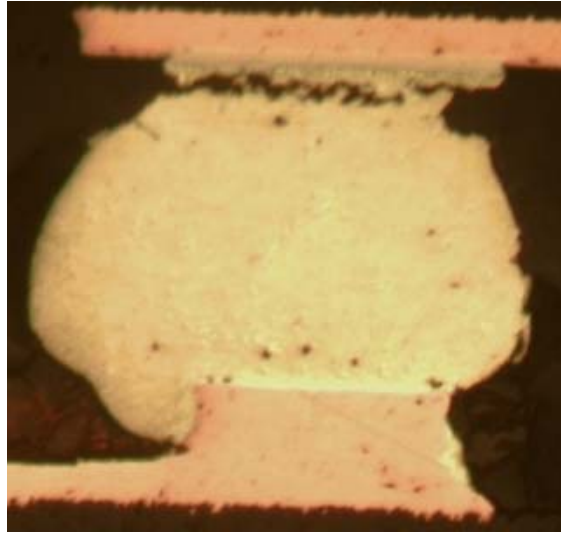


Figure 2-15: Damage moved to the component side for the most durable specimens

### 2.1.9. Statistical analysis of durability as response variable

Commercial software was used to calculate the factor effects for durability as response variable. The factor effect diagram showing the main factor effect for different process variables for the CTBGA component are presented in Figure 2-16.

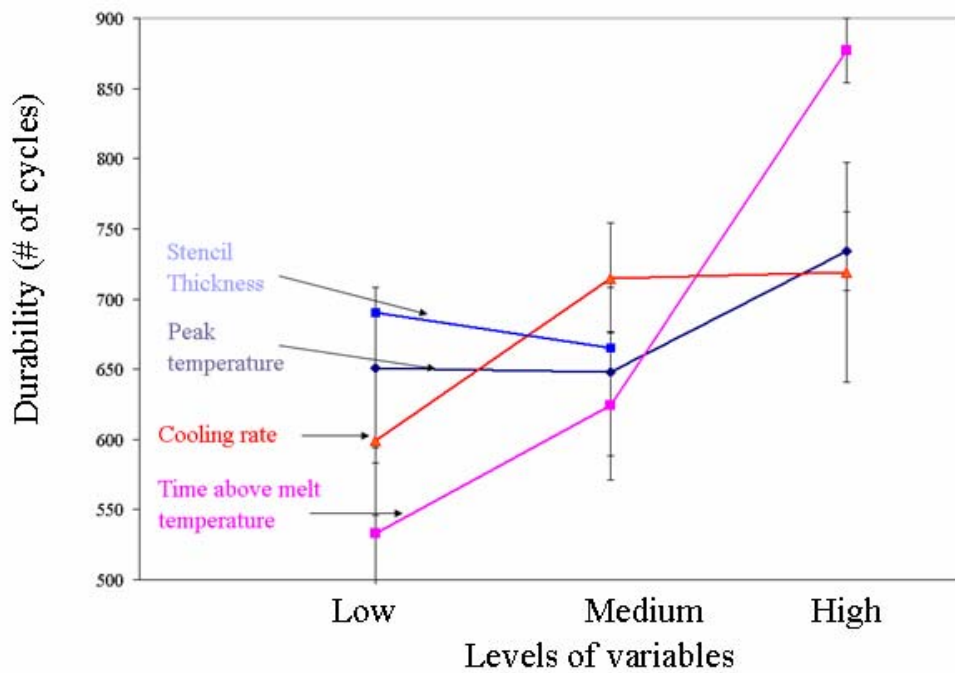


Figure 2-16: factor effect plots for different variables for durability as response variable

As seen in the figure, durability increases at higher levels cooling rate, peak temperature and time above melt temperature. Due to high scatter the only significant factor is time above melt temperature. As seen in Figure 2-8, the void percentage also increases as the time above melt temperature increases.

Comparing these results with the result of statistical analysis of voids as response shows that higher levels of voids did not result in lower durability. This indicates that variation in the process may have resulted in different types defects that have higher impact on durability. To validate this hypothesis the micro-structural failure analysis is conducted and presented in the next section

#### **2.1.10. Summary and conclusion of Study 1**

A taguchi experiment was designed and conducted to make voided specimens and to investigate the effect of reflow and printing variables on void formation and durability of Pb-free solder joints. Error-seeded specimens were assembled by varying selected process variables according to an L18 Taguchi DoE array. The response variables are thermal cycling durability and void area percentage.

Statistical analysis of void percentage and durability as response variables show that higher percentage of voids did not result in lower durability. The micro-structural failure analysis showed that other types of defects exist in the specimens that are caused due to variation in the process. This may indicate that effect of other types of defects dominate the effect of voids, hence higher levels of variables that resulted in higher void percentage, but in better intermetallic formation and wetting resulted in higher durability. Because of the difficulties encountered in isolating the effect of voids from other defects

on durability, result of this experiment was not deemed useful in correlation with modeling. So results of another existing experiment [Osterman et al., 2006] were used to qualitatively study the effect of voids. Next section discusses study 2 that was used to establish a modeling technique.

## 2.2.Study 2

The purpose of the test was to evaluate the long term reliability of Pb-free solder joints. The test was conducted by Hong Kong University of Science and Technology for boards with low glass temperature and high glass temperature. The test matrix for low glass temperature FR4 board is provided in Table 2-7.

Table 2-7: Test Matrix used in long term Pb-free consortium project [Osterman et al., 2006]

Board	Solder	Pad Finish	Component	Component Terminal Metallurgy
Low Tg (130°C) FR4	Sn37Pb	HASL	CLCC,PBGA, LQFP, 2512 resistor 1210 resistor	SnPb
	Sn3.0Ag0.5Cu	ENIG,ImAg, ImSn, OSP		CLCC: SnAg PBGA: SnAgCu LQFP: Sn, SnCu, SnBi Resistor: Sn

Due to high void density in test specimens produced in this test the result of this test was used in order to qualitatively verify the modeling approach.

### 2.2.1. Test condition

The test was conducted using a similar test chamber as DOE test. However, the test was conducted under a different temperature cycle. Minimum and maximum temperature for this test was -40°C and 125°C respectively. Cooling and heating ramp rates were equal and of 11°C per minute. Dwell time at high and low temperature was 15 minutes. The total time for one cycle was 1 hour or 60 minutes. Schematic of this temperature

cycle is shown in Figure 2-17. The specimens went under temperature cycling for 3500 cycles.

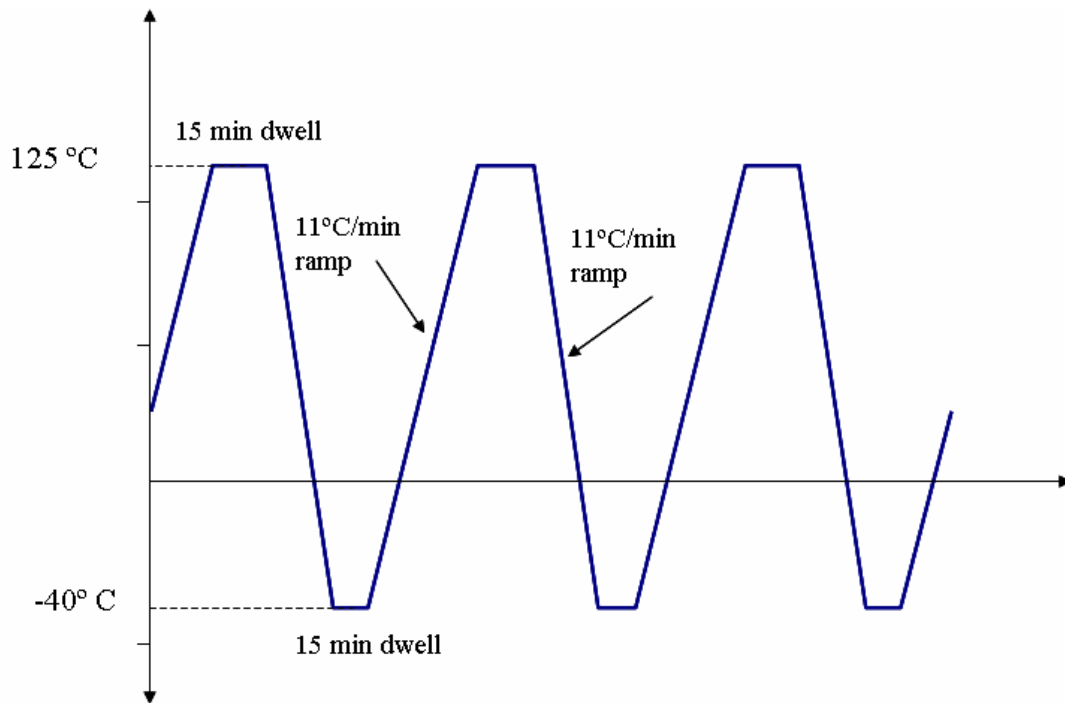


Figure 2-17: Temperature cycle used in long term Pb-free solder consortium project

### 2.2.2. Test specimen

Components were assembled on FR4 boards with different surface finishes; Hot Air Solder Leveling (HASL), Immersion Sn (ImSn), Immersion Ag (ImAg), Electroless Nickel /Immersion Gold (ENIG), and Organic Solderability Preservatives (OSP). The test specimen contained different types of components, such as BGAs, LQFPs, CLCCs, and chip resistors. A picture of the board is shown in Figure 2-18.

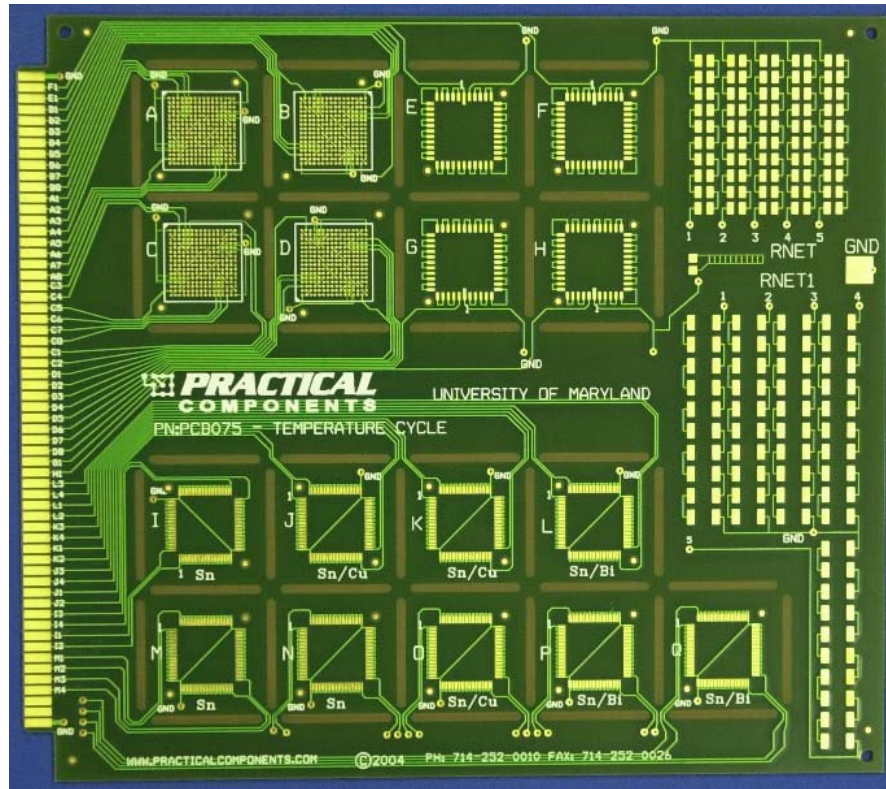


Figure 2-18: test board used for thermal cycling test for long term Pb-free consortium project [Osterman et al., 2006]

### 2.2.3. X-ray Analysis

BGA samples were of interest of this study so BGA samples from different boards were selected to be analyzed. Before conducting destructive failure analysis, the specimens were inspected using a MicroRTB X-ray imaging system. The X-ray analysis was conducted for BGAs from boards with different surface finishes. The internal BGA module was used to calculate the void percentage for each specimen. Figure 2-19 shows one example of X-ray analysis done for one part of BAG for the Im-Sn surface finish. As seen in Figure 2-19 there are many voids in the solder balls. Some balls even failed because of high void area percentage based on the internal device criteria. The analysis was conducted for BGAs from different boards and compared to select the best case for destructive failure analysis. The specimens with the highest void percentage (ImSn

finish) were selected for destructive failure analysis to increase the probability of getting voids and cracks in the same solder ball.

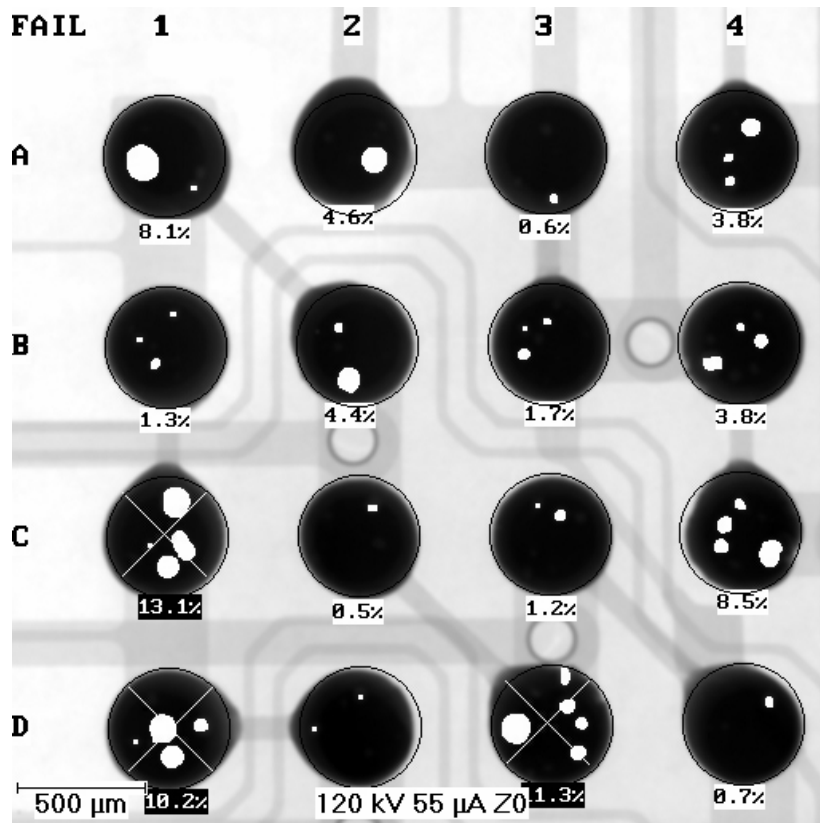


Figure 2-19: Example of X-ray analysis for Im-Sn surface finish

#### 2.2.4. Destructive failure analysis

Destructive failure analysis was conducted to determine the location of the failed solder ball and find out the location of cracks and voids. Many interesting examples were observed which some are used to correlate the modeling results discussed in later chapters. Two examples are shown in Figure 2-20, Figure 2-21, where partial crack is observed with a big void in the middle of the ball and small void close to the edge of the solder ball. Another example is shown in Figure 2-22, where a relatively big void is located close to edge of the solder ball, no crack observed in this solder ball. Some of

these cases were selected to be modeled using a global local approach explained in the next chapter.



Figure 2-20: Relatively big voids located in the middle of damage path



Figure 2-21: Small void located close to damage initiation site

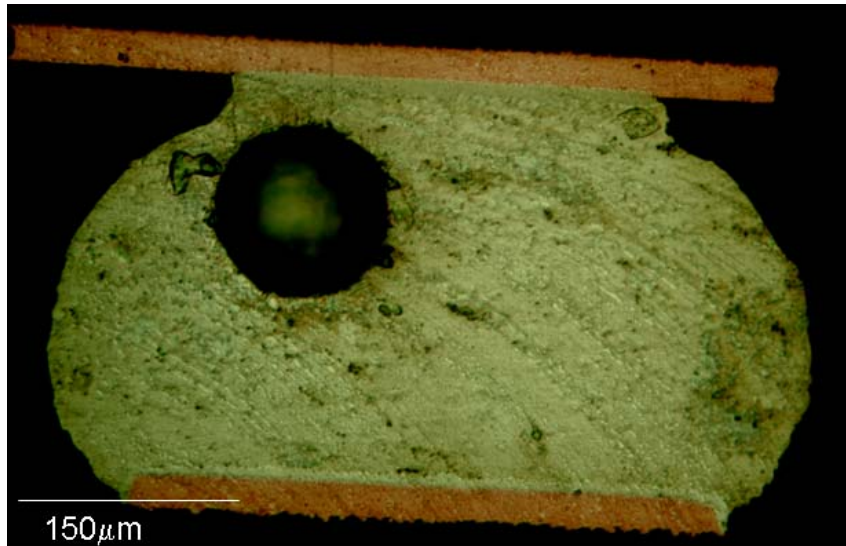


Figure 2-22: Relatively big void located close to initiation site

### **2.2.5. Summary and Conclusions of Study 2**

Nondestructive and destructive failure analyses were conducted for Pb-free BGA specimens produced with different surface finishes. The result show that board finish of ImSn produces more voids than other types of board finishes.

### **2.3. Summary and Conclusions**

Void characterization and durability results for both studies show that higher percentage of voids does not necessarily reduce durability. However, due to variabilities in experiment and test specimens, this conclusion is very qualitative. Therefore, detail modeling of the voided specimens is suggested to evaluate the effect of voids by isolating voids and eliminating other defects. The details of modeling approach and methodology is presented in the next chapters.

### **3. Durability modeling: effect of voids on durability**

One of the main objectives of this study is to study the effect of void size, location and distribution on durability of solder balls in BGA packages. The results of experiment from previous chapters indicate that effect of voids might not be as strong as other types of defects. However the comparison was done very qualitatively due to existence of many types of defects at the same time in specimens. To isolate the effect of voids, a modeling approach is suggested to be used. The objective of this chapter is to establish and qualitatively verify a modeling approach for parametric study of voids. A global local modeling is proposed to model the selected solder balls in the package. Use of successive initiation method is suggested to study the effect of voids on damage initiation time and propagation time and path and the procedure is documented. Five cases for which the experimental data were available and explained in chapter 2 were selected to be modeled and results of modeling and experiment are compared. This modeling approach then was used to parametrically model voids in chapter 4.

#### **3.1. Investigating effect of voids on thermo-mechanical durability**

Voids are usually small compared to the size of packages and joints. Modeling voids and their effect on durability is difficult when modeling the full package with finite element. Therefore, modeling a void inside a solder joint or solder ball requires a global-local finite element modeling strategy. The procedure is shown in Figure 3-1. First a global model of the package on the board is generated. Package symmetry can be exploited to model parts of the package. Creep and plastic work is monitored in all viscoplastic elements.

The critical ball is then identified as the one that has highest energy densities and therefore the highest damage and the shortest life. The next step is to generate a more

detailed local model of the critical ball. All the nodes at the top and bottom of the copper pads at the top and bottom of the critical ball are listed in the global model. Then, the time history of the displacements at top and bottom nodes of the critical ball is recorded in the global model for subsequent use in the local model. The local model is error-seeded with void(s) and the displacement histories obtained in the global model are mapped to the corresponding boundaries of the local model. The temperature history of the local model is varied in phase with displacement history for three consecutive temperature cycles. The creep-fatigue damage in the solder is then calculated using the energy-partitioning (E-P) damage mode described in chapter 1.

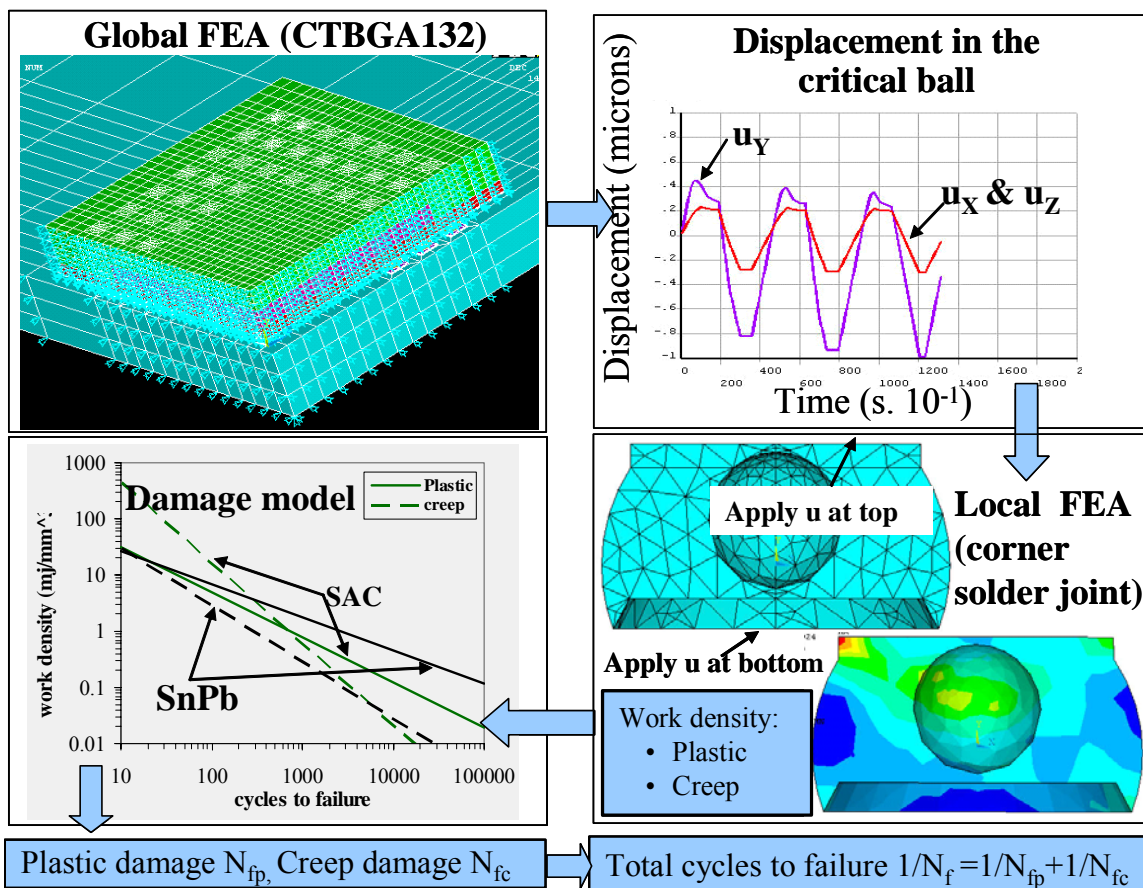


Figure 3-1: Global – local modeling approach

### **3.1.1. Investigating durability of voided joints using averaging techniques**

To estimate solder life using the E-P model, the damage has to be extracted from certain elements. Because of local stress concentration, using only one element in FEA is not accurate. Most authors have reported good correlation of the damage models to experiments if the stress, strain and energy values are averaged over a certain domain in the neighborhood of the potential failure sites. Using the technique recommended by Zhang [Zhang, 2004] in this study, damage was therefore averaged over a circular slice, with thickness of two layers of finite elements enclosing the critical site. This averaging technique however is not a good approach in cases where the damage path needs to be monitored. It only provides information about the overall durability of balls and does not separate the damage initiation life from the damage propagation life. The damage constants that were obtained from literature are for specific reference geometry of solder balls. Thus the initiation life is assumed to have a set ratio to the propagation life, when these damage constants are used in conjunction with this averaging method. In cases where the ratio of initiation life to propagation life is vastly different from the reference case, for example, in long joints, these constants cannot provide a good correlation with experiment. For this study, since the damage path and initiation and propagation time are important factors in evaluating the effect of voids, an approach developed by Okura [Okura, 2001] is enhanced and used to predict the life, and the ratio of damage initiation to propagation, as well as damage path. This approach is explained in next section.

### 3.1.2. Durability of voided joints using successive initiation technique

The information obtained using simple averaging techniques is an approximation of the life of the solder joints, including both time for initiation of damage as well as the time needed to propagate the damage all the way to the failure. The averaging technique, does not give enough information about the damage initiation, and damage growth. Neither can information be gathered about propagation path. Several different methods have been proposed and used in literature to predict the initiation and propagation time. Darveaux [Darveaux, 1995] durability model is one approach that separates the initiation time from propagation time and can be used to determine the initiation time of damage. Paris [Paris, Erdogan, 1997] proposed a method based on Linear Elastic Fracture Mechanics (LEFM), which related the damage propagation rate to damage metric and was used to predict the durability of solder material by [Deplanque, et al, 2006 and Lau, et al, 2002]. The form of such model follows:

$$D = C_{cp} \left( \frac{da}{dN} \right)^{n_{cp}} \quad \text{Equation (3-1)}$$

Where D is the chosen damage criteria (could be Inelastic Strain Range (ISR), Work densities ( $\Delta W$ ), or Total Strain Range (TSR)),  $\frac{da}{dN}$  is the damage propagation per cycle and  $C_{cp}$ , and  $n_{cp}$  are material constant. As mentioned earlier the Fracture mechanics based damage models are not recommended for solder material. Fracture mechanics considers propagation of a single dominant crack through an otherwise undamaged material. However, the damage mechanism in solder is different. In solder, damage is propagated by growth, coalescence and the interconnection of micro-cracks and voids distributed all

over the stresses region of ball. Therefore, use of a continuum damage model is more appropriate.

Okura introduced a method called successive initiation [Okura, 2001] which can be used with any damage model. Successive Initiation analysis involves several steps and is implemented with the help of finite elements in this study. The damage initiation site is first identified with the help of a suitable damage model (the E-P model is used in this study), for a typical cyclic loading history. A set of finite elements surrounding the initiation site, with damage higher than a selected threshold value, are identified as the damage initiation zone. This threshold value should be determined based on parametric studies. For demonstration purposes in this study, the initiation threshold is set to 60% of the maximum damage. The damage is averaged over this initiation zone using the E-P model. This determines the initiation life as follows:

$$N_{f1} = N_I = \frac{1}{D_{cycle1}} \quad \text{Equation (3-2)}$$

Where  $N_{f1}$  is the number of cycles needed to completely fail the set of finite elements in the initiation zone and  $D_{cycle1}$  is the average of damage over eliminated elements.

The propagation path for maximum damage is then monitored as follows. The initial damage zone is removed from the structure by eliminating or “killing” the damaged finite elements in the initiation zone. Damage due to the  $N_{f1}$  cycles is accumulated ( $D_{accum}$ ) in all the surviving elements. The FEA modeling of cyclic loading is repeated on the remaining structure and new critically damage zones are identified based on the residual damage endurance of the remaining structure, as in Equation (3-14). The time (or cycles) to fail the next local critically damaged zone is estimated from:

$$N_{fi} = \frac{(1 - D_{accumi})}{D_{cyclei}} \quad \text{Equation (3-3)}$$

The process is repeated, until a complete failure path is established and the structure loses its ability to carry any further mechanical loads. The total life is the summation of the number of cycles needed in each step to successively propagate the damage through the next successive critical zone.

$$N_f = \sum_{i=1}^{i=n} N_{fi} \quad \text{Equation (3-4)}$$

The flow chart of the method is provided in Figure 3-2.

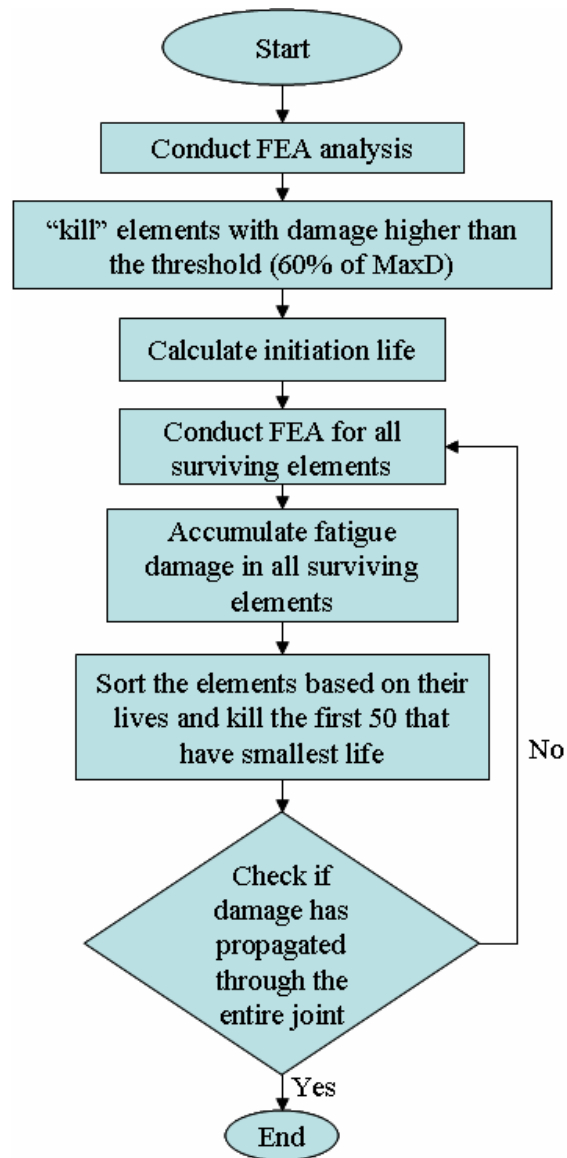


Figure 3-2: Damage propagation using successive initiation

This method was used by Okura [Okura, 2001] to predict the damage propagation path in two-dimensional models of void-free flip chip solder joints. This study represents the use of successive initiation in 3D cases of voided BGA solder interconnects. An Ansys post-processing code was written to estimate the damage in each element, using the Energy-Partitioning damage model after each step, and to “kill” the failed elements.

The effect of voids on damage propagation step and on the damage path can be studied using this method. The ratio of damage initiation life to damage propagation life can also be estimated using this method. It should be noted that “initiation life” is somewhat subjective, depending on the threshold value used in the failure criterion. The effect of this threshold value needs to be investigated in future studies.

### **3.1.3. Implementation of successive initiation approach: Case studies**

A full-array PBGA component with 256 balls mounted on an FR4 PWA (specimen from Study 2), is modeled under accelerated thermal cycling condition. Failure data for this assembly for 3500 thermal cycles are available in the literature [Osterman et al, 2006] which had undergone 3500 cycles, second study were selected to be modeled. The global-local approach introduced the beginning of this chapter is implemented for these examples. Then 5 cases that were of more interest were selected to be modeled locally. The cases were observed in destructive analysis of different samples in Study 2. The detail about the temperature cycle and test condition is provided in Chapter 2. As seen in Figure 3-3 the voided balls being examined are located in different spots in the package. The examples were observed after 3500 cycles of thermal cycling. In some cases the crack had propagated through the whole joint, such as case 4, but in some cases the crack has partially propagated, such as case 1, and 3. The global-local approach implemented is discussed in more detail in following sections.

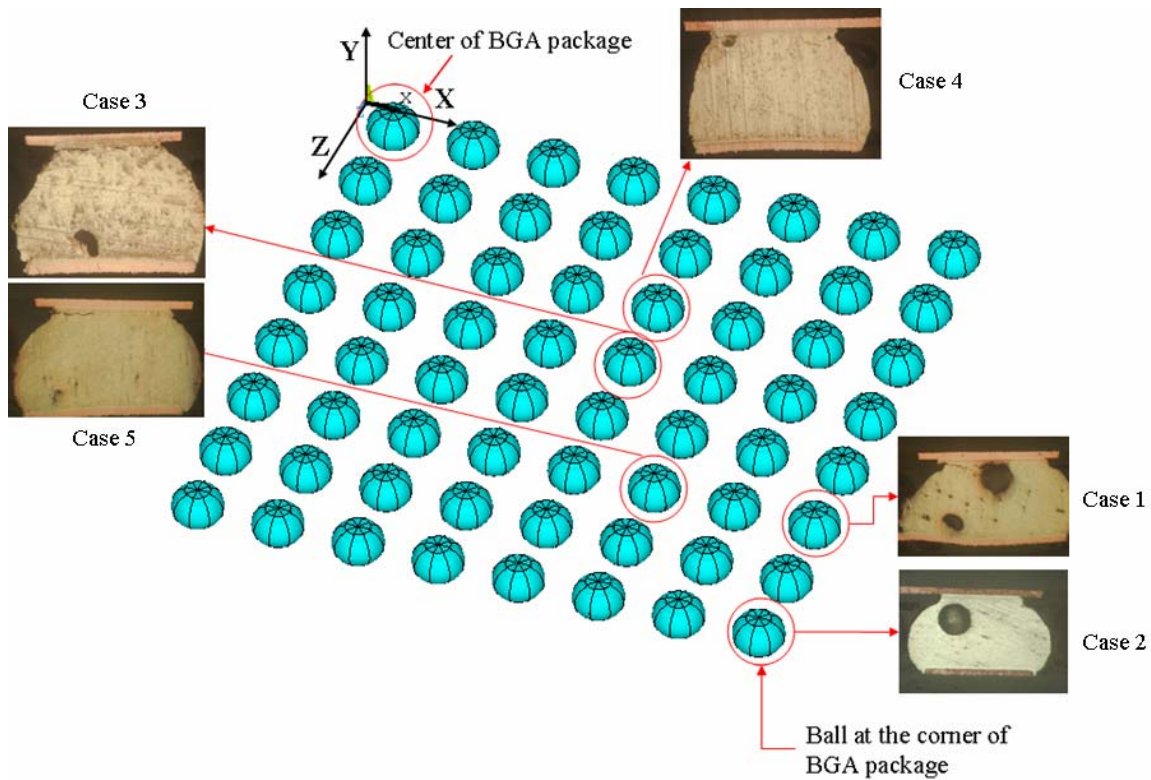


Figure 3-3: Map of the balls of one quarter of the package and cases studies in detail

### 3.1.4. Solder joint material properties

To model a package globally on the board, the following information is needed; dimension of the assembly, and properties of materials used in the assembly. In this case material properties include constitutive properties (including partitioned creep, plastic and elastic properties for viscoplastic materials) and damage properties for the solder. This section included material properties used for this modeling.

Material deformation can be broken into two groups; “elastic” deformation and “inelastic” deformation. Elastic deformation is deformation that can be recovered when the load is removed. Inelastic deformation is deformation that is retained even after the load is removed. Inelastic deformation can happen quickly or slowly as a function of time. The term “plastic” deformation is used when inelastic deformation happens almost instantaneously and the term “creep” is used when inelastic deformation happens slowly.

The first type of deformation (plastic) is sometimes termed “rate independent” deformation and the second type (creep) is called “rate dependent” deformation. The term “visco” is added to either the elastic or plastic terms when the deformation is a function of time, so visco-elastic means elastic deformation that is a function of time and is recovered when the load is removed. Visco-plastic means permanent deformation that is a function of time and will be retained in the body even after the load is removed. All different combinations of deformations are possible in engineering materials.

Usually elastic deformation is described by Hooke’s law. For plastic deformation the power law relationship is used [Darveaux et al, 1995];

$$\sigma = C_{pl} \varepsilon_{pl}^n \quad \text{Equation (3-5)}$$

Where  $\sigma$  is equivalent stress,  $\varepsilon_{pl}$  is equivalent plastic strain,  $C_{pl}$  is the strength coefficient and  $n$  is the plastic hardening exponent. Creep is a very common and important inelastic deformation mechanism in solder joints, because the solder is above half of its melting point at operating temperatures. A typical constant-load creep deformation is composed of primary, secondary, and tertiary sections, as shown schematically in Figure 3-4.

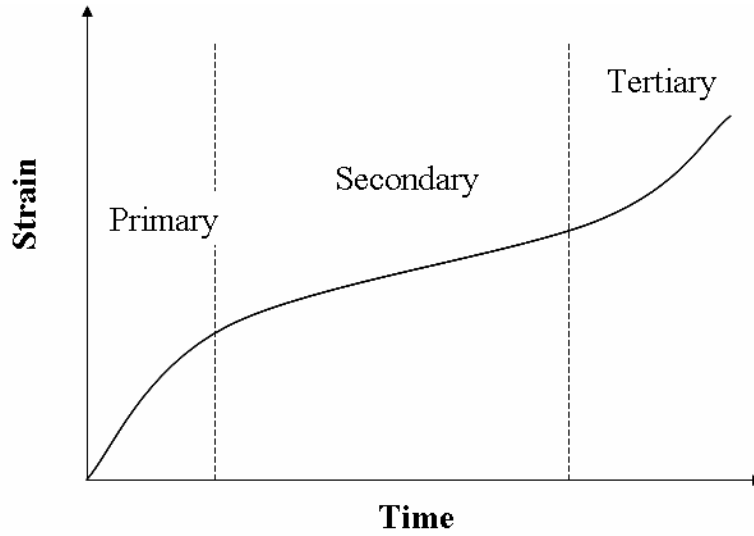


Figure 3-4: Typical constant load creep deformation

The transient or primary creep is generally expressed by following models [Drvaeux et al, 1995]:

$$\frac{\gamma_{pcr-sat} - \gamma_{pcr}}{\gamma_{pcr-sat}} = \exp(-A_{pcr} t) \quad \text{Equation (3-6)}$$

$$A_{pcr} = C_1 \tau^{n_1} \exp\left(-\frac{C_2}{T}\right) \quad \text{Equation (3-7)}$$

Where  $\gamma_{pcr-sat}$  is the saturated primary creep,  $C_1$ ,  $C_2$  and  $n_1$  are material constants.

Steady state creep deformation of solder alloys at high temperature exhibits different characteristic behaviors at different levels. If the steady state creep strain  $\gamma_{scr}$  is plotted versus stress on a log log scale as shown in solders behave differently at different stress levels. The dominant deformation mechanisms in these regions are: Nabarro-Herring matrix diffusion creep in (region 1) [Nabarro, 1967, Herring, 1950], super plasticity due to grain boundary sliding (Region 2) [Gifkin, R.C., 1976], and climb control dislocation creep (Region 3) [Weertman, 1955]. At high stresses the steady state creep rate  $\dot{\gamma}_{scr}$

increases more rapidly with the shear stresses and the power law behavior breaks down. Therefore this region is called “power law breakdown region” [Schubert et al., 2001] (Region 4). Generally Region 1 and 2 are grain size controlled regions, whereas Regions 3 and 4 are independent of grain size. Relationship that often is used is in the form of power law to represent the stress dependency with dependency to temperature through Arrhenius (exponential relationship) as follows:

$$\frac{d\gamma_{scr}}{dt} = A\sigma^{n'} \exp\left(-\frac{Q}{RT}\right) \quad \text{Equation (3-8)}$$

Where R is the universal gas constant (= 8.31 m<sup>2</sup>Kg/s<sup>2</sup>Kmol), T is the absolute temperature in Kelvin, Q is activation energy in J/mol, and A is constant.

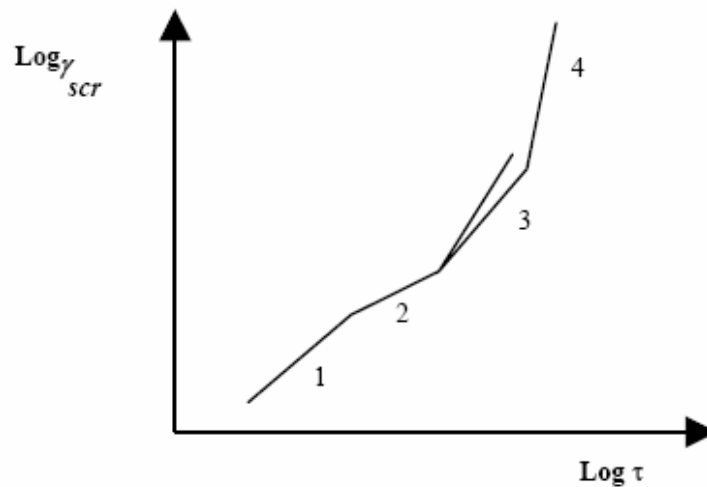


Figure 3-5: Schematic of a log-log plot of the shear secondary creep strain Vs. shear stress [Zhang, 2005, Schubert et al., 2001]

Most typical load levels in solder interconnect of electronic assemblies fall in region 3 and 4 and a hyperbolic sine model is often used to model the steady state creep in these regions as follows [Garofalo, 1965];

$$\frac{d\varepsilon_{cr}}{dt} = A'(\sinh(\alpha\sigma))^{n''} \exp\left(-\frac{Q}{RT}\right) \quad \text{Equation (3-9)}$$

where  $\sigma$  is the applied equivalent stress,  $\varepsilon_{scr}$  is the equivalent strain, R is the universal gas constant ( $=8.31451 \text{ m}^2\text{kg/s}^2\text{kmol}$ ), T is the temperature in K, Q is the activation energy in J/mol, A' and  $n''$  are model constants.

Elastic deformation occurs by changing the distance between atoms. Inelastic deformation including plastic and creep deformation is caused by dislocation slip motion, and grain boundary motion and grain boundary diffusion. In solder material all three different deformations happen at the same time. In this study we will use Garofalo's equation for creeps and the power law (Hollomon [Hollomon, 1946]) equation for plasticity.

A partitioned viscoplastic constitutive law is employed in this FEA analysis, as shown below, to facilitate the use of the Energy-Partitioning fatigue model:

$$\varepsilon = \varepsilon_e + \varepsilon_p + \varepsilon_{sc} \quad \text{Equation (3-10)}$$

Where  $\varepsilon$  is total strain;  $\varepsilon_e$  is elastic strain;  $\varepsilon_p$  is rate-independent plastic strain; and  $\varepsilon_{sc}$  is rate-dependent steady-state (secondary) creep strain. The transient primary creep strains are neglected here because damage in thermal cycling is believed to be dominated by steady-state creep deformations due to slow rate of loading. The rate-independent plastic strain is given in equation 3-16. Since we use equivalent strain,  $C_p$  and N are scalar values. The steady state secondary creep strain rate is described by the Garofalo equation. The plastic and creep constitutive constants are summarized in Table 3-1

Table 3-1: Solder creep and plastic properties [Zhang, 2004]

Solder alloy	Plastic constants		Creep constants			
	$C_p(\text{MPa})$	$N$	$A$	$\alpha$ (1/MPa)	$n_c$	$Q$ (J/Mol)
Sn3.9Ag0.6Cu	121.6-0.4* $T(^{\circ}\text{C})$	0.29- $0.00046 * T(^{\circ}\text{C})$	1.5E 3	0.19	4.0	7.13E4

### 3.1.5. Global modeling for BGA256 (Study 2 specimen)

To obtain the correct dimensions of the package for global modeling, one sample was cross sectioned and the dimensions of the package were measured using an optical microscope. The dimensions are shown in Figure 3-6 and values of these dimensions are provided in Table 3-2.

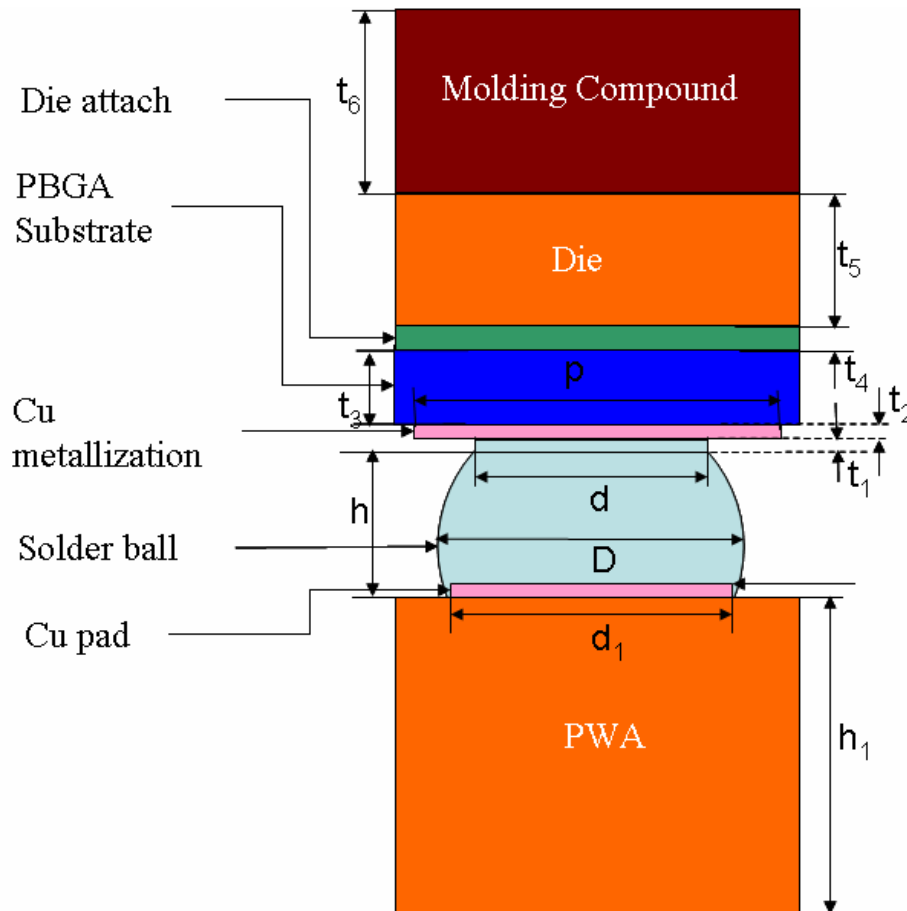


Figure 3-6: Dimension of the package

Table 3-2: Dimension of the package in microns

Ball diameter (D)	630
Neck diameter (d)	325
Pad thickness ( $t_2$ )	25
Neck thickness ( $t_1$ )	40
Substrate thickness ( $t_3$ )	300
Die-attach thickness ( $t_4$ )	100
Die thickness ( $t_5$ )	330
Molding compound thickness above the die ( $t_6$ )	470
Pad size (p)	480
Board pad size ( $d_1$ )	500
Board plating thickness	25
Ball height (h)	370
Board thickness ( $h_1$ )	1570
Die dimension (L)	4000

Figure 3-7 shows quarter of a PBGA256 component modeled on the PWA. The component is a full-array BGA with 256 I/O of 1 millimeter pitch. The assembly is subjected to thermal cycling. The temperature profile is between  $-40^{\circ}\text{C}$  to  $125^{\circ}\text{C}$  with  $11^{\circ}\text{C}/\text{min}$  cooling and heating ramps, and 15 minutes dwell in both low and high extreme temperatures. The temperature profile used for modeling is shown in Figure 3-9.

Non-linear viscoplastic finite element analysis was conducted with ANSYS-8. Due to symmetry in geometry, material properties, boundary conditions and loading, a three-dimensional quarter model was built for a BGA256. Modeling one eight of the package was refrained Because of issues related to applying boundary condition and meshing difficulties encountered in modeling.

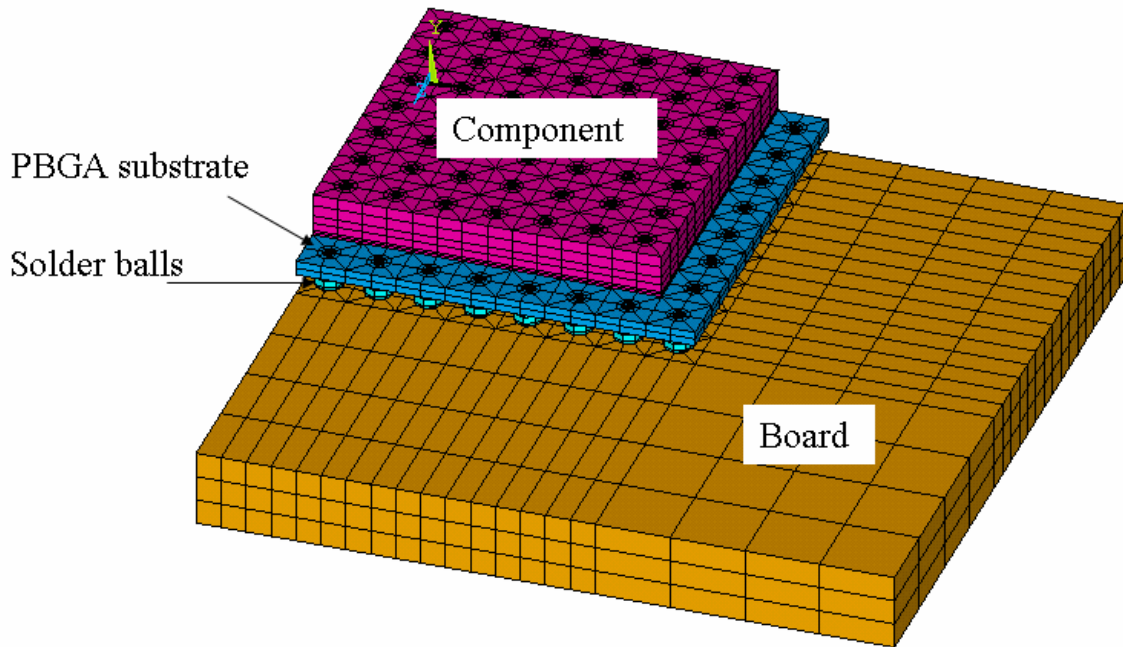


Figure 3-7 Global FEA model for BGA256

An 8-noded solid brick element with linear interpolation functions, with the capability of modeling plasticity, creep, large deflection and large strain, is used.

The displacement boundary conditions are:

- 1) All nodes on the symmetry surfaces  $x = 0$  and  $z = 0$  are fixed in the  $z$  and  $x$  directions, respectively.
- 2) The node at the origin ( $x = y = z = 0$ ) is constrained in all three directions (refer to Figure 3-8).

Since a global-local model approach is used, solder balls at all different locations on the package were meshed with the same mesh density. The total number of elements is about 43,000. Three complete thermal cycles are simulated in order to obtain a stable hysteresis loop for energy computation. Inelastic behavior is ignored in all materials, except the solder. Material properties are obtained from literature and manufacturer and are provided in Table 3-3.

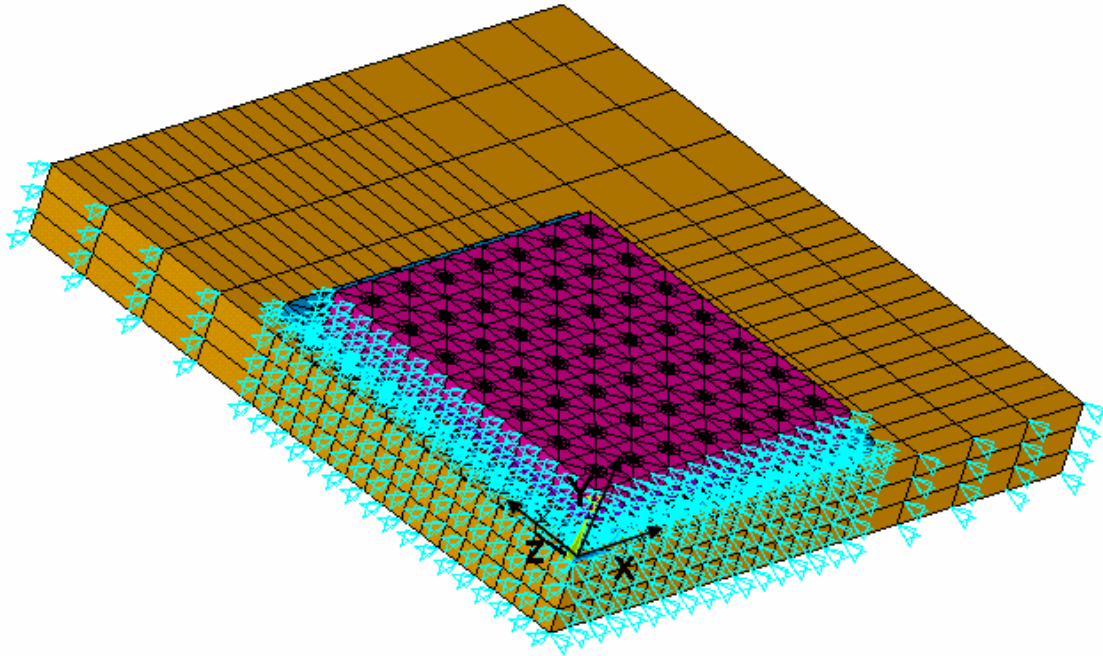


Figure 3-8: Global FEA model for PBGA256, with applied boundary conditions

Table 3-3: Material properties used in FEA modeling [Zhang, 2004]

Material	Elastic Modulus (MPa)	CTE (ppm/°C)	Poisson Ratio	Shear Modulus (GPa)
PWA in-plane	17685	15.74	0.38	6.908
PWA out-of - plain	7709	15.9	0.38	3.47
Molding compound	23.6E3	9	0.3	-
Chip	191E3	2.095	0.28	-
Die attach	1.2E3	110	0.42	-
Substrate (BT material)	17.89E3	12.42	0.3	-
Solder	4.37E4-22.3T(K)	20.9	0.4	-
copper	13E3	14.5	0.35	

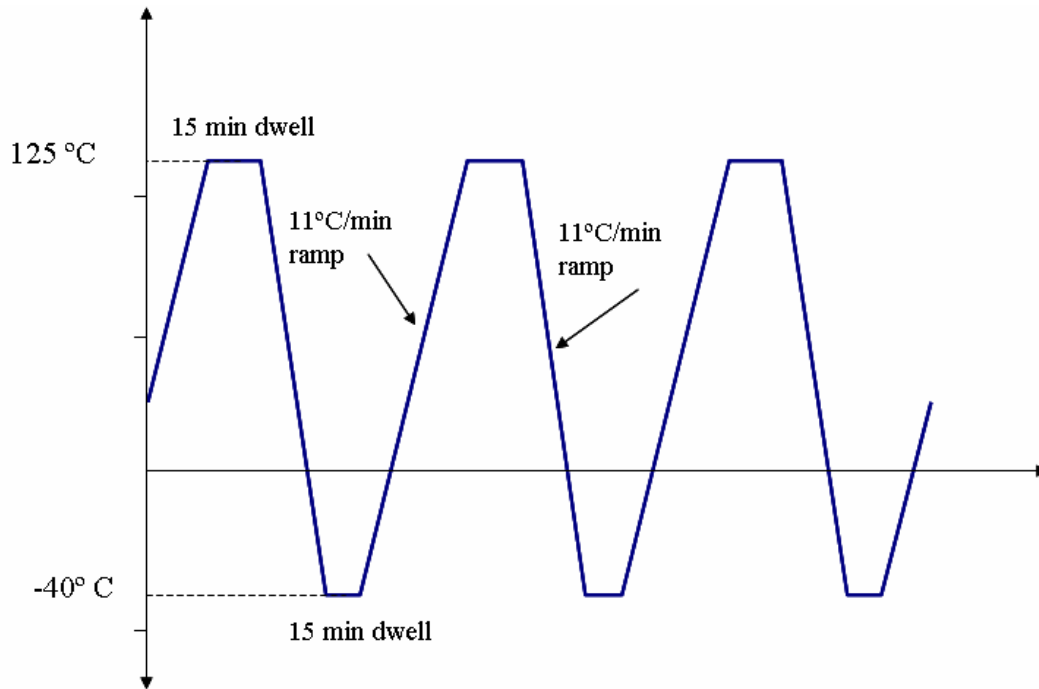


Figure 3-9: Temperature profile used in FEA modeling

Creep and plastic work densities are monitored in the solder ball for all the balls. The Energy Partitioning (E-P) damage model described in chapter 1 is used to calculate the damage. An ANSYS APDL code is written to calculate and plot the damage for all elements in the ball, based on E-P damage models. The damage constants are obtained from literature [Zhang, et al, 2003] and are provided in Table 3-4.

Table 3-4: Thermo-mechanical Energy Partitioning damage model constants for Sn3.8Ag0.7 solder [Zhang, et al. 2003]

	Sn3.8Ag0.7 Solder
c	-0.8
$W_{p0}$	198
d	-1.4
$W_{c0}$	1.23E4

Figure 3-10 shows the contour plot of the cyclic fatigue damage for all the balls in the package. It is seen that the ball under the die shadow has the maximum damage and thus fails earlier. The displacements at the top and bottom of the ball for the cases that were indicated in Figure 3-3 were obtained from this global model to be used in local modeling of selected solder balls with the successive initiation technique. x, y and z displacement at all nodes at the top and bottom of the balls were recorded from time history post processor in ANSYS (Post27) to be applied as a boundary condition to the local model as reported in Chapter 3.1.

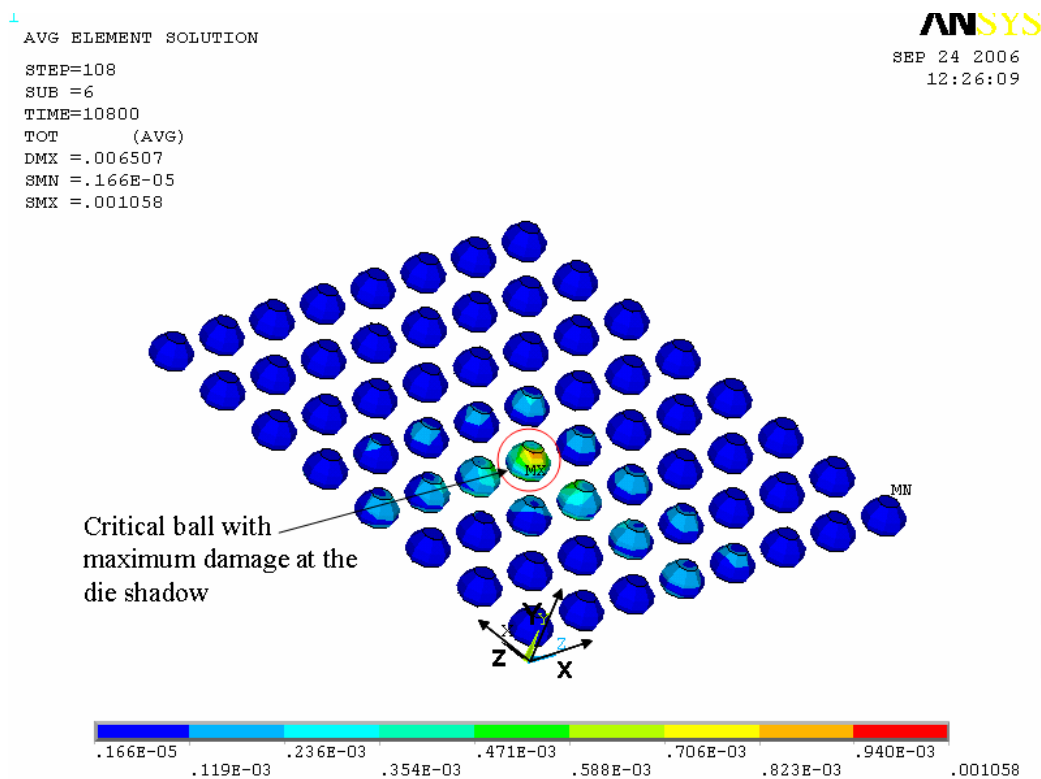


Figure 3-10: Contour plot of cyclic fatigue damage calculated based on E-P model

### 3.1.6. Local modeling of voided solder balls

The cyclic damage in each solder ball was first calculated first using the E-P model and the averaging technique discussed in section 3.1.1. The normalized damage, with

respect to the critical ball, is shown in Figure 3-11. As expected, the critical ball is under the die shadow experiences the highest amount of cyclic fatigue damage. Failure sites observed by cross sectioning were also mostly around the die shadow, which confirms the FEA results. Five cases of voided solder joints were then modeled in detail, using E-P model and method of successive initiation presented in section 3.1.2. Each of these cases are circled and labeled in Figure 3-11. As seen in Figure 3-11 same amount of damage has been predicted by FEA using E-P damage model for Case 1, 2 and 5 but as seen in the figures the crack has already initiated in case 1 and 5 but not in case 2. Case 1 and 5 have the same amount of propagation, however due to presence of void the amount of the crack has propagated more significantly in case 1. Comparison between case 3 and 4 shows that these balls also have the same amount of damage, however, the crack has already propagated through the whole joint in case 4, but only propagated partially in case 3. This could indicate the effect of crack arrest for small voids [Lau and Erasmus, 2002]. These five cases are selected to be modeled using a global local approach explained in Chapter 3. The result of modeling is compared with experiment qualitatively and a global local model is established to study effect of voids parametrically.

Details of each case are described and compared to FEA model prediction in sections 3.1.6.1 to 3.1.6.5.

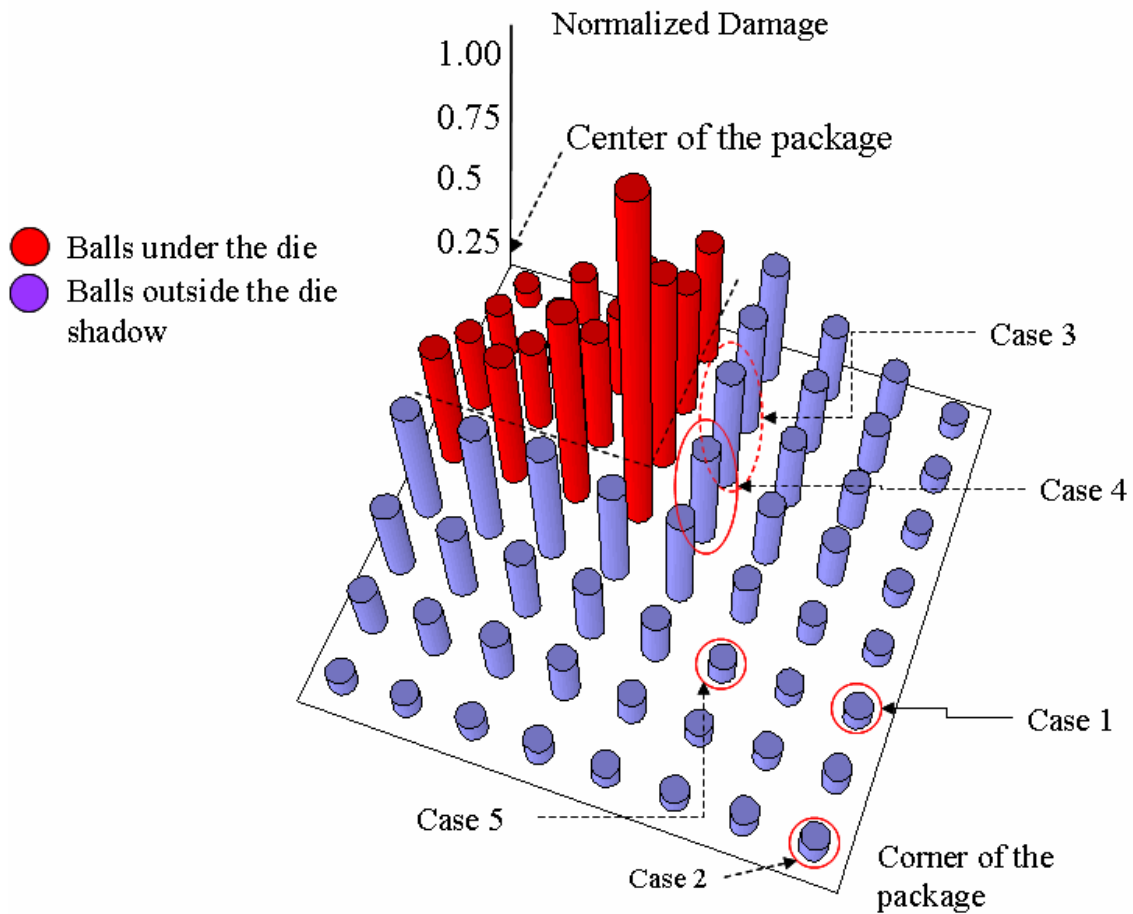


Figure 3-11: Normalized damage with respect to critical ball

An 8-noded solid brick element with linear interpolation functions, which has the capability of modeling plasticity, creep, large deflection and large strain, is used. Solder balls were meshed with free mesh with average number of 4000 elements. The solder ball was modeled with copper pads at top and bottom. Hard points are assigned to the surfaces at the top and bottom of the copper pad at the corresponding global nodes, to assure creation of nodes at those points in the local model. The ball is modeled under the same

temperature cycle as the global model, for three consecutive cycles. Figure 3-12 shows the cross section of the local model. Contour plot of cyclic fatigue damage is shown in Figure 3-13 for critical ball. The damage tends to start from the interface of solder with copper traces at component side. FEA predicts initiation site to be inner corner of the ball at component side.

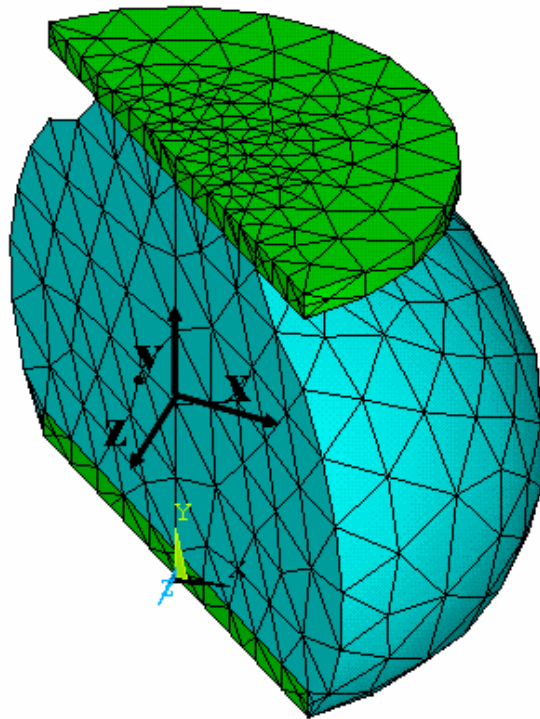


Figure 3-12: 3-D local model

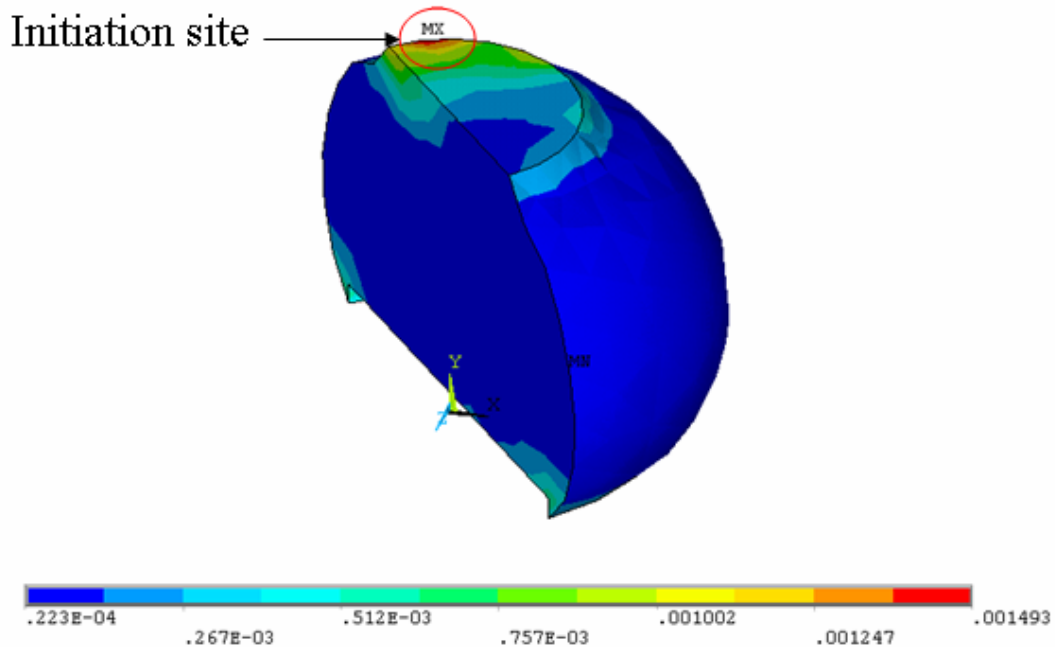
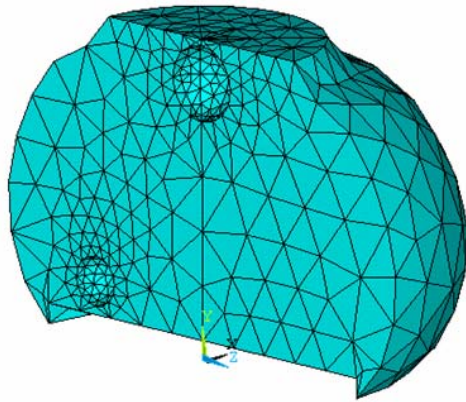


Figure 3-13: Contour plot of cyclic fatigue damage

### 3.1.6.1. Case 1: void in the middle with partial crack

Case 1 is a ball in the outer row of the package with a partial crack, a relatively big void in the middle, and two smaller voids. Cross section picture, X-ray image and the corresponding local FEA model built for this case are provided in Figure 3-14. One of the two small voids has been ignored due to small size and due to lack of information about its vertical location. The principal vertical plain indicated in x-ray image shows the vertical plain that passes connects the center of the ball to the center of the package.



FEA model of case 1

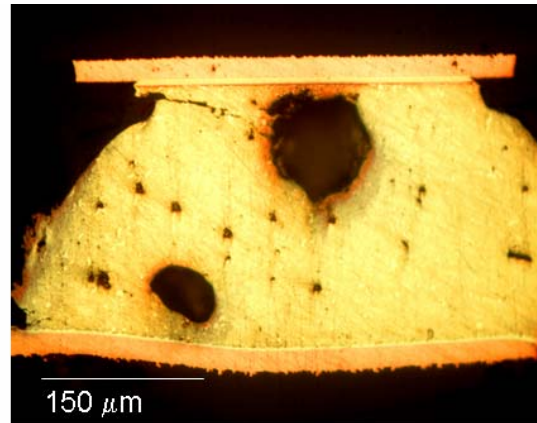
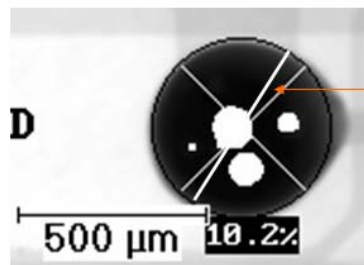


Image of cross section of case 1



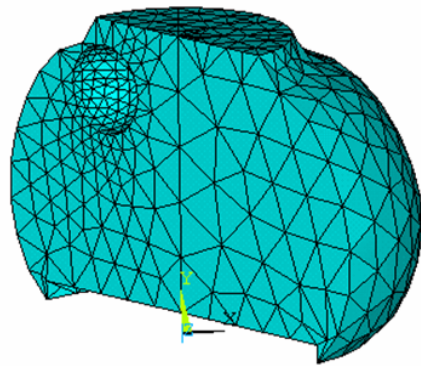
X-ray image of case 1

Figure 3-14: Case 1: Solder ball with relatively big void in the middle near the component

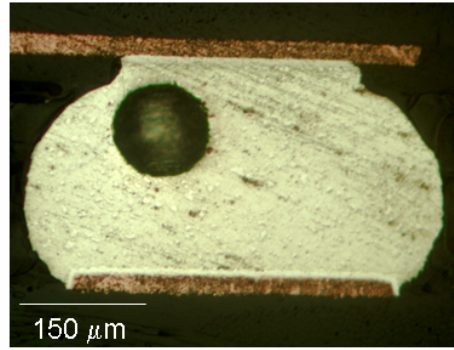
### 3.1.6.2. Case 2: void close to initiation site

Case 2 is the ball in the corner of the package that has a big void located close to the damage initiation site. The damage initiation site is at the inner diagonal corner of the ball near the component bond pad, as shown earlier in

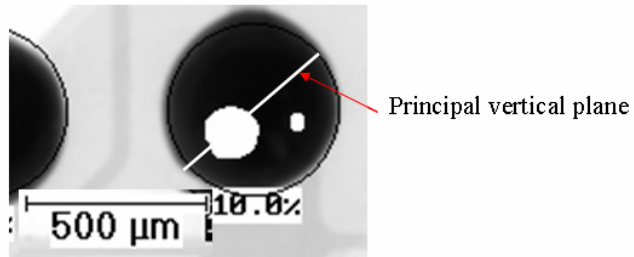
Figure 3-13. The cross section, X-ray image and FEA model built for this case are provided in Figure 3-15.



FEA model of case 2



Cross section image of case 2

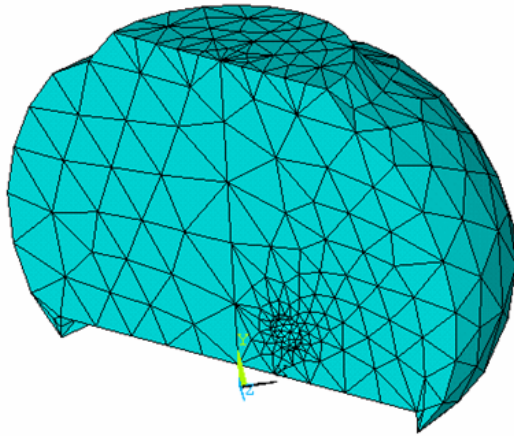


X-ray image of case 2

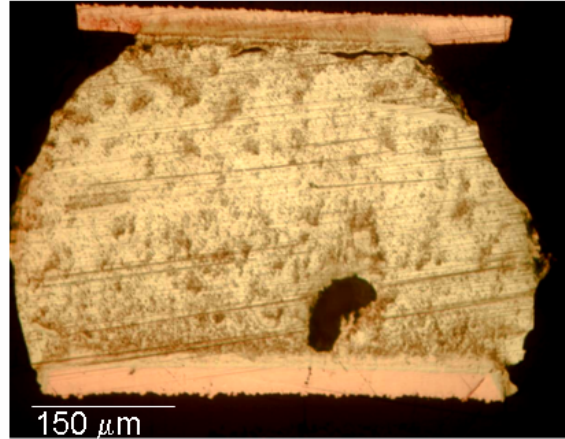
Figure 3-15: Case 2: big void located close to damage initiation site

### 3.1.6.3. Case 3: full crack with void far away from damage path

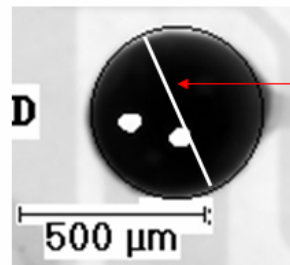
Case 3 is a ball located in fifth row and close to the critical ball shown in Figure 3-3. This ball has and a void close to PWA bond pad. The FEA model, X-ray and cross section of the ball is shown in Figure 3-16.



**FEA model of case 3**



**Cross section image of case 3**



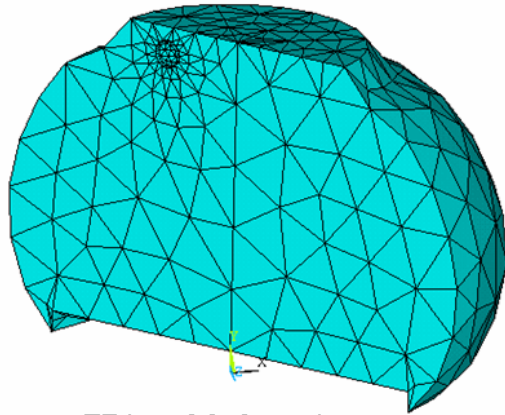
**Principal vertical plane**

**X-ray image of case 3**

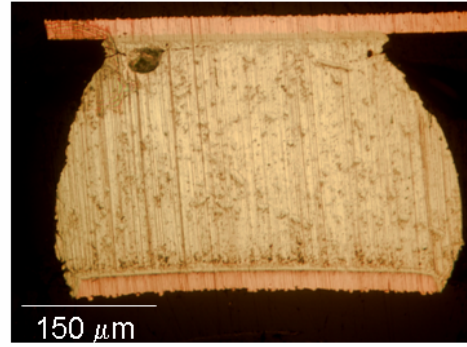
Figure 3-16: Full crack with small void close to PWA bond pad

#### **3.1.6.4. Case 4: small void in crack path**

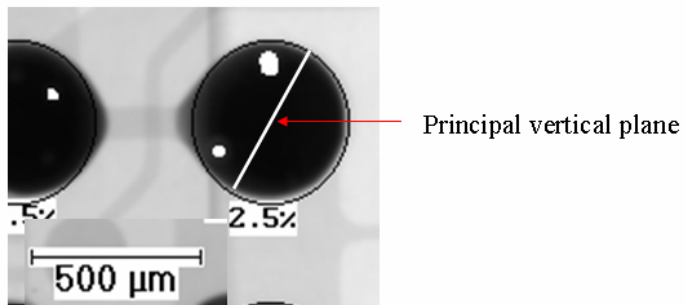
Case 4 is a ball in perimeter of die that has a small void close to initiation site. The small void evidently arrested the crack and made the propagation time longer. The cross section image, X-ray and FEA model built for this case is shown in



FEA model of case 4



Cross section image of case 4

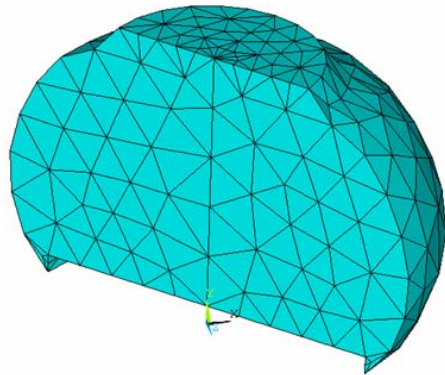


X-ray image of case 4

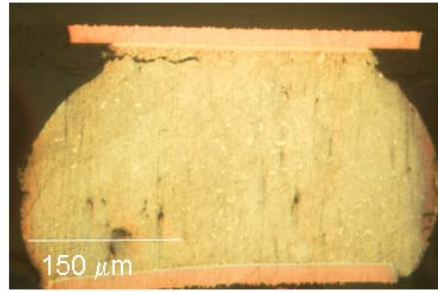
Figure 3-17: Small void close to damage initiation site

### 3.1.6.5. Case 5: no void, partial crack

Case 5 is a ball in the 6th row on the diagonal symmetry line of the package. The ball has no void, and it is modeled for the purpose of base line comparison. This ball has a partial crack as shown in Figure 3-18.



FEA model of case 5



Cross section image of case 5

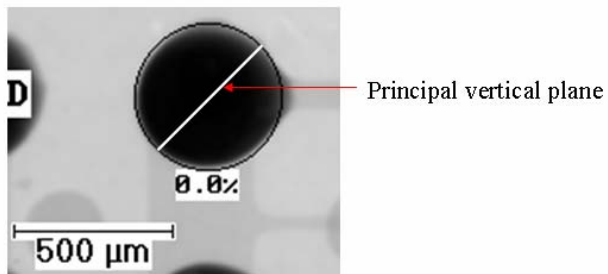


Figure 3-18: Case 5, solder ball with no void and partial crack

### 3.1.7. Results of successive initiation technique

The five cases explained at the last section were modeled with detail local FEA model. A full local ball model with the copper pad at the top and bottom was created. The displacement histories of the nodes at the top and bottom of the copper pad are obtained from the global model and are mapped as boundary conditions for to the local model. One example of displacement obtained from global model for ball located on diagonal symmetry line of the package using POST26 at one node, as a function of time, is shown in Figure 3-19.

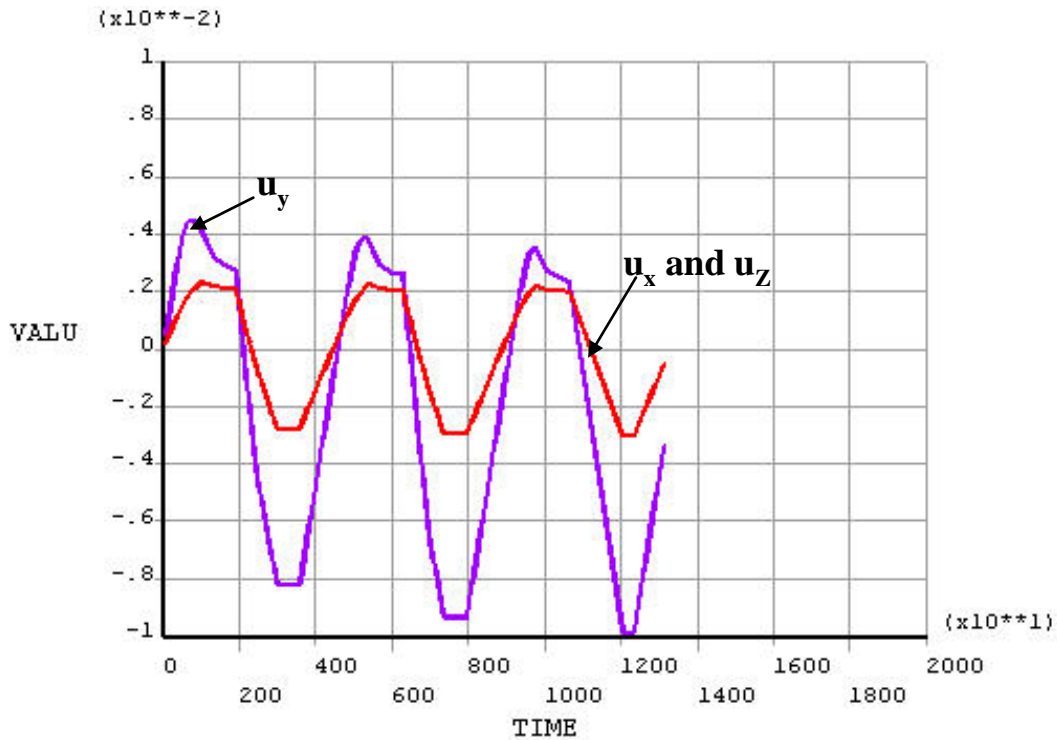


Figure 3-19: Example of displacement history at one node at top of the joint

Hard points are assigned to the surfaces at the top and bottom of the copper pad at the corresponding global nodes, to assure creation of nodes at those points in the local model. The local modeling of the ball is subjected to the same temperature history as the global model, for three consecutive cycles.

Creep and plastic work densities are monitored in the solder ball for each of the five cases discussed in section 3.1.6. The Energy Partitioning (E-P) damage model is used to calculate the damage. An ANSYS APDL code was written to calculate and plot the damage for all elements in the ball, using E-P damage models. An automated program was developed to conduct successive initiation for these cases using the algorithm presented in 3.1.2. The damage constants are obtained from literature [Zhang, Dasgupta and Haswell, 2004] and are provided in Table 3-5.

Table 3-5: Thermo-mechanical Energy Partitioning damage model constants for Sn3.8Ag0.7 solder [Zhang et al., 2003]

	Sn3.8Ag0.7 Solder
c	-0.8
$W_{p0}$	198
d	-1.4
$W_{c0}$	1.23E4

### 3.1.8. Result of case Studies: qualitative comparison

FEA analysis predicts two competing damage paths, a circumferential damage path that starts at the component side and another that starts at interface of the ball with the copper pad on the PWA side. Damage initiates faster from the inner corner of the solder ball at the component side. It also develops faster at inner corner of the solder ball at the component side. Figure 3-20 shows one example of these damages started from top and bottom of the ball.

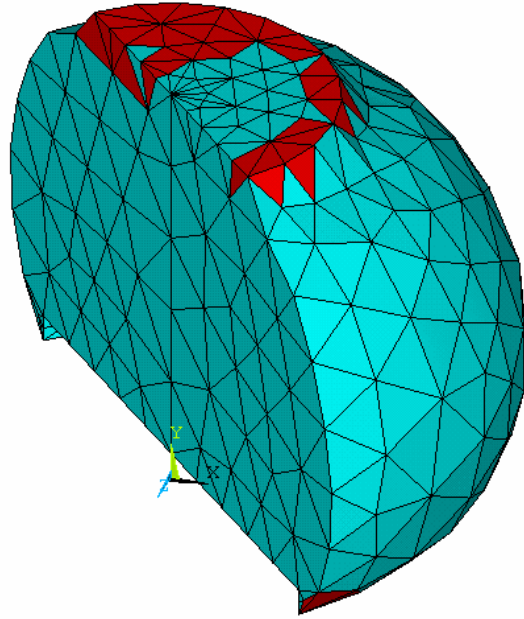


Figure 3-20: Example of damage starting circumferentially from the top and bottom of the ball for un-voided joint

FEA analysis for case 1 shows that damage starts from inner corner of the ball. It develops around the joint at the component side, but the elements at top of the void also have relatively high damage and are killed in sequential steps. Figure 3-21 shows the contour plot of cyclic damage in case 1.

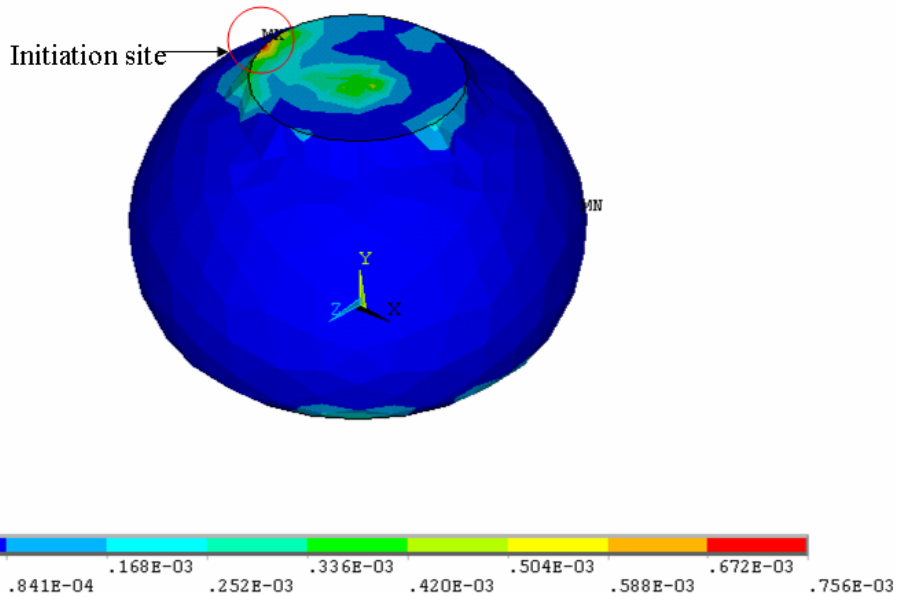


Figure 3-21: Contour plot of damage in solder ball with a void in the middle

Comparison between the Case 1 and 5 shows that the rate of damage propagation is almost the same in both cases until the damage zone reaches the void. The propagation rate increases gradually until the damage zone reaches the large central void in case 1 as shown in Figure 3-22, since the elements at the top of void have already been killed. In this case the void causes the propagation time to decrease. The void in Case 1 does not help in arresting the crack due to its central location. The disadvantage of this void location is that damage along the circumference and grows radially in towards the void from all sides and finally reaches the void. Experimental observation confirms the damage propagation in both cases as seen in Figure 3-14 and Figure 3-18. However, only partial crack can be observed from cross sections. There is possibility of crack developed around the circumference which cannot be inspected in the cross section picture.

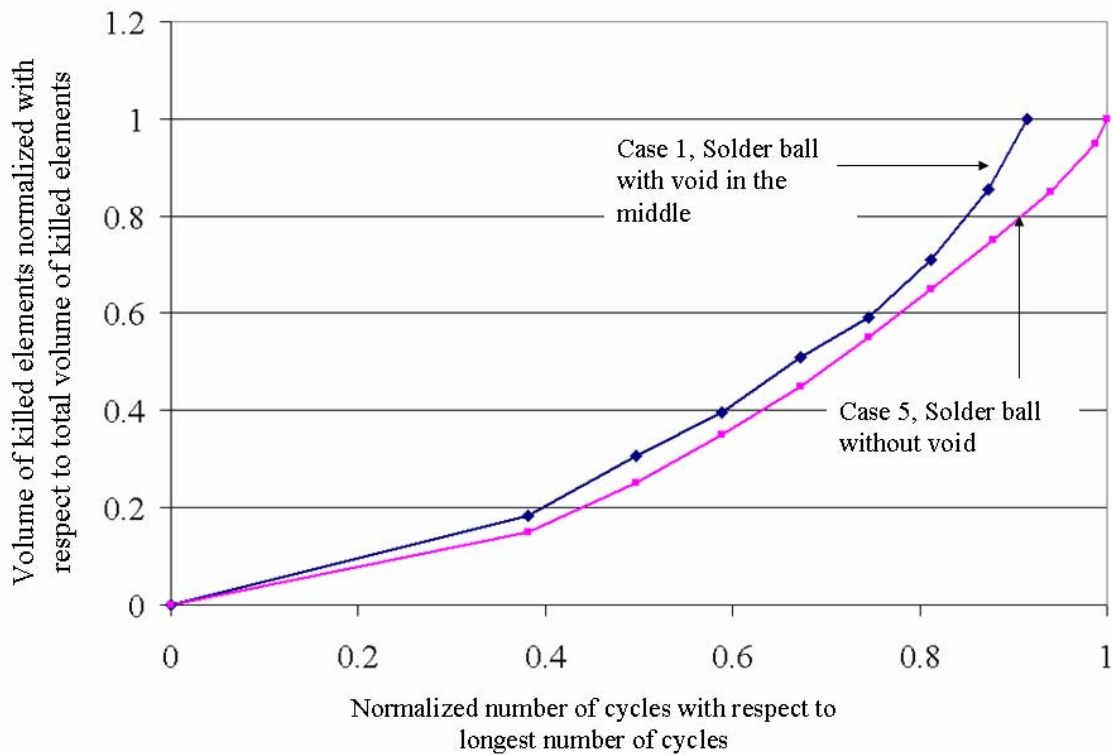


Figure 3-22: Comparison between Case 1 and 5 solder ball with big void in the middle and solder ball without void

Comparing Case 2 and Case 1 and 5 in Figure 3-11 shows that these cases have the same amount of average damage. However the initiation time is predicted to be longer for case 2 than case 1 and 5. The initiation time normalized with Case 5 is shown in Figure 3-23. As seen from the figure, the initiation time is much longer in case 2 relative to case 1 and 5. This is also observed in cross section pictures provided in Figure 3-15, Figure 3-14 and Figure 3-18. As seen in figures the damage has not initiated in Case 2. Hypothesis is that the void makes the ball locally compliant and delays the initiation time. More explanation about this phenomenon is provided in chapter 4.

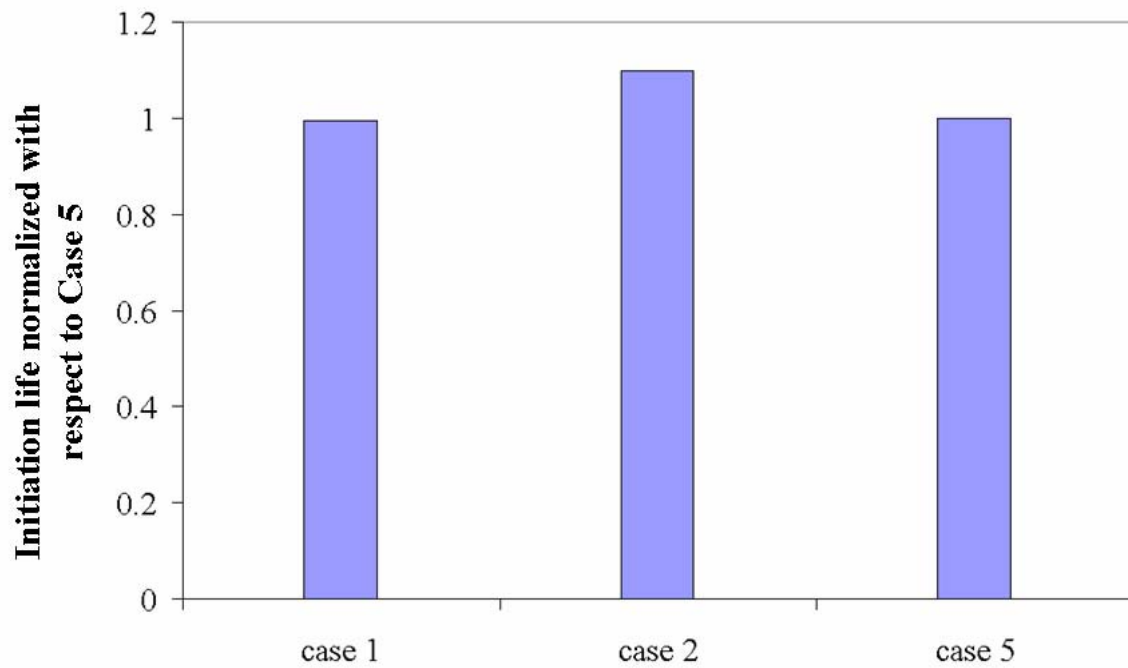


Figure 3-23: Comparison between the initiation time for case 1, 2 and 5

Between case 3 and 4 the rate of propagation of damage started from inner corner of the solder ball close to small was measured and compared. The initiation site is shown in both cases in Figure 3-24

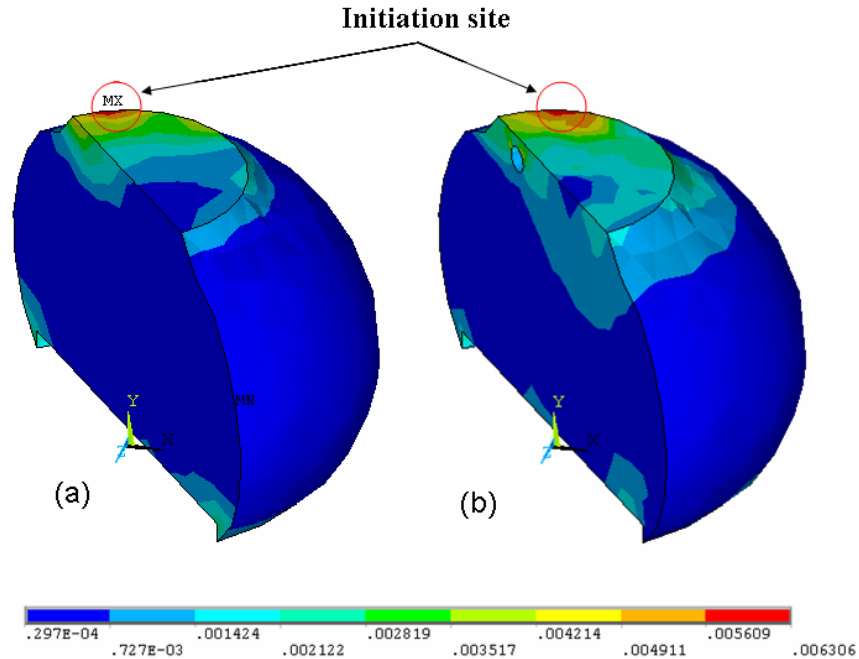


Figure 3-24: Initiation site in Case 4, solder ball with void far from crack and Case 3, solder ball with small void on the crack path

In both cases the damage initiates relatively at the same number of cycles. However, it propagates with a faster rate in the case without void. The small void located in the crack path in the case 4 arrests the crack for several steps. But this void only arrests the damage started from inner corner. The damage started from other sides of the ball still has the same rate of propagation. The damage propagation length normalized with respect to total damage path started from the corner where the void is located is shown in Figure 3-25. The damage length is defined as the length of the crack started from the corner where the void is located. The total length here is therefore the final length of the damage started at that corner which is about half of the joint length. As seen the overall propagation rate is smaller in case 4 than case 3. The two steps in which the damage is arrested are shown in Figure 3-26 and Figure 3-27.

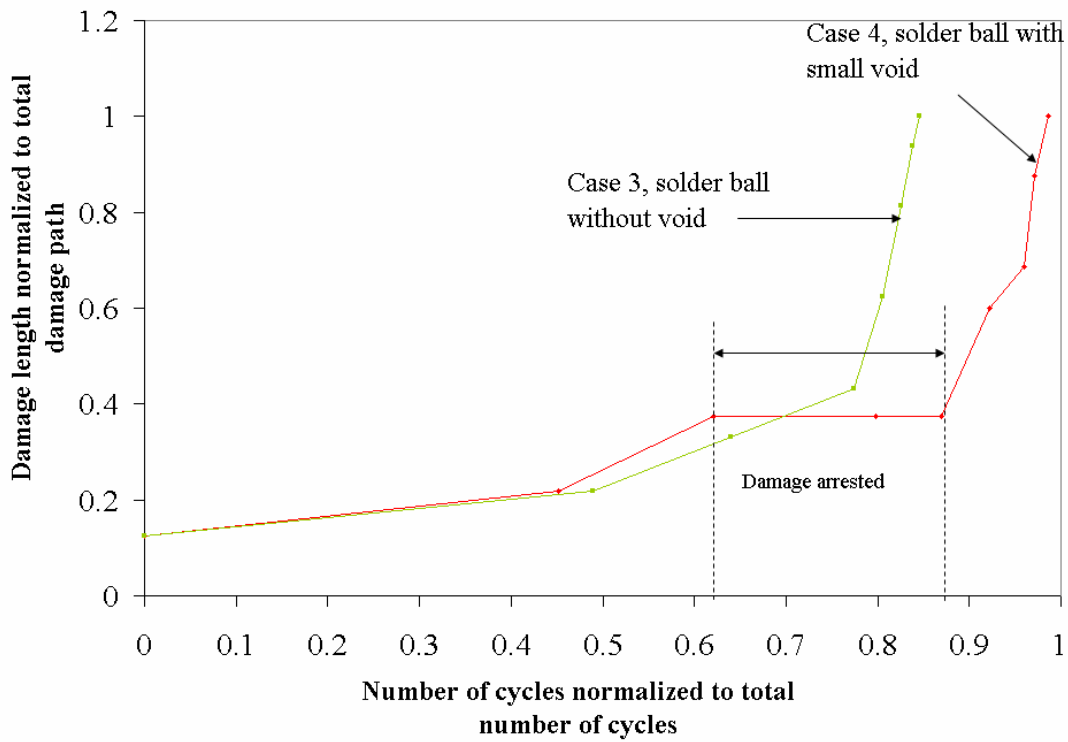


Figure 3-25: Damage propagation length normalized with respect to total path length

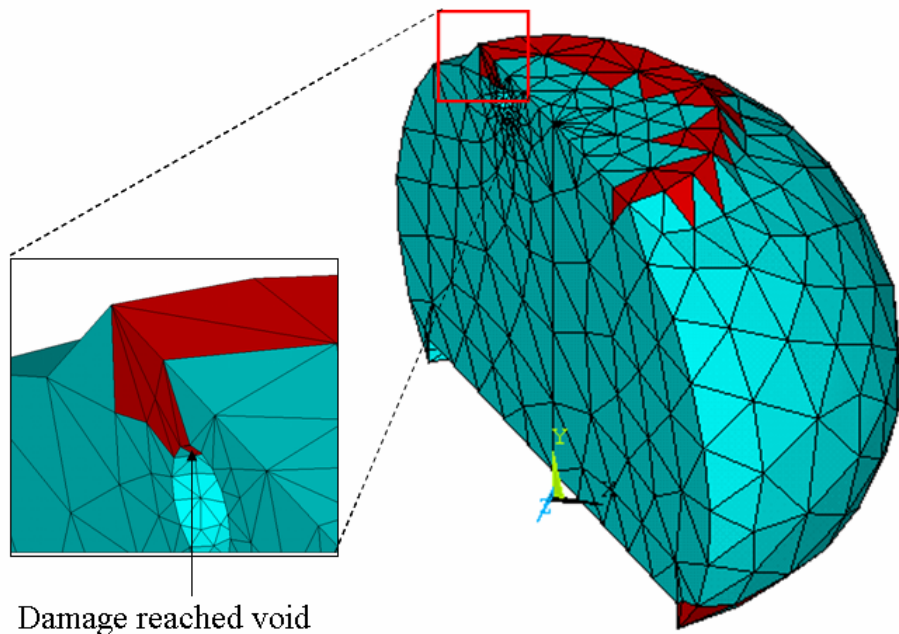


Figure 3-26: Damage propagated in second step of successive initiation, when it reached the void

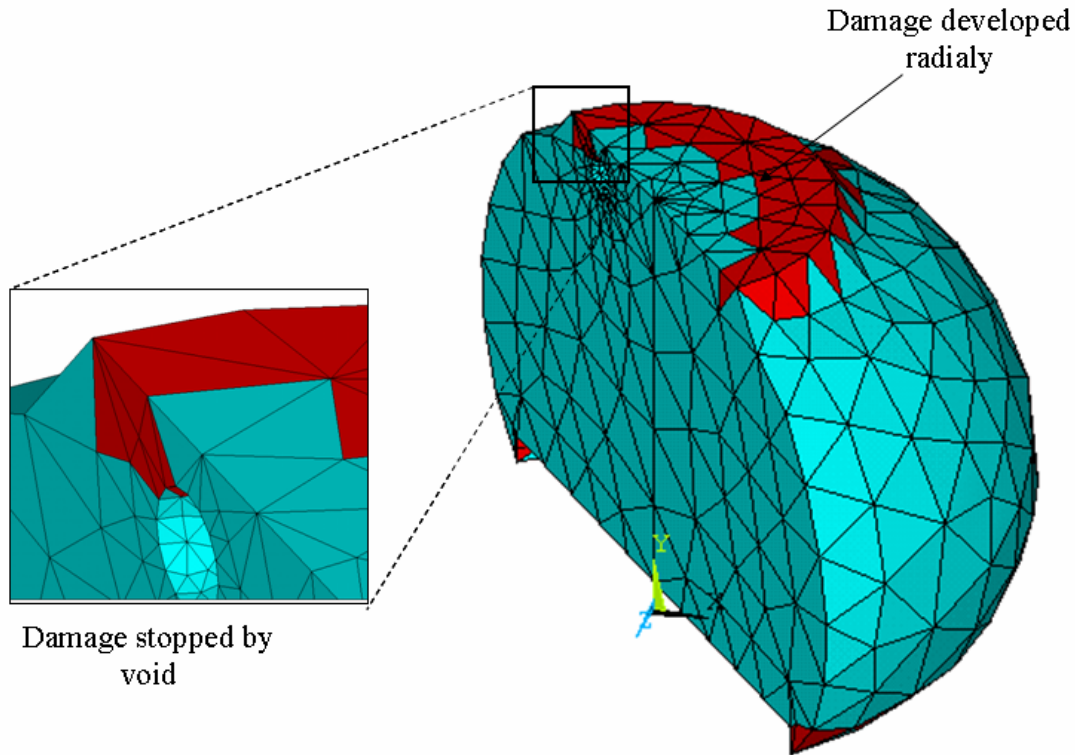


Figure 3-27: Damage propagated in third step of successive initiation, stopped by void locally

### 3.2. Summary and conclusion

This chapter summarizes the procedure of establishing a global local modeling which is used in the next chapter to study the effect of voids parametrically. A successive initiation method is suggested to be used with E-P damage model to predict the damage initiation site and propagation path. Five different cases were selected from experiment to be analyzed using this approach. The result of FEA modeling have been analyzed and compared with experiment. As observed in experiment FEA results also show that small void could delay damage propagation and big void in the middle of solder ball can shorten the propagation time as expected. Interestingly results also show that a big void close to initiation site may delay the initiation by making the solder ball compliant locally. These hypotheses will be discussed in further details in chapter 4.

#### 4. Parametric study of voids

In order to effectively understand the influence of voids, their size, and locations on durability a parametric study of voids in conducted. The chapter contains different approaches used for evaluating the effect of voids. The global local approach explained in previous chapters and successive initiation technique is used to model the solder ball with voids.

##### 4.1.Global modeling of CTBGA132 (Study 1 specimen)

To obtain the correct dimensions of the package for global modeling , one sample was cross sectioned before testing and the dimensions of the package were measured using the cross section a images . The dimensions are shown in Figure 3-6 and values of these dimensions are provided in Table 4-1.

Table 4-1: Dimension of the package in microns

Ball diameter (D)	300
Neck diameter (d)	250
Pad thickness (t2 )	25
Neck thickness (t1)	20
Substrate thickness (t3 )	100
Die-attach thickness (t4)	40
Die thickness (t5)	200
Molding compound thickness above the die (t6 )	260
Pad size (p)	400
Board pad size (d1)	280
Board plating thickness	35
Ball height (h)	137
Board thickness (h1)	1000
Die dimension (L)	5600

Figure 4-1 shows one- eight of a CTBGA component modeled on the PWA. The component has 132 I/O with 0.5 millimeter pitch and is subjected to thermal cycling. The

temperature profile is between -55°C to 125°C with 10°C/min and 6°C/min cooling and heating ramps, respectively. The temperature profile used for modeling is shown in Figure 4-4.

Non-linear viscoplastic finite element analysis was conducted with ANSYS-8. Due to symmetry in geometry, material properties, boundary conditions and loading, a three-dimensional quarter model was built for a CTBGA.

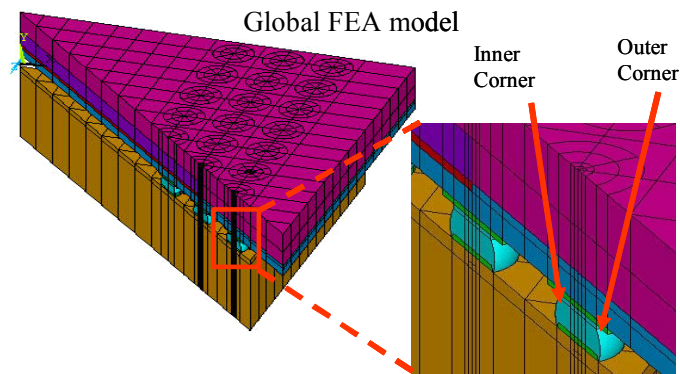


Figure 4-1 Global FEA model for CTBAG132 and the critical ball at the outer corner

An 8-noded solid brick element with linear interpolation functions, which has the capability of modeling plasticity, creep, large deflection and large strain, is used.

The displacement boundary conditions are:

- 1) All nodes on the symmetry surfaces  $x = 0$  and  $z = 0$  are fixed in the  $z$  and  $x$  directions, respectively.
- 2) The node at the origin ( $x = y = z = 0$ ) is constrained in all three directions (refer to Figure 4-3).

Fine meshing is employed for the critical solder joints which are normally located at the outer corners of the package or at the corner of the die shadow. From the four critical

solder balls, only three are selected due to symmetry. The remaining solder joints are meshed with far fewer elements in order to reduce the mesh size & computation time. The total number of elements is about 23,000. Three complete thermal cycles are simulated in order to obtain a stable hysteresis loop for energy computation. The Temperature cycle used is shown in Figure 4-4. All materials, except the solder, are assumed to behave in a linear elastic manner. Solder plastic and creep deformations are assumed to follow the power law equation and the Garofalo secondary creep formula, respectively. Solder material properties are obtained from the literature [Zhang, 2004]. All other package material properties are obtained from the manufacturer, except the PCB properties that have been calculated for a multilayer transversely isotropic laminate. The materials properties are provided in Table 4-2.

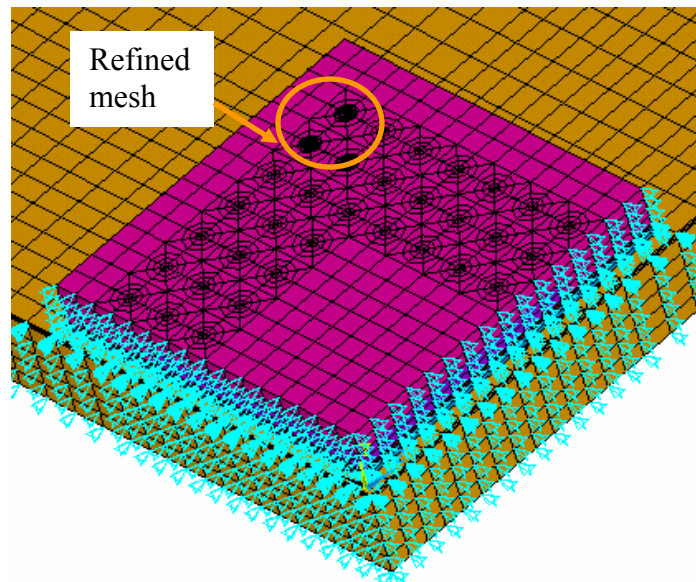


Figure 4-2: Global FEA model for CTBAG132, with applied boundary conditions

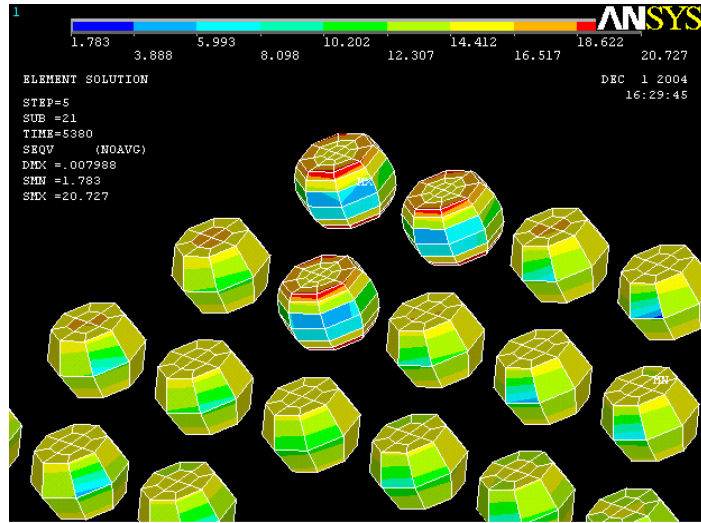


Figure 4-3: Contour plot of equivalent stress in balls

Table 4-2: Material properties used in FEA modeling

Material	Elastic Modulus (MPa)	CTE (ppm/°C)	Poisson Ratio	Shear Modulus (GPa)
PWA in-plane	38E3	15.74	0.38	11.602
PWA out-of - plain	21.7E3	15.9	0.38	2.4
Molding compound	23.6E3-	9	0.3	-
Chip	191E3	2.095	0.28	-
Die attach	1.2E3	110	0.42	-
Substrate (BT material)	17.89E3	12.42	0.3	-
Solder	4.37E4- 22.3T(K)	20.9	0.4	-
copper	13E3	14.5	0.35	-

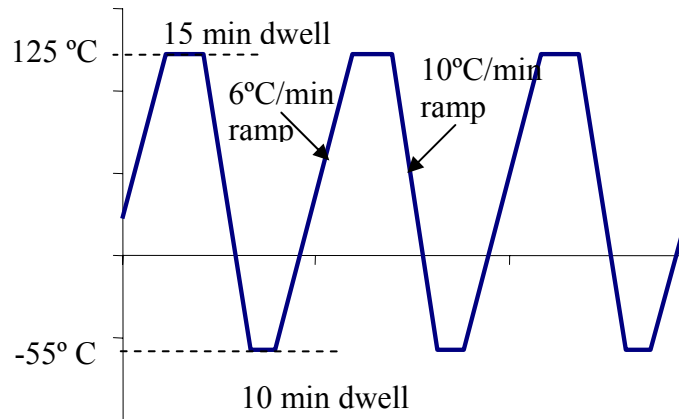


Figure 4-4: Temperature profile used in FEA modeling

The result of the global FEA model shows that the critical ball is located at the outer corner of the package and not at the die shadow. x, y and z displacement at all nodes at the top and bottom of the balls were recorded from time history post processor in ANSYS (Post27) to be applied as a boundary condition to the local model.

#### **4.2. Local modeling of solder balls**

Local model is done at the joint level. A full critical ball model with the copper pad at the top and bottom was created. Ball radius and height are 150 and 137 microns, respectively.

The ball is meshed with free mesh with an average of 4000 elements. Hard points are assigned to the surfaces at the top and bottom of the copper pad at the corresponding global nodes, to assure creation of nodes at those points in the local model. The ball is modeled under the same temperature cycle as the global model, for three consecutive cycles. This procedure is repeated for a “perfect” ball without any voids and a ball with different void sizes at different locations. Figure 4-5 shows a half ball without any voids and with a big void in the middle.

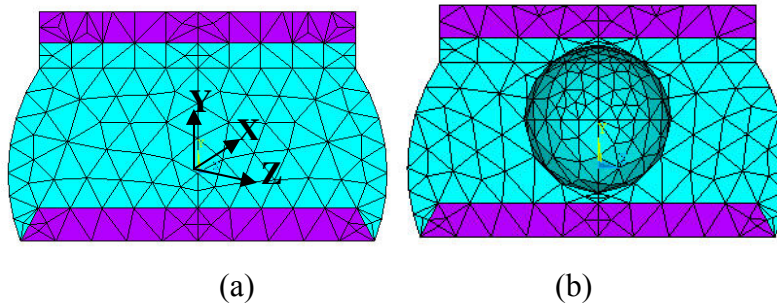


Figure 4-5: Local modeling of the ball (a) without and (b) with voids

A total of 20 different cases were modeled. Each case was modeled with only one void at a time. Voids are located at four corners of the ball as well as middle. Small voids up to an area fraction of 9% were modeled at the four corners of the ball. Big voids with area fractions of 15% were modeled in three different locations in the ball and very big voids with area fractions of 25, 35, 45, and 49% were modeled only in the middle of the ball. Voids are modeled as spheres and in the cases where voids are big, the voids get truncated by the copper pad. Area fraction is defined as the area of the void to area of the ball. In other word, the area of the void is the area of a circle with void radius and area of the ball is area of a circle with radius of the ball. Figure 4-6 shows the cases studied. Table 4-3 shows the nomenclature of geometric configuration. Figure 4-7 shows an example of a meshed ball with void area fraction of 49%.

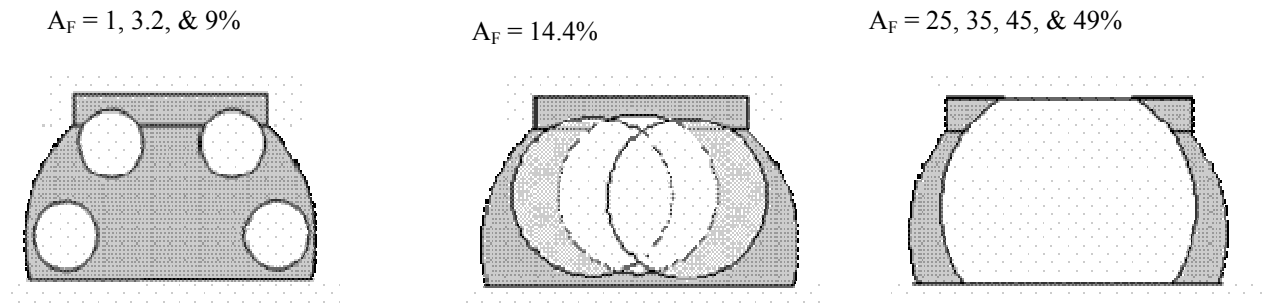


Figure 4-6: Cases studied

Table 4-3: Nomenclature of geometric configuration

Symbol	Description
C-I	Close to component and inner corner of the ball
C-O	Close to component and outer corner of the ball
PWA-I	Close to PWA and inner corner of the ball
PWA-O	Close to PWA and outer corner of the ball
15-C-I	Single void with radius of 15 micron located close to component and inner corner of the ball

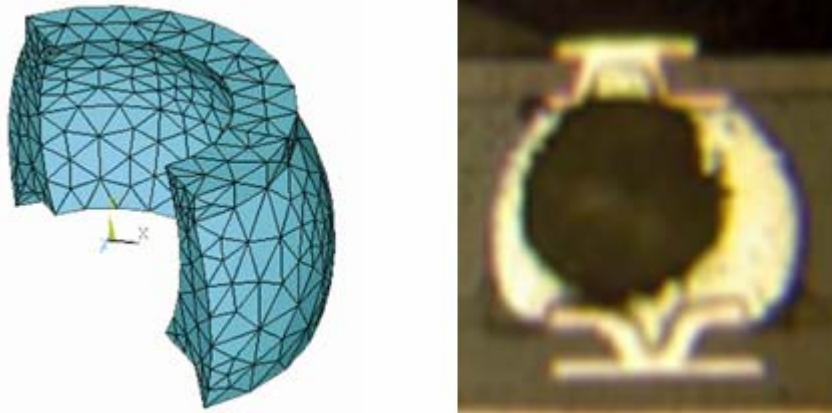


Figure 4-7: Example of void with area fraction of 49% located in the middle of the ball, figure courtesy of Brizoux et al. 2005.

#### 4.2.1. FEA model analysis using averaging technique

Explicitly modeling damage using successive initiation is a very time consuming process. To avoid conducting this process for many cases, first the averaging technique is conducted to identify the critical cases of void location and size. The critical cases then are further studied using successive initiation.

Creep and plastic work densities are monitored in the solder ball for each different case. The Energy Partitioning (E-P) damage model is used to calculate the damage. An ANSYS APDL code is written to calculate and plot the damage for all elements in the ball, based on E-P damage models. The damage constants are obtained from literature [Zhang et al., 2003] and are provided in Table 4-4.

Table 4-4: Thermo-mechanical Energy Partitioning damage model constants for Sn3.8Ag0.7 solder [Zhang et al., 2003]

	Sn3.8Ag0.7 Solder
c	-0.8
W <sub>p0</sub>	198
d	-1.4
W <sub>C0</sub>	1.23E4

A case of a ball without void was modeled and used as a baseline. The durability results of the voided joints are normalized by this baseline case. The result of the base line model shows that E-P damage model predicts that the damage initiates from the inner corner of the ball. Figure 4-8 (a) shows a contour plot of the damage for the baseline case. The initiation site is indicated in a circle.

A strain based damage model is also used to calculate the damage for the purpose of comparison. For this study, the Coffin Manson model is selected in which the total inelastic strain is the damage criteria. This damage model is based on the following equation;

$$N_f = \left( \frac{\Delta \varepsilon_{equ}}{C} \right)^{\frac{1}{n}} \quad \text{Equation (4-1)}$$

Where n and C, Coffin-Manson's durability parameters for Pb-free solder are 1.087 and 11.89 respectively. n and C were calculated by running an ANSYS model and using literature failure data 95.  $\Delta \varepsilon_{equ}$  is the total inelastic strain range in the third cycle.  $\Delta \varepsilon_{equ}$  is calculated by subtracting the equivalent strain at the end of hot dwell from equivalent strain at the end of cold dwell. The total equivalent strain is estimated by summation of



In the case of an un-voided joint, both the EP and the strain-based fatigue models show the maximum damage in the neck to be near the component bond pad, but at opposite corners. The E-P model predicts damage initiation at the inner corner while the strain-based model predicts damage initiation at the outer corner.

The E-P damage modeling based on the FEA shows that maximum damage occurs in the neck of the solder, mostly near the interface of the solder and copper pad, but not around the voids. The only exception is the example case presented here (refer to Figure 4-10), in which the small void is located very close to the site of maximum damage and causes the damage to concentrate around the void.

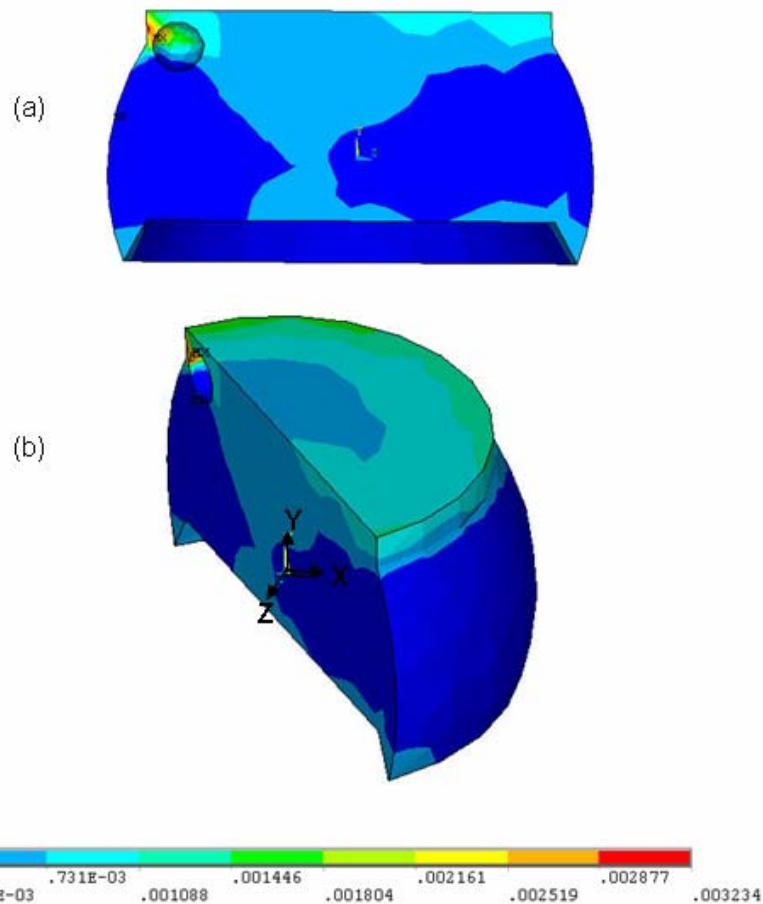


Figure 4-9: E-P damage contour plot in critical solder ball, for small void located at inner corner, towards the component bond pad (a) front view (b) Isometric view

To estimate solder life using the E-P model, the damage has to be extracted from certain elements. Because of singularities in the FEA analysis, assuming only one element is not accurate. Most authors have reported good correlation of the damage models to experiments if the stress, strain and energy values in the neighborhood of the potential failure sites are assessed by employing approximate averaging techniques. In this study, damage was therefore averaged over a circular slice, with thickness of two layers of finite elements centered around the critical site.

This averaging technique is used to predict the life for voided joints based on E-P and strain based methods. These two methods show good correlation as long as the void is small enough to fit inside the ball. As soon as the voids become larger and get truncated by the copper pads, these two method predictions start contradicting. The results of these two methods for voids up to 15% where both methods correlate are provided in Figure 4-11. Figure 4-12 shows a bar chart of the same results obtained for both methods. As it is seen both the E-P method and the strain based method show the same trend.

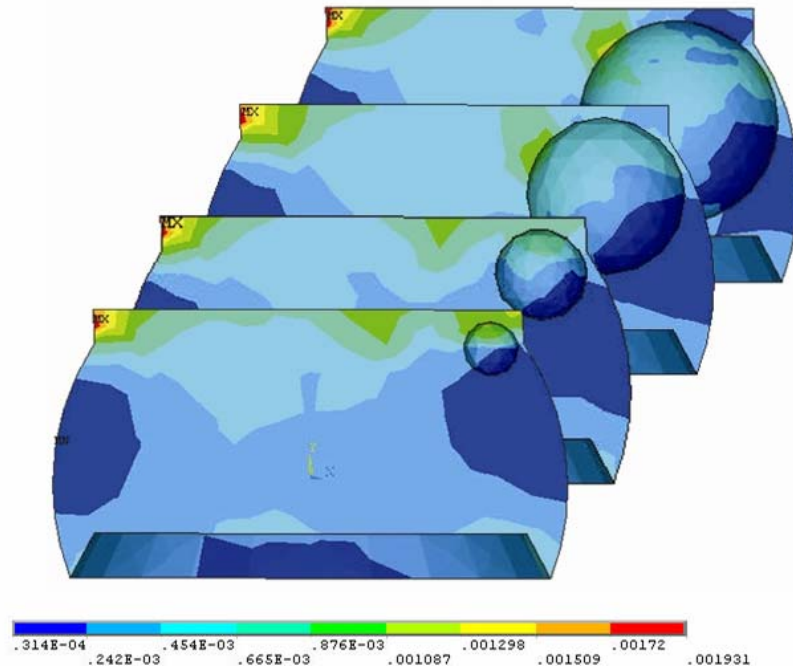


Figure 4-10: Contour plot of damage based on E-P model for ball with different void sizes at the outer corner close to component interface

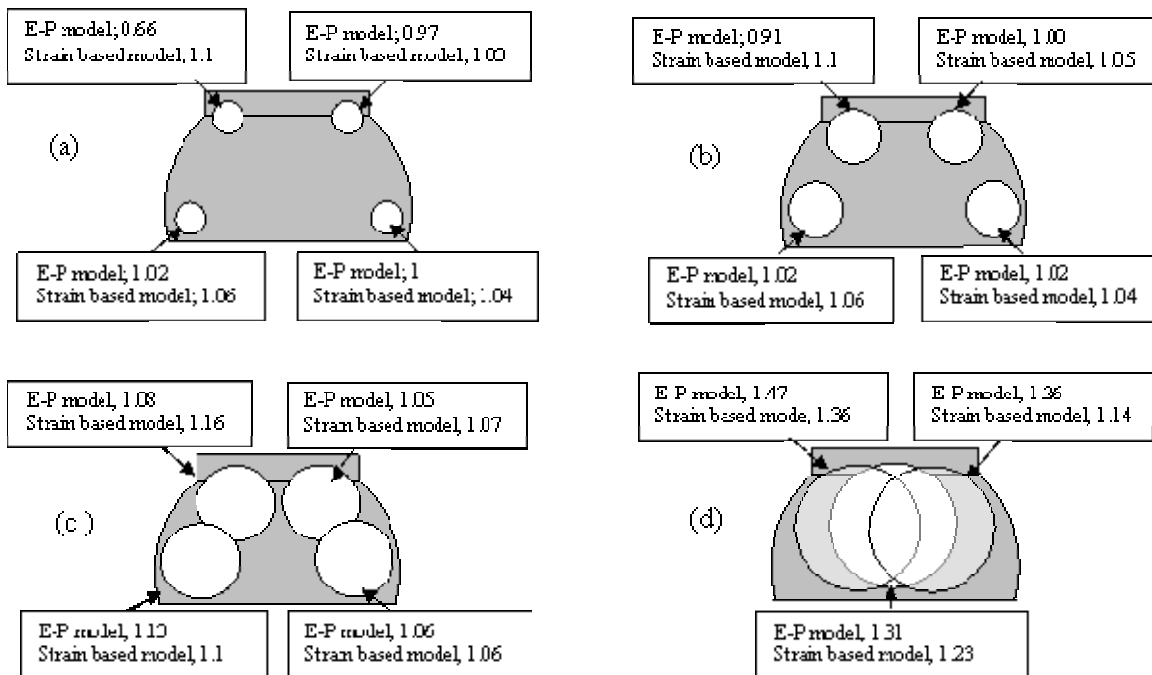


Figure 4-11: Life estimate using E-P model and Strain based model, normalized with respect to un-voided joint with different void  $A_F$  (a) 1%. (b) 3.2% (c) 9% (d) 14.4%

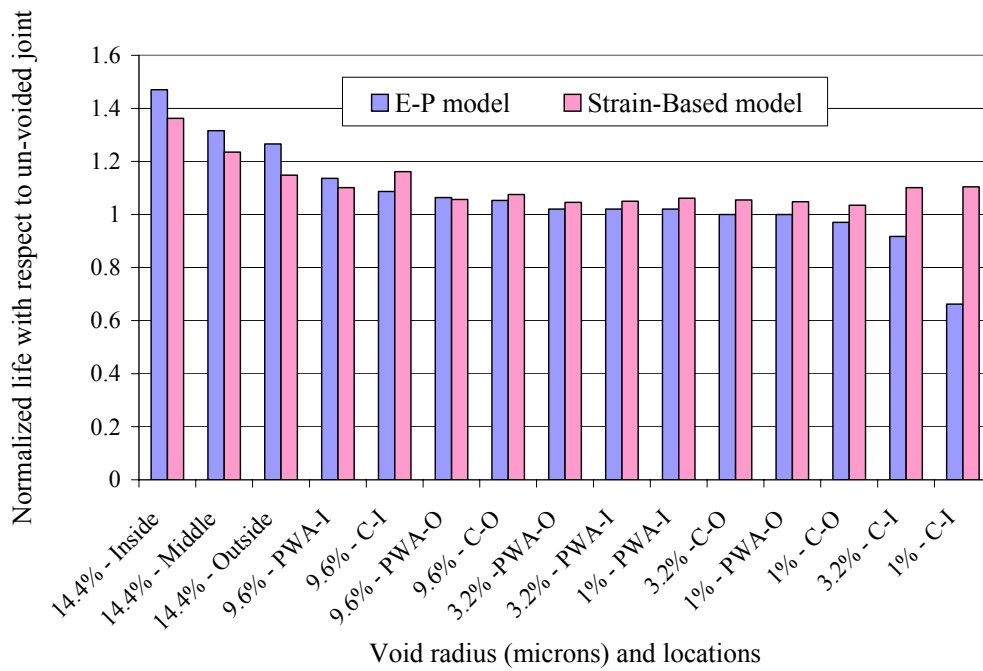


Figure 4-12: Normalized durability for voided joints with different void area fractions; Comparison between E-P and strain based method

Comparison of the results for the E-P model for different void locations shows that as expected, life decreases as the void location approaches the damage initiation site and propagation path. An example is provided in Figure 4-13.

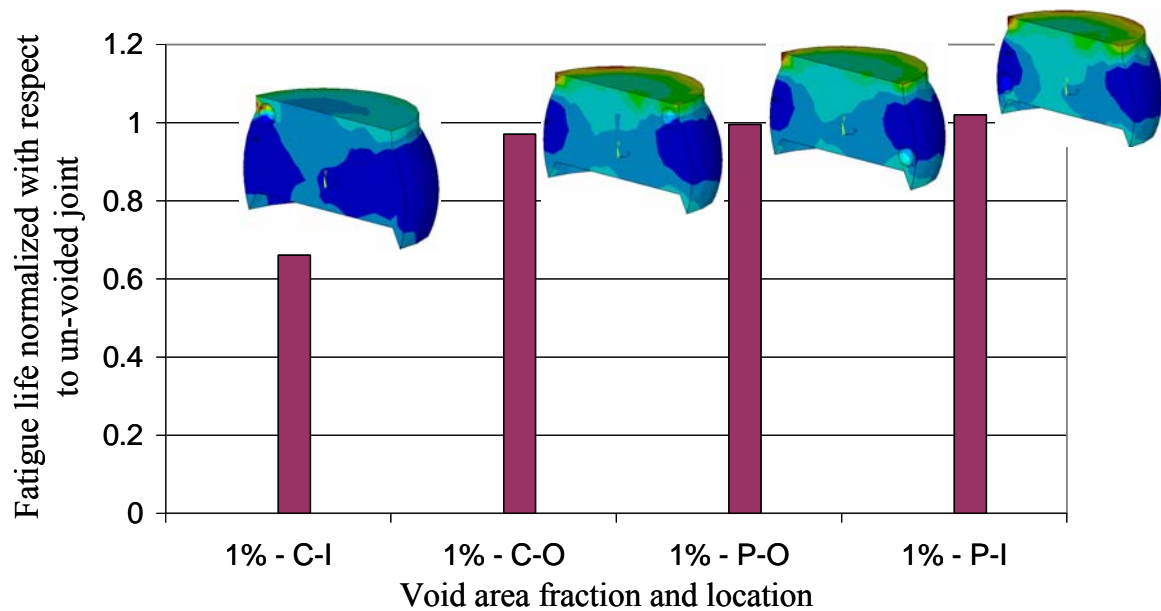


Figure 4-13: Effect of void location on durability

Comparison of the FEA results for the E-P damage model, for voids of different sizes shows that durability is a non-monotonic function of void size. Durability increases with void size up to a void area fraction of 14.4%. For voids bigger than 14.4% life decreases as voids become larger, up to void area fraction of 49%. The results are shown in Figure 4-14.

These results are probably due to the effects of several competing factors. As voids become bigger, the ball structure becomes more compliant and therefore the stress (and energy) reduces, increasing life. As the void area fraction becomes larger than 14.4%, it gets truncated by the copper pad, and the stress concentration around the void at the interface of copper pad and ball increases. The cross sectional area and therefore the crack path decreases. These two factors, increased stress concentration and decreased crack path and cross section area, cause durability to decrease. This hypothesis is illustrated in Figure 4-15.

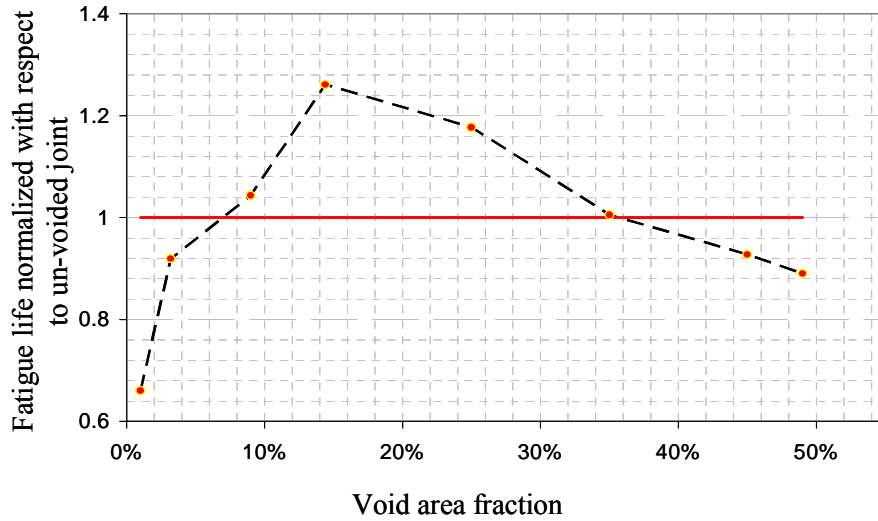


Figure 4-14: Effect of Void Size on durability

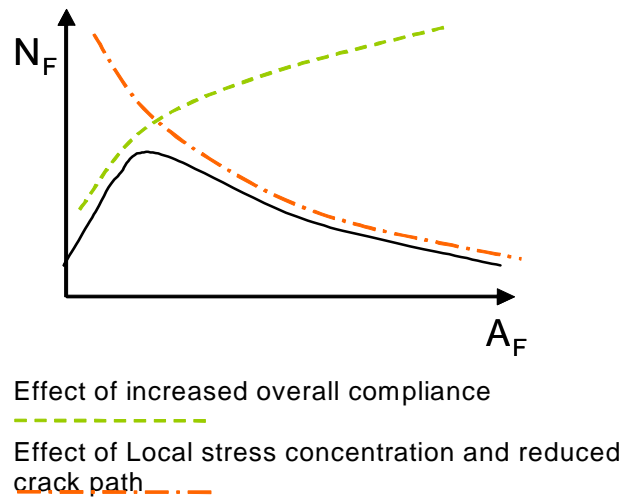


Figure 4-15: Hypothesis of effects of competing factors

Figure 4-16 shows the interaction between void size and location. The overall durability is compared when the void is located close to component pad and PWA pad. The difference between these two cases is seen to decrease as the voids become larger. Therefore, as void size increases the effect of size dominates the effect of location. In

other words, sensitivity of  $N_f$  to the distance of the void from the crack path decreases, as void size increases.

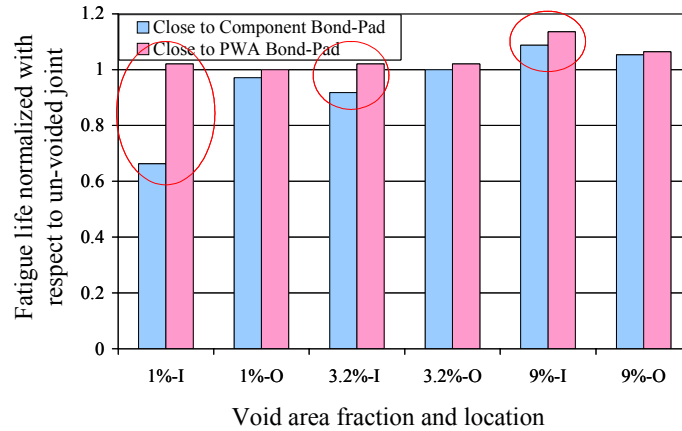


Figure 4-16: Interaction effect between void size and location

#### 4.2.2. Effect of multiple voids

One case was studied with multiple voids located on damage path. The area fraction of small voids was about 36% of that of the ball, and each void had radius of 15 micron. A FEA meshed ball is shown in Figure 4-17. Analysis of the results using the E-P damage model and strain based damage model show significant decrease in life of the joint due to the presence of many small voids. The damage contour plot shows that damage is concentrated in the neck and starts from the inner corner of the ball as shown in Figure 4-18 (a). As shown in the contour, maximum damage is about 0.008. Further evaluation of damage contours for this case shows that the concentration of damage is very high (0.007) and close to maximum damage in regions between voids (Figure 4-18-b). So the probability of damage starting between the voids is very high in the case of multiple voids located on damage path. Explicit modeling of damage propagation shows that

about 50% of elements in the neck of the solder ball are eliminated in the first step, resulting in an unstable structure that cannot stand loading.

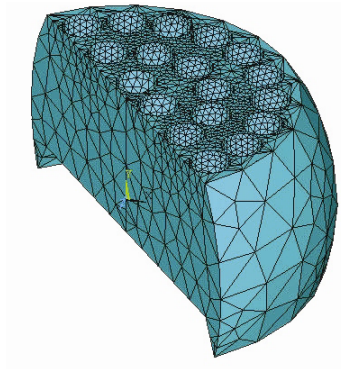


Figure 4-17: Meshed ball with multiple voids on damage path

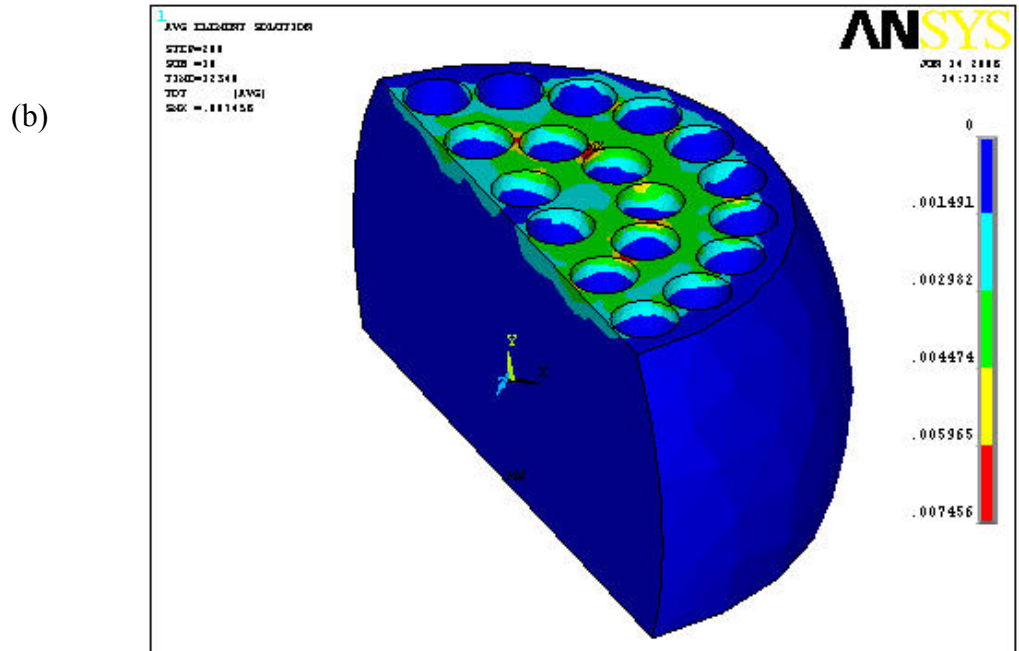
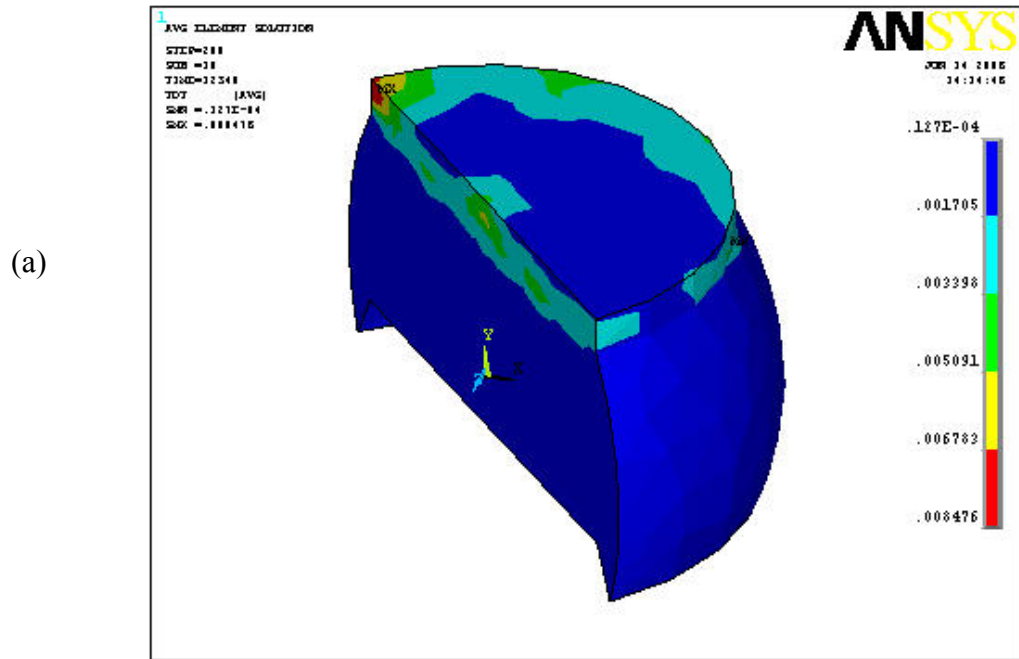
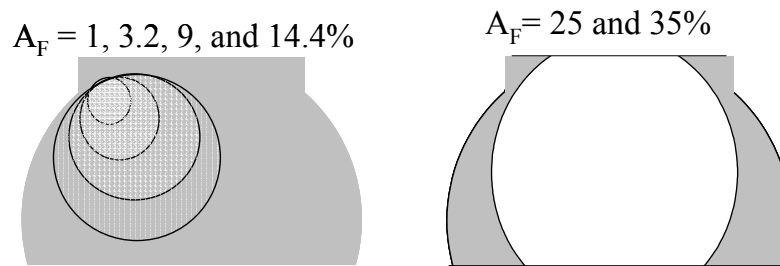


Figure 4-18: Contour plots of damage calculated using E-P damage model in the ball with multiple voids: (a) concentration in the neck, (b) Distribution over the surface and between the voids

### 4.2.3. Investigating voids using successive initiation

Results of FEA modeling using averaging technique indicated that critical location of the voids is on damage path. So 6 more cases with voids with different sizes on damage path were selected to be studied using successive initiation method.

Damage propagation rates were studied using the method of successive initiation, for a ball with 6 different void sizes; (1%, 3.2%, 9%, 14.4%, 25% and 35% area fraction) located along the damage path, close to the damage initiation site. Figure 4-19 shows cases that initially were modeled using Successive Initiation method.



$$A_F = A_{\text{void}}/A_{\text{ball}} * 100$$

Figure 4-19: Cases studied using Successive Initiation Method

The initiation and propagation lives were calculated using the method discussed above and the results were normalized with respect to the void-free case. Figure 4-20 shows the normalized initiation life. For demonstration purposes, a threshold value of 60% of maximum damage is used for the failure criterion, for all cases. This value was chosen for convenience of implementation and its effect will be examined in a future study. As seen in Figure 4-20, the initiation life increases as the void size increases to about 15% area fraction. For voids larger than 15%, the initiation life starts to decrease. The possible reasons for this non-monotonic trend are discussed below.

For void sizes between approximately 1% and 15%, as the void becomes larger the stress is redistributed inside the ball and stress concentration at the initiation site becomes smaller. As a result, initiation life increases. When the void becomes large enough to get truncated by the copper pad, the stress concentration at the initiation site begins to increase again due to reduced load carrying area. Therefore the initiation life decreases.

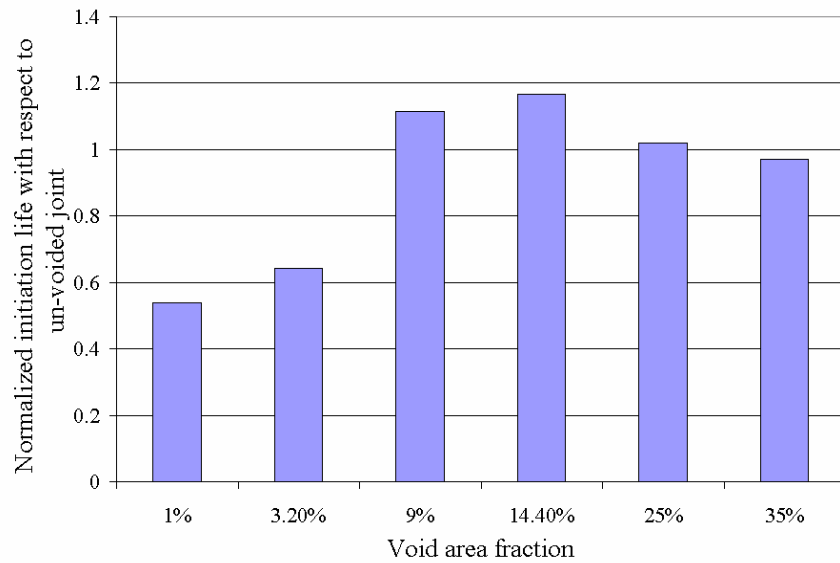


Figure 4-20: Damage initiation life, normalized with respect to results for a void-free joint

The damage propagation life was calculated as discussed in and then normalized with respect to the un-voided case. The result is shown in Figure 4-21. As expected, the propagation life is seen to decrease monotonically as the void becomes larger, due to shortening of the path available for damage propagation.

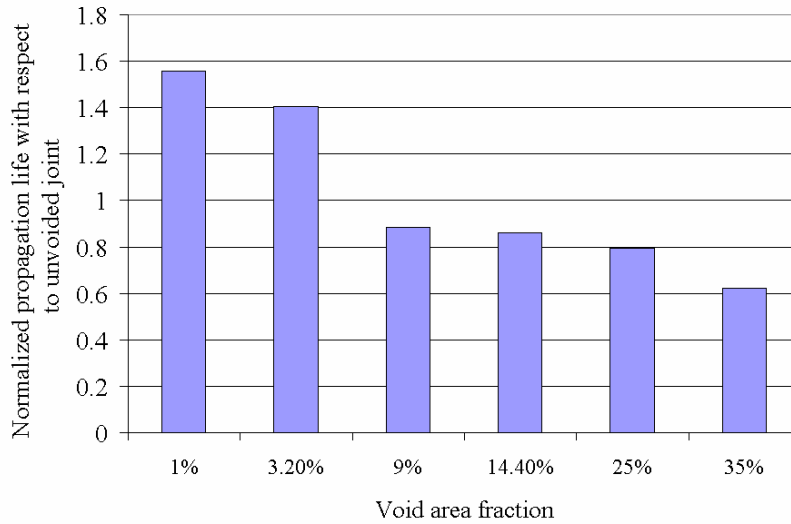


Figure 4-21: Damage propagation life, normalized with respect to results for a void-free joint

An interesting point for this study is that for small voids, the propagation life is longer than for the void-free case. The reason was studied and found to be because of a damage arrest mechanism. In the simulation this was manifested as a drop in the damage propagation rate in the vicinity of the void. Figure 4-22 shows the length of the damaged zone, as a function of cycles. It can be seen that the damage propagation rate decreases around the void. This arrest of the damage propagation rate is a direct result of blunting of the tip size of the damage zone. This is found to be the case for most of the small voids located close to the damage propagation path.

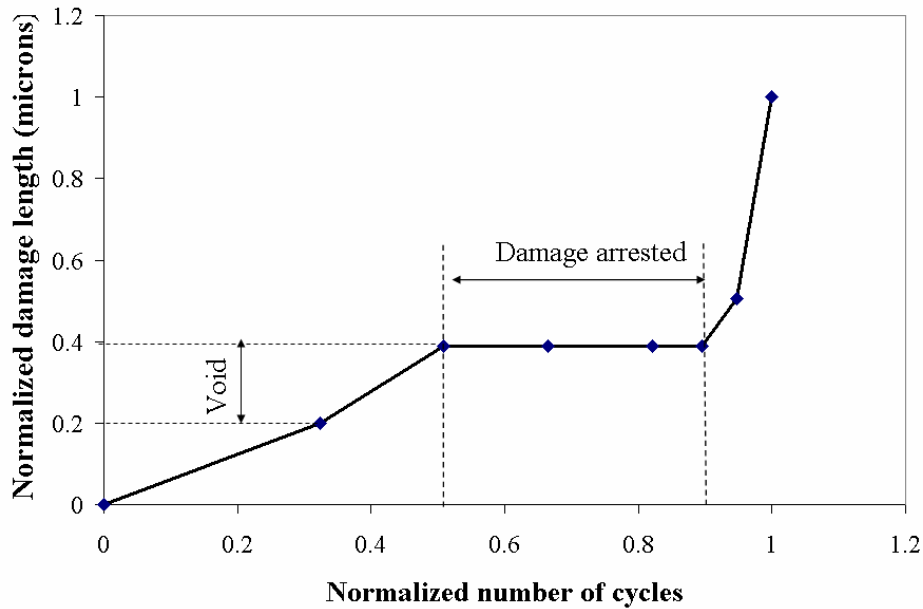


Figure 4-22: Growth of damaged zone with temperature cycling

Total life is obtained by adding the initiation and propagation lives for each case. The results are provided in Figure 4-23 and show that durability is a non-monotonic function of the void size, due to competing effects. The same conclusion was reported by the authors in earlier sections of this chapter, but using an averaging technique instead of successive initiation. For small voids, the initiation life is shorter due to the stress concentration around the void, close to damage initiation site. After the damage initiates, propagation is slowed down by void and therefore the propagation life is increased. In the case of bigger voids (up to approximately 15%) damage initiation life is longer, but due to shorter damage path the propagation life is shorter. Therefore, the summation of initiation and propagation shows a small increase in life with increasing void size (up to approximately 15%). Bigger voids, truncated by the interface, suffer from both effects of shorter damage initiation and shorter damage propagation, which causes the durability to decrease even faster for these voids. The result of this non-monotonic trend is that there

are two regions in Figure 4-23 with reduced durability relative to un-voided joints. These include small voids close to damage initiation site and big voids at the interface of the solder and copper pad.

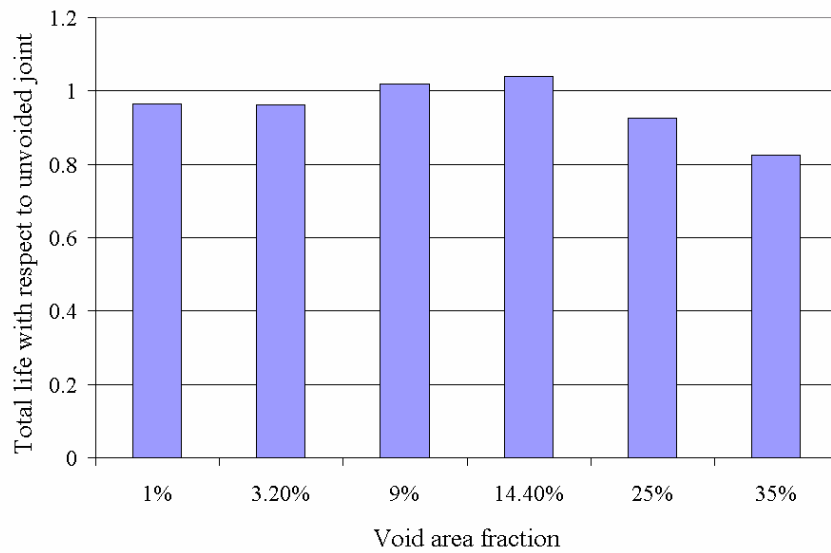


Figure 4-23: Total life normalized with respect to a void-free joint

In order to study the effect of location of void on durability and crack arresting a small void was selected to be modeled in different locations on damage path. 5 different cases have been conducted. These cases are shown in Figure 4-24. The results for durability are shown in Figure 4-25.

Comparison between durability predicted for these cases show that void is not very effective in arresting the crack in further distances from initiation. The main reason is that the damage starts circumferentially and therefore although void helps preventing crack from developing from one side, but the damage continues to grow from other sides. The void in the middle almost has no effect on damage arrest and even decreases the durability very slightly by shortening the damage path. So in general small voids on the

crack path do not help to increase reliability and in some cases when the void is located very close to initiation site, it detracts reliability.

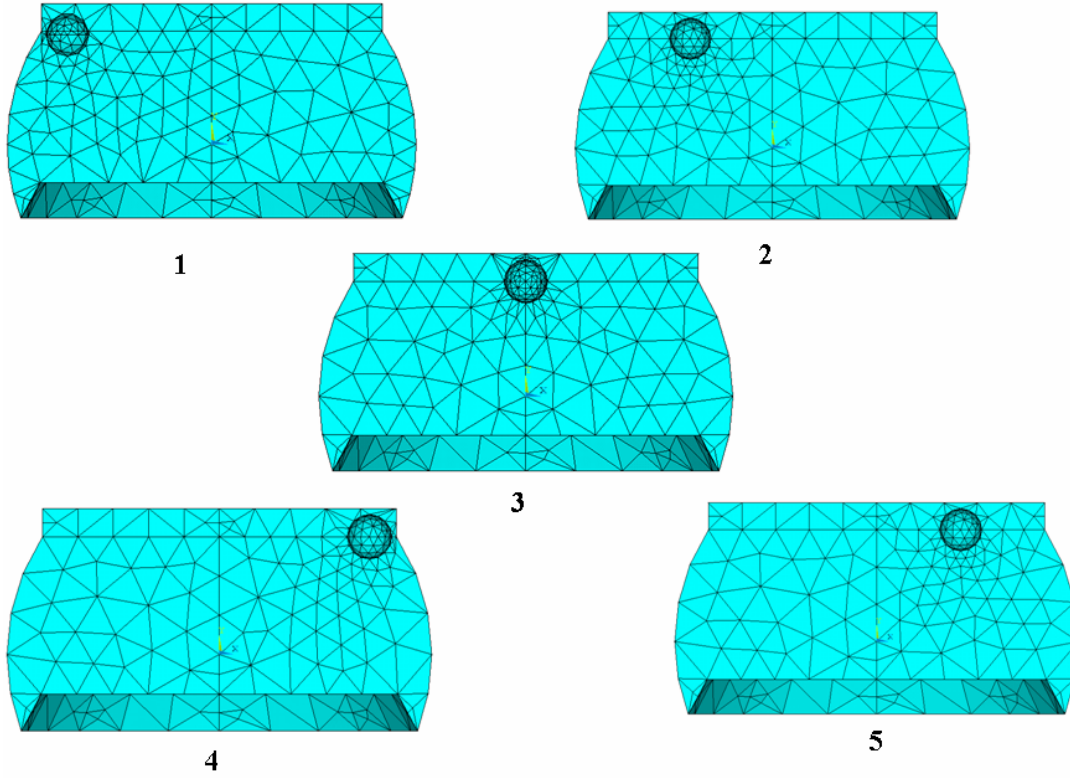


Figure 4-24: Different cases of solder ball modeled with void in different location on damage path

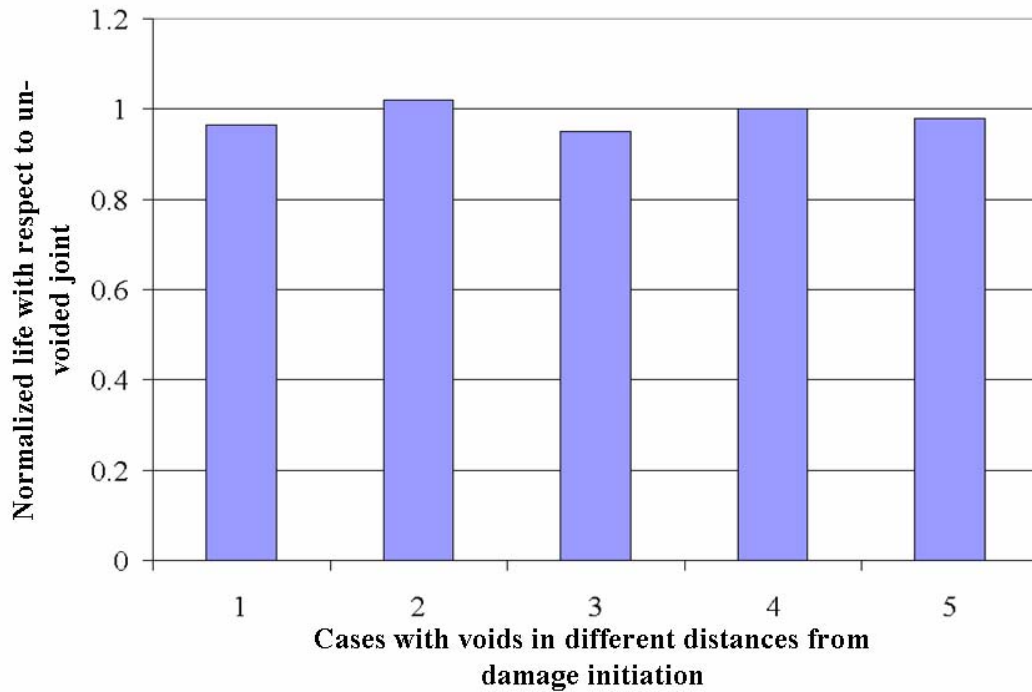


Figure 4-25: Total life for different cases with small void located in different distances from initiation site on damage path

### 4.3. Summary and conclusions

A global-local model was used to study the effect of voids on thermo-mechanical durability of solder ball using Energy Partitioning damage model. The model then was modified by use of successive initiation technique. Damage initiation and propagation times were estimated for different cases with different void sizes. The result of modeling predicts that reliability is not reduced for voids up to 15% of area fraction. However if small voids were located close to initiation site, initiation time was severely decreased and although the small voids helped increase the propagation time by arresting the crack, the total life was reduced by significant reduction in initiation life. Changing the location of the small void does not help to increase reliability since damage develops circumferentially.

This study also showed that many small voids located at the propagation path decrease the life significantly by causing stress concentration between the voids and distributed damage.

## **5. Damage evolution due to cyclic loading**

Conventional mechanics approach assumes that all materials are perfect or defect-free. However, material deterioration and stiffness degradation known as damage is induced due to the change of microstructure in a material element under load.

Material properties change as material goes under cyclic loading. There are several factors contributing to this change. For polycrystalline material cyclic loading sometimes causes coarsening. It also causes micro cracks and voids to initiate and propagate.

### **5.1. Problem statement**

Due to damage caused by creep and fatigue the material degrades, the load bearing capacity of the material reduces and constitutive properties of material changes. This is seen in the literature that for example Young's modulus of SAC solders material decreases as the number of thermo-mechanical cycling increases 93. The other constitutive properties of material also changes as function of number of cycles.

Figure 5-1 and Figure 5-2 show examples of damage observed in two different solder materials. As it was mentioned in previous chapters, conventional fatigue modeling does not consider damage evolution due to thermo-mechanical or isothermal cycling and consider the material properties to be constant during the cycling. These conventional models are usually calibrated to experiment and can predict the durability fairly well in most of the cases. However, these constants are not applicable when the initiation and propagation are studied separately. For example using E-P damage model constants in successive initiation may result in an inaccurate prediction since the E-P constants are not mean to model initiation and propagation separately. It also makes more sense to include all the physical phenomenon that happens in real applications. One of the important events that is mostly neglected in modeling is cyclic damage or softening of material.

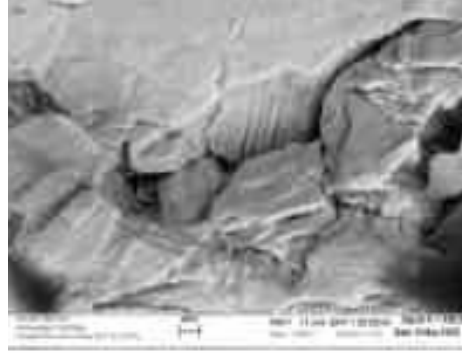


Figure 5-1: Extrusion and damage observed for Sn3.5Ag after 350 thermal cycles 82

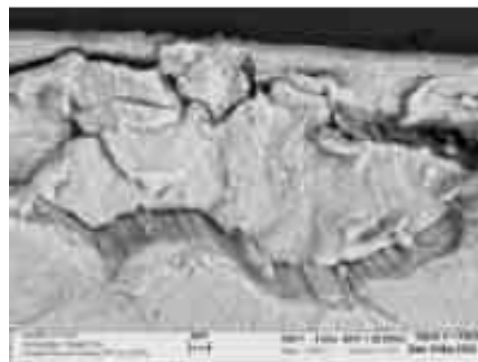


Figure 5-2: Extrusion and damage observed in Sn3.9Ag0.7Cu after 290 thermal cycles 82

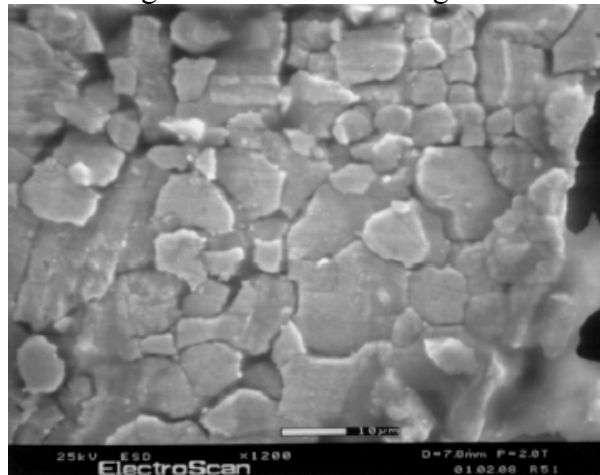


Figure 5-3: Post test ESEM micrograph of Sn3.9Ag0.6Cu solder joint (high creep cyclic conditions 125°C, 7.9 % inelastic strain range control  $4.5 \text{ E-4 S}^{-1}$  shear strain rate, 55% total load drop) [Zhang, 2004]

In order to accurately predict the life of joints in the package, the degradation of material also has to be considered in modeling especially when a successive process is used. Due

to the following reasons the approaches mentioned in literature review section is not applicable to this study:

- The approach was proposed for Sn-Pb solders and constants derived not applicable for Pb-free solders such as Basaran, et al., Huang, et al.
- The approach only modeled dislocation motion and thus only modeled damage caused by plastic deformation such as micro-mechanic approach used by Keer et al. and Huang, et al.
- The approach was not a mechanistic approach, was for a very limited strain range and rate, or it was coupled in a unified damage model such as keer, et al., Chaw, et al., and Ernic et al.

There is still need for a simple experimental approach that is convenient and can be used for broader range of applications.

An experimental approach is proposed here to estimate the degradation in material and change in constitutive properties of solder due to thermo- mechanical cycling. An Energy Partitioning Damage Evolution Method (EPDE) is proposed to be coupled into energy partitioning damage model and predict the material degradation using plastic and creep work densities dissipated in the first few cycles of cyclic loading. Next section explains this method in more details.

## **5.2. Energy Partitioning Damage Evolution (EPDE) method**

The idea of Energy Partitioning Damage Evolution Method was inspired by Wen and Keers work [Wen et al., 2001] on micro-mechanics of Pb-free solders, where damage was considered to have a power law relationship with the number of cycles. The power law

relationship of damage with number of cycles was also mentioned by Kachanov long before that. The relationship is defined as follow:

$$\left(\frac{D}{D_c}\right) = \left(\frac{w}{w_c}\right)^\eta \quad \text{Equation (5-1)}$$

Where  $D$  is damage ratio in this study,  $D_c$  is critical damage and  $w$  is the portion of grains that are damaged and  $w_c$  is the percolation limit according to the percolation theory [Wen et al., 2001]. The metric  $w$  grows with the cycle number  $N$  and micro-cracks percolate within the material until  $w = w_c$  at which point the structure becomes unstable of completely damaged.

This relationship is plotted in Figure 5-4 for different values of  $\eta$ . The value of  $\eta$  depends on the material and assumed to be constant for specific material.

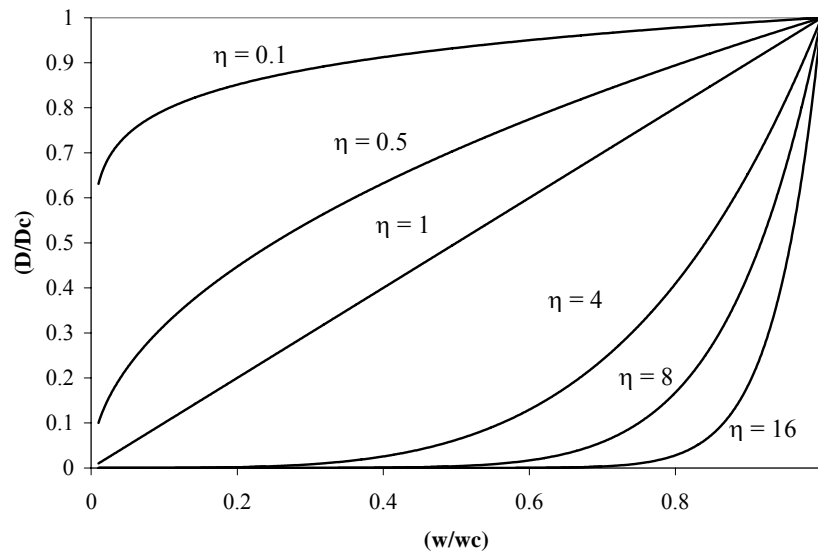


Figure 5-4: Plot of  $D$  Vs.  $w$  for different values for  $\eta$

The number of cycles is related to  $w$  through the following equation [Wen et al., 2001]:

$$\left(\frac{N}{N_f}\right) = \left(\frac{w}{w_c}\right) \quad \text{Equation (5-2)}$$

Wen and Keer used a micromechanics approach based on Mura and Nakasone's [Mura and Nakasone, 1990] dislocation model to predict the micro-crack density and then calculate  $w$ . Even though some of creep deformation in Pb-free solders is caused by dislocation motion (climb), there is also possibility of diffusion. Mura and Nakasone's dislocation model is used mostly for only plastic deformation. In other words, Wen and Keer failed to include damage caused by creep. There is also another issue with the model where they assumed  $\eta = 1$ , or linear damage evolution, which will be discussed and modified in later sections.

Inspired by this model and the point that plastic and creep deformation result in different types of material damage as seen in various partitioned damage models such as, Strain Range Partitioning [Halford et al., 1992] and Energy Partitioning damage model [Dasgupta et al, 1992], a mechanism based model was proposed to include both plastic and creep damage in separate terms.

Based on this model Damage is broken into two parts; damage caused by plastic deformation and damage caused by creep deformation as follow:

$$\left(\frac{D}{D_c}\right) = \left(\frac{N}{N_{f_p}}\right)^{\eta_p} + \left(\frac{N}{N_{f_c}}\right)^{\eta_c} \quad \text{Equation (5-3)}$$

Where  $D$  is called damage ratio,  $D_c$  is critical damage ratio,  $N$  is number of cycles,  $N_{f_p}$  is number of cycles to failure for plastic damage,  $N_{f_c}$  is number of cycles to failure for creep damage,  $\eta_p$  and  $\eta_c$  are damage exponents for plastic and creep that can be obtained by fitting experimental data.

$N_{fp}$  and  $N_{fc}$  can be calculated using Energy Partitioning Damage model as it was explained in former sections according to the following equations:

$$N_{fp} = \left(\frac{W_p}{W_{p0}}\right)^{1/c} \quad \text{Equation (5-4)}$$

$$N_{fc} = \left(\frac{W_c}{W_{c0}}\right)^{1/d} \quad \text{Equation (5-5)}$$

In earlier sections Kachanov [Kachanov, 1986] definition of damage was mentioned. The same definition for damage is used in this context which is load drop or decrease in load bearing. The main assumption here is that damage develops isotropically. Therefore load drop can be assessed as a metric for damage.

### **5.2.1. Experimental Approach**

The experiment was conducted by Zhang, and Dasgupta [Zhang et al, 2003]. The result of the experiment was used to develop the damage function. The experiment was performed on a custom test setup. Thermo-mechanical Micro-scale (TMM) setup designed by Haswell [Haswell, 1999]. This setup is designed to conduct monotonic test as well as cyclic test. The important feature of this test setup is that the size of specimen is very small and so can represent the scale in real application of solder joints in micro electronics [Zhang, 2004]. Due to small size of the solder, and to provide gripping area, the solder is soldered to two small copper plates. An Iosipescu specimen was used for this test. The dimension and shape of the specimen is shown in Figure 5-5. The test setup is shown in Figure 5-6. The test setup is designed to cycle the specimen under different loading conditions and rates. It can hold the total or inelastic strain range constant.

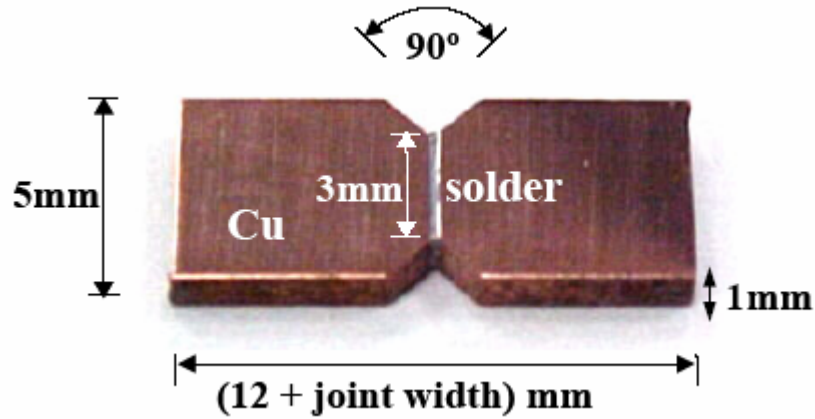


Figure 5-5: TMM specimen schematic [Zhang, 2004]

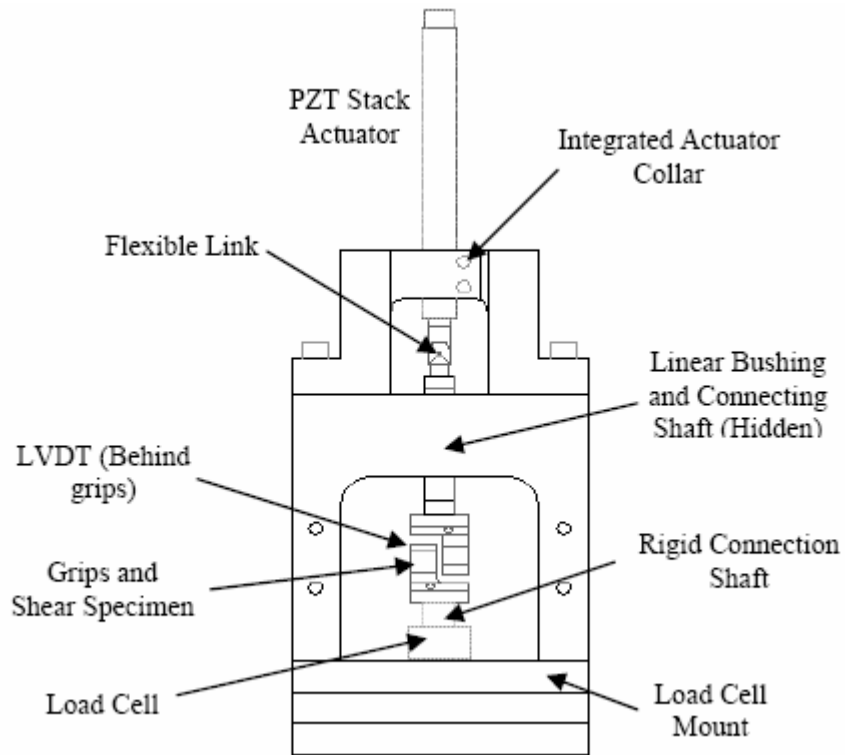


Figure 5-6: TMM test frame [Zhang, 2004]

Strain and stress can be measured using the TMM test set up. Zhang finished cycling of material in different inelastic strain ranges in two different temperatures. Since the mechanism of damage is different for plastic and creep deformation it is desirable to choose a test condition to isolate these two effects. To isolate the plastic and creep

deformations, Zhang carried the test at two different temperatures; room temperature and very high strain rate to minimize the creep and at 125°C and very low strain rate to maximize the creep. He referred to the first condition as creep minimized or regime one and to the second condition as creep maximized or regime two.

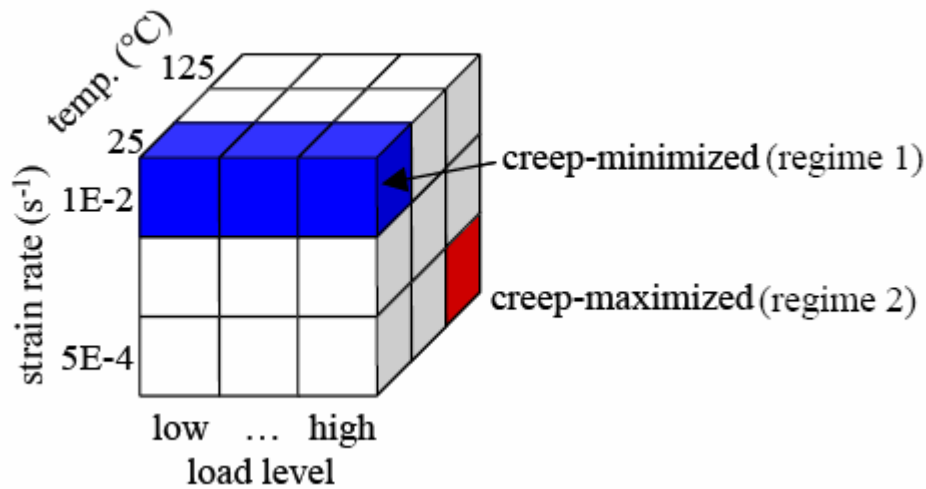


Figure 5-7: Tex Matrix used in Zhang Studies [Zhang, 2004]

Outcome of Zhang test was used to derive  $\eta$  for plastic and creep damages.

### 5.2.2. Analysis of Result of Experiment

Figure 5-8 shows an example of hysteresis loop for a Pb-free specimen for different number of cycles. Load drop is defined as:

$$\phi_N = \frac{P_{MAX} - P_N}{P_{MAX}} \quad \text{Equation (5-6)}$$

Where the load drop parameter is  $\phi_N$  at cycle N is determined by  $P_N$  the amplitude measured at cycle N and  $P_{MAX}$  is the maximum cyclic amplitude measured at within the first few cycles of the test. As seen in Figure 5-8 the maximum stress or load drops as the

number of cycles increase. In this context damage is defined as amount of load drop according to Kachanov. The failure criterion is considered 50% of load drop. Zhang evaluated the durability models with different load drop levels (50% to 80%) and concluded that durability exponent does not change with different load drop criteria but durability coefficient increases monotonically and that 50% load drop failure criterion is enough to capture major characteristic of durability of solder materials. Thus in this context the critical damage is considered to be 0.5. Figure 5-9 shows a typical load drop curve versus number of cycles when the inelastic strain range is kept constant.

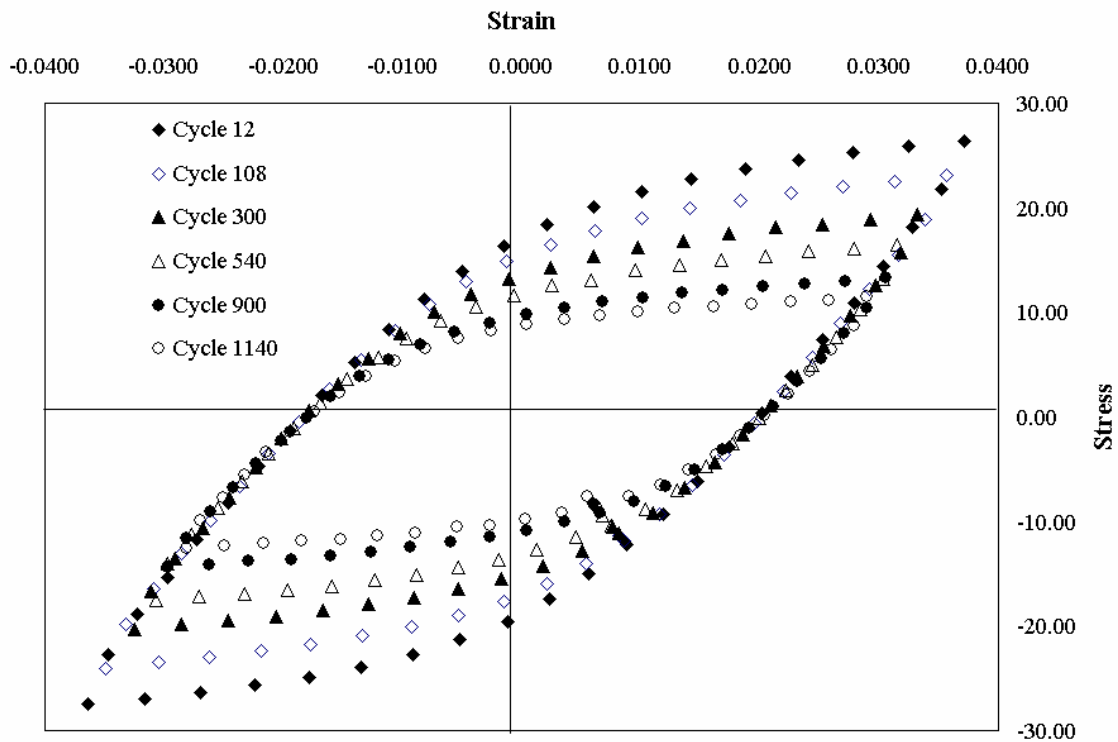


Figure 5-8: Example of Hysteresis loops at 25°, strain rate of 0.05 s<sup>-1</sup> and inelastic strain range of 0.04

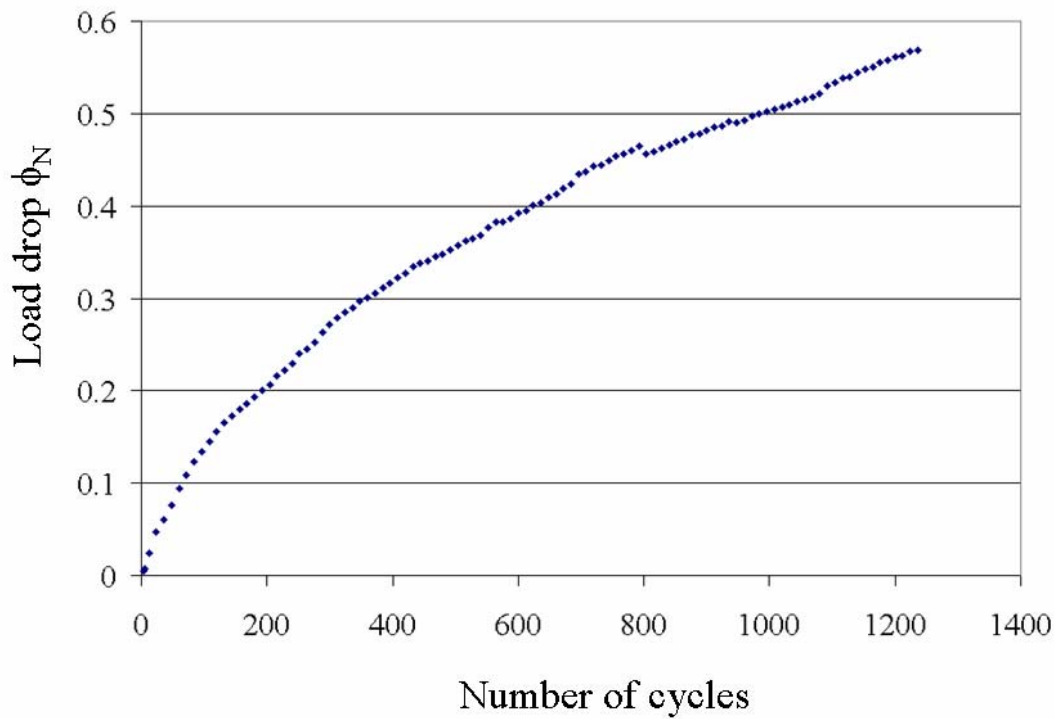


Figure 5-9: Typical load drop observed in cyclic loading

As it was mentioned earlier the test was conducted in two regimes, low creep and high creep. Calculating creep at low temperature and high strain rates used in this test show that creep deformation is negligible and therefore for the low minimum creep regime the creep has been ignored. So the damage equation can be limited to only plastic term as follows:

$$\left(\frac{D}{D_c}\right) = \left(\frac{D}{0.5}\right) = \left(\frac{N}{N_f}\right)^{n_p} \quad \text{Equation (5-7)}$$

Where  $N_f$  is the number of cycles at which the load drop is 50% or damage ratio is 0.5.

Taking logarithm of both side of the equation will result in:

$$\log\left(\frac{D}{D_c}\right) = \eta \log\left(\frac{N}{N_f}\right) \quad \text{Equation (5-8)}$$

The slope of the linear plot of this equation is  $\eta$  which is intended to be calculated for this study. The value of  $\eta$  is considered to be 1 in Wen and Keer's study. However the result of the test shows disagreement with this value. As it is seen in Figure 5-10, the value of  $\eta$  is varied for different inelastic strain ranges. The value of  $\eta$  is believed to be constant [Wen and Keer, 200391 for specific material. Therefore the average of the values is used for  $\eta$  which is 0.47.

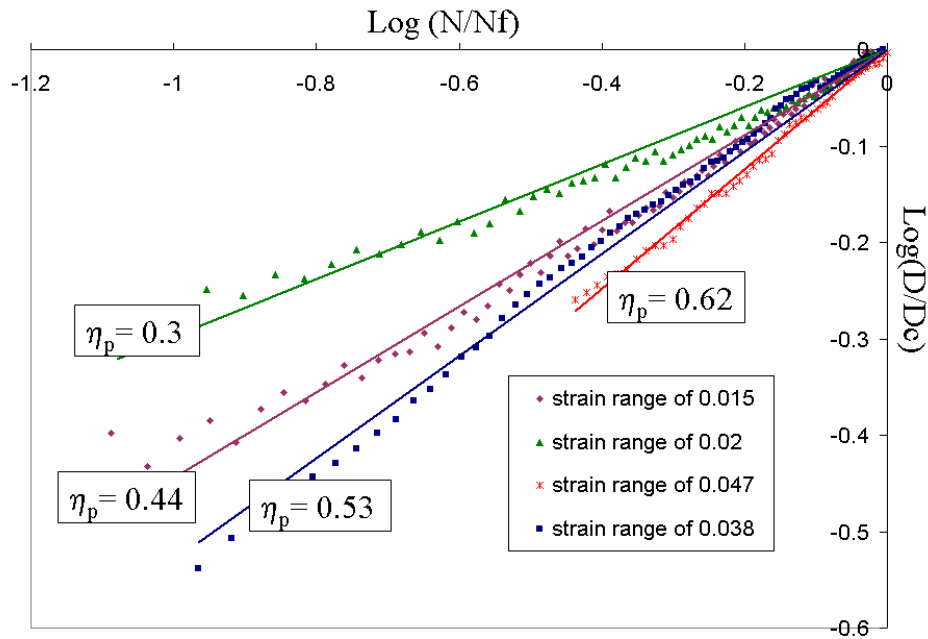


Figure 5-10: Logarithmic plot of damage versus number of cycles to failure

For the second regime of high creep, the main equation has to be used. In this regime the creep deformation cannot be ignored. The value of  $\eta_p$  is kept constant between these regimes.

$$\left(\frac{D}{D_c}\right) = \left(\frac{N}{N_{fp}}\right)^{n_p} + \left(\frac{N}{N_{fc}}\right)^{n_c} \quad \text{Equation (5-9)}$$

The values of  $N_{fp}$  and  $N_{fc}$  are calculated using energy partitioning model which was introduced in previous sections. Isothermal mechanical damage constants are used to calculate the values of  $N_{fp}$  and  $N_{fc}$  according to the following equations:

$$N_{fp} = \left(\frac{W_p}{W_{p0}}\right)^{1/c} \quad \text{Equation (5-10)}$$

$$N_{fc} = \left(\frac{W_c}{W_{c0}}\right)^{1/d} \quad \text{Equation (5-11)}$$

$c$ ,  $W_{p0}$ ,  $d$  and  $W_{c0}$  E-p damage constants for isothermal mechanical cycling that have been generated by the same set of data and are available in literature [Zhang et al., 2003].

The constants for these equations for Pb-free solder have been obtained from literature [Zhang et al., 2004] and provided in Table 5-1.

Table 5-1: Isothermal-mechanical constants for Sn3.9Ag0.6Cu

c	-0.46
$W_{p0}$	72.7
d	-0.9
$W_{c0}$	174.6

To calculate the plastic and creep work densities the hysteresis loop was modeled using a 1 dimensional analytical model [Zhang, 2004]. The model is shown in Figure 5-11. The solder is considered to have elastic, plastic and creep deformations and each type of deformation is modeled using a mechanical part. The strain is calculated using the following equation:

$$\gamma = \frac{\tau}{G} + C_p(\tau)^n + \int_{t=0}^t A \sinh(\alpha\tau)^n \exp\left(\frac{-Q}{RT}\right) dt \quad \text{Equation (5-12)}$$

Constitutive properties for this model was obtained from literature and calibrated to the test. For details about this model please refer to Zhang, 200495. The work densities were calculated by integrating the hysteresis loop.

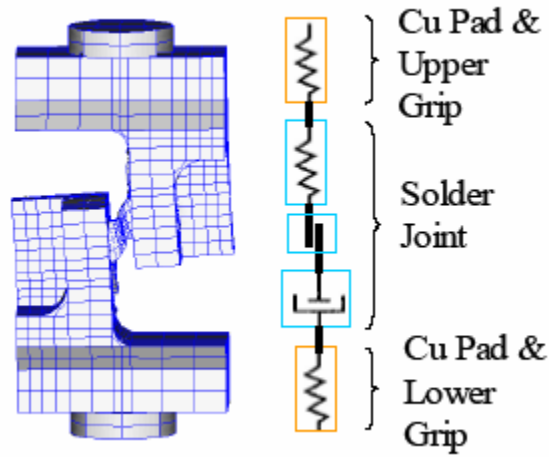


Figure 5-11: Schematic of Analytical model used in TMM test

Having  $N_{fp}$ ,  $N_{fc}$ ,  $N$ ,  $D$ ,  $D_c$  and  $\eta_p$ ,  $\eta_c$  can be easily calculated using the following equation:

$$\log\left(\frac{D}{D_c}\right) - \left(\frac{N}{N_{fp}}\right)^{\eta_p} = \eta_c \log\left(\frac{N}{N_{fc}}\right) \quad \text{Equation (5-13)}$$

As seen in Figure 5-12, the value of  $\eta_c$  is in the range of 0.47 to 0.57. The average value of  $\eta_c$  is 0.52.

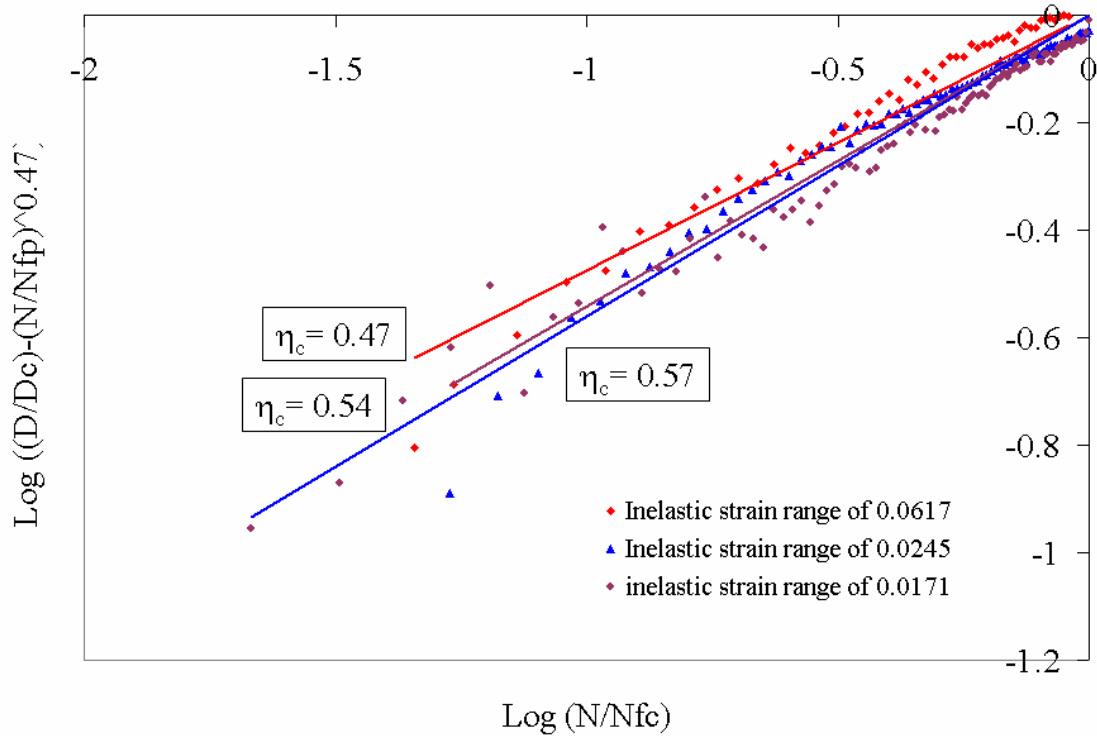


Figure 5-12: Plot of  $\eta_c$  for different values of inelastic strain ranges

### 5.2.3. Implementation of damage evolution approach

In this section the approach introduced and explained in last sections is implemented in a FEA model and predicted life is compared with the case without damage evolution approach.

Critical solder ball in CTBGA132 package was selected to be modeled with successive initiation, with and without damage evolution. Successive initiation technique with E-P damage model was used to predict the life.

In order to include damage evolution and cyclic softening in successive initiation the material constitutive properties are to be updated in each step of process.  $D$  is calculated using Equation 5-9.  $N_{fp}$ ,  $N_{fc}$ , used in this equation are determined using the FEA

analysis and averaging technique. That means that  $N_{fc}$  and  $N_{fp}$  are calculated by averaging energy densities over 10% of volume of the solder joint around the critical site. E-P isothermal mechanical damage constants are used to predict  $N_{fp}$ , and  $N_{fc}$ .  $D_c$  as mentioned earlier is considered 0.5 for this study. D or damage ratio is calculated in each step of successive initiation using the following equation:

$$\left(\frac{D}{D_c}\right) = \left(\frac{N}{N_{fp}}\right)^{n_p} + \left(\frac{N}{N_{fc}}\right)^{n_c} \quad \text{Equation (5-14)}$$

$N_{fp}$  and  $N_{fc}$  are calculated based on averaging technique by averaging work densities over 10% of volume around the critical site.

Softening is caused by damage in material, thus changing the constitutive properties of material. These changes are taken into account by incorporating damage into constitutive properties. If  $\tau_0$  is related to undamaged material and  $\tau$  shows the stress in damaged material then:

$$\tau = \frac{\tau_0}{(1-D)} \quad \text{Equation (5-15)}$$

$$\gamma = \frac{\tau_0}{(1-D)G_0} \quad \text{Equation (5-16)}$$

$$G = G_0(1-D) \quad \text{Equation (5-17)}$$

Where  $G_0$  is shear modulus for undamaged material and  $G$  is the shear modulus of damaged material. Plastic coefficient also can be found as follows:

$$\gamma = \left(\frac{\tau}{C_p}\right)^{1/n} \quad \text{Equation (5-18)}$$

$$\gamma = \left(\frac{\tau_0}{C_p(1-D)}\right)^{1/n} \quad \text{Equation (5-19)}$$

$$C_p = C_{p0}(1-D) \quad \text{Equation (5-20)}$$

For creep coefficient

$$\gamma = \int_{t=0}^t A \sinh\left(\alpha_0 \frac{\tau_0}{1-D}\right)^n \exp\left(\frac{-Q}{RT}\right) dt \quad \text{Equation (5-21)}$$

$$\alpha = \frac{\alpha_0}{(1-D)} \quad \text{Equation (5-22)}$$

Where  $C_{p0}$  and  $\alpha_0$  are plastic coefficient and creep coefficient for undamaged material.

The update in material constitutive properties is conducted in each step of successive initiation after killing elements.

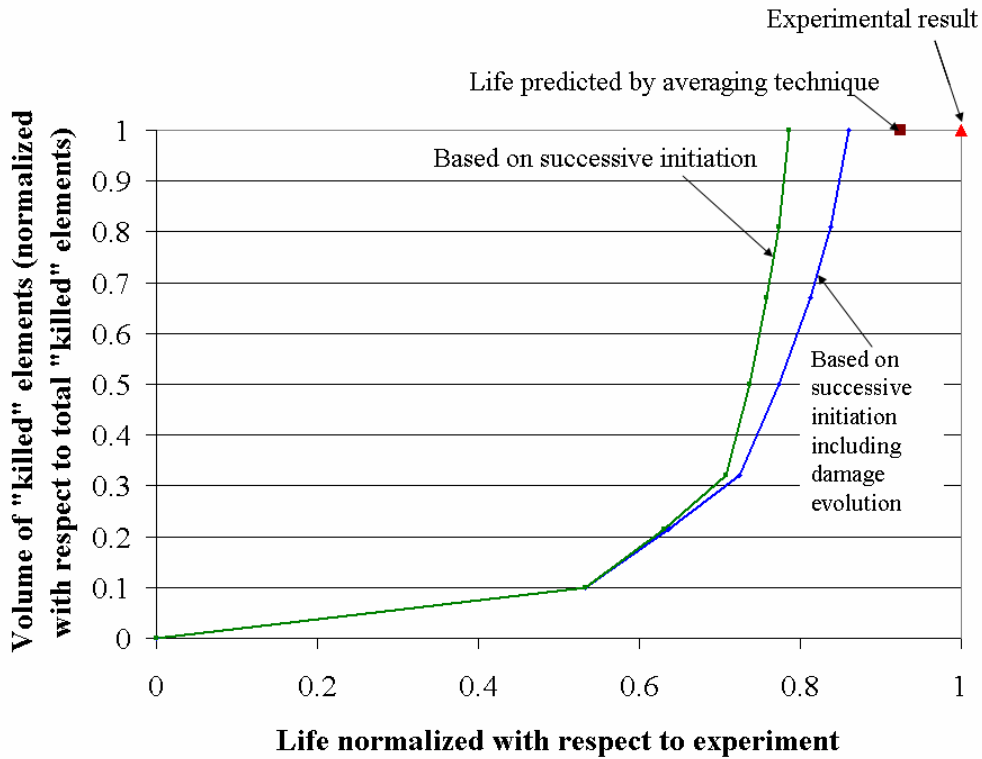


Figure 5-13: Comparison of damage propagation calculated using successive initiation with and without damage evolution

Result of FEA predicts a longer life than successive initiation itself when the material degradation is taken into account. The reason is that in each step when the elements are killed in FEA, the life of the elements that are averaged over the killed elements is predicted by creep and plastic energy densities which decrease as the material degrades or softens and the hysteresis loop becomes smaller as observed in Figure 5-8 . FEA analysis also confirms this as shown in Figure 5-14. Certain elements inside the ball which were not on the crack path were selected for this hysteresis loop. The largest component of shear stress ( $\tau_{xz}$ ) versus shear strain is plotted for two models at the same number of cycles. The first model did not include damage evolution, but the second model included the damage evolution. As seen in this figure the hysteresis loop becomes

smaller when damage evolution is taken into consideration, thus causing the life predicted by successive initiation to be longer.

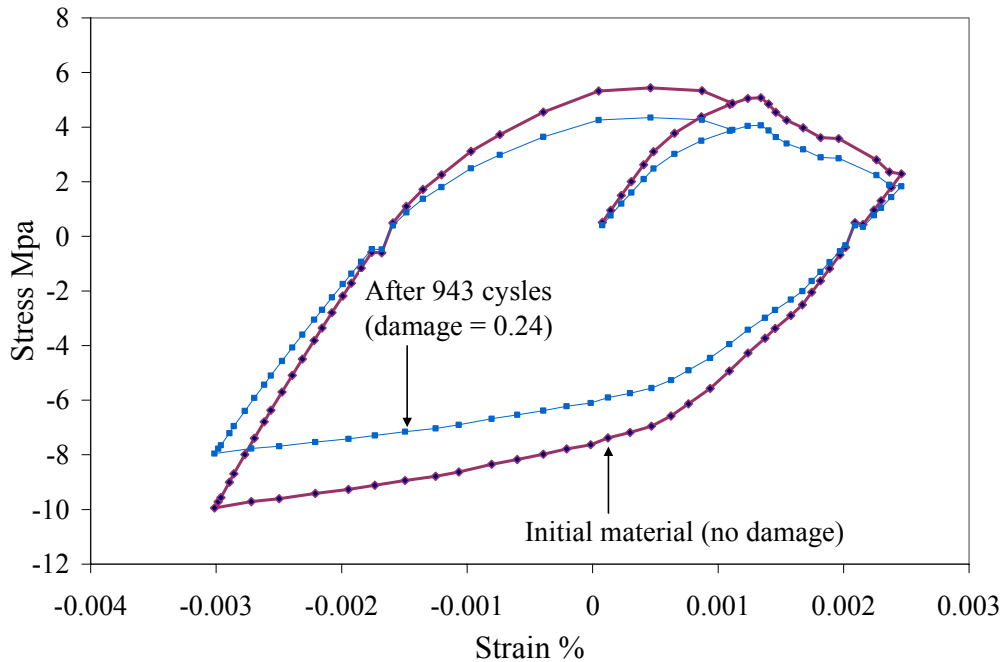


Figure 5-14: Hysteresis loop predicted by FEA for undamaged and damaged material (Damage is averaged over the entire joint)

### 5.3. Summary and conclusions

An Energy Partitioning Damage Evolution (EPDE) method is developed based on experiment and available micro-mechanic based damage models to predict the cyclic damage and softening of material due to mechanical cyclic loading. The constants for partitioned plastic and creep damage were obtained. The method then was implemented in successive initiation method. Comparison of results shows increase in life predicted by successive initiation if the damage evolution is taken into consideration. The increase is due to decrease in work densities in each step of successive initiation. Since E-P constants have been calibrated to experiment and already contain all the effects, if these

constants are used in successive initiation with and without damage the resulting predictions would not be accurate. To solve this problem the E-P constants have to be calibrated to be adapted into successive initiation method with and without damage evolution. Next Chapter addresses this issue.

## **6. Calibrating Energy Partitioning Constants**

The Energy partitioning constants that were used in the successive initiation technique, reported in section 1.3.1.4 from the literature [Zhang et al., 2003] were obtained from experimental data. The experimental data (and hence the E-P constants) already include both initiation and propagation phases and are hence not the most appropriate constants to be used in the successive initiation approach. Furthermore, these constants are obtained by using the undamaged constitutive material properties for partitioning the hysteresis energy and change in material properties due to cyclic loading are not considered. Thus these constants need to be calibrated in order to predict the life accurately. The next sections explain calibration of E-P constants for successive initiation with and without damage evolution. Two calibration schemes are explained here; calibration with respect to the results of the averaging technique and calibration with respect to the results of thermo-mechanical cycling experiment explained in chapter 2.

### **6.1. Calibration of E-P constants for successive initiation**

There are 4 damage constants in E-P model that need to be calibrated; plastic and creep coefficients and exponents. These existing E-P constant are presented in Table 6-1. Due to limited data only creep constants are calibrated here in this study. Further calibration is suggested for future work.

Table 6-1: Thermo-mechanical Energy Partitioning damage model constants for Sn3.8Ag0.7 solder [Zhang et al., 2004]

	Sn3.8Ag0.7 Solder
c	-0.8
$W_{p0}$ (mj/mm <sup>3</sup> )	198
d	-1.4
$W_{c0}$ (mj/mm <sup>3</sup> )	1.23E4

To calibrated two creep constants two FEA model were used. Two different packages were modeled; CTBGA132 and BGA256. The critical ball in CTBGA132 which is located at the outer corner of the package was selected and modeled locally.

FEA results predicted close life for critical balls in these two packages. Therefore to obtain enough spread in data, another ball that was predicted to have a longer life, and for which the experimental results were available [Osterman et al., 2006] was selected to be modeled locally. The location of this solder ball is shown in Figure 6-1.

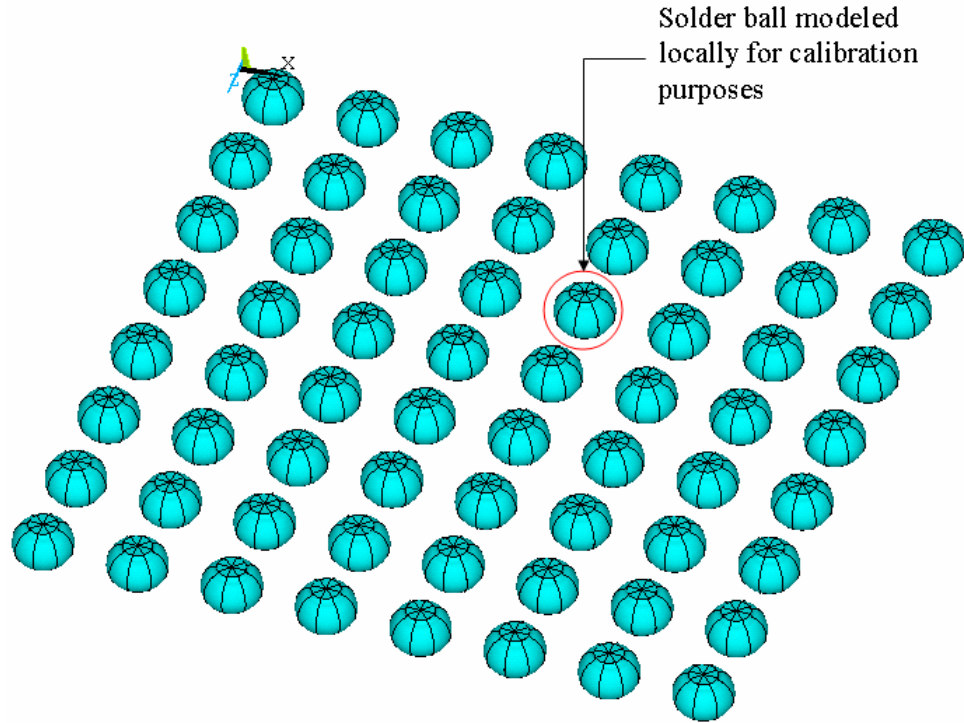


Figure 6-1: Selected ball from BGA256 model in local modeling for calibration purposes

As explained in chapter 3 for successive initiation technique, the total life can be obtained by:

$$N_f = \sum_{i=1}^{i=n} N_{fi} \quad \text{Equation (6-1)}$$

Where  $N_{fi}$  is the average life of elements killed in each step of successive initiation and obtained as follows:

$$N_{fi} = \frac{(1 - D_{accumi})}{D_{cyclei}} \quad \text{Equation (6-2)}$$

$$D_{accumi} = \sum_{j=1}^i N_{fj} * D_{cyclej} \quad \text{Equation (6-3)}$$

Where  $N_{fj}$  is the number of cycles in each step and  $D_{cyclej}$  show the damage for elements for  $J$ th step. Substituting the E-P damage constants and Equation (6-2) and (6-3) into Equation (6-1) we obtain:

$$N_f = \sum_{i=1}^n N_{fi} = \sum_{i=1}^n \left[ \frac{1 - \left( \sum_{j=1}^i N_{fj} * D_{cyclej} \right)}{\left( \frac{W_{pi}}{W_{p0}} \right)^{(-1/c)} + \left( \frac{W_{ci}}{W_{c0}} \right)^{(-1/d)}} \right] \quad (6-4)$$

Where  $W_{c0}$  and  $d$  are constants that are being calibrated. The two other constants;  $W_{p0}$  and  $c$  are kept unchanged.  $N_f$  is obtained from the averaging technique and equals 1169 for CTBGA132 and 3364 for BGA256. To solve Equation (6-4), the histories of elements killed in each step have to be determined by FEA. For each set of elements killed not only energy densities for final step has to be determined, but also to calculate the amount of damage accumulation, the energy densities in all previous steps have to be determined.

Using the same procedure the constants were also calibrated to experiment. The experimental results show  $N_f$  of 1264 cycles for CTBGA and 3407 cycles for BGA256 [Osterman et al., 2006]. The calibrated constants are provided in Table 6-2.

Table 6-2: E-P creep constants calibrated for successive initiation

Reference for $N_f$	$d$	$W_{c0}$ (mj/mm3)
Experiment [Osterman et al., 2006]	-1.07	2.1E4
Prediction by averaging technique	-0.92	4.34E2

E-P constants calibrated for successive initiation to averaging was used to reproduce the life for BGA132 and the plot with calibration and without calibration is provided in

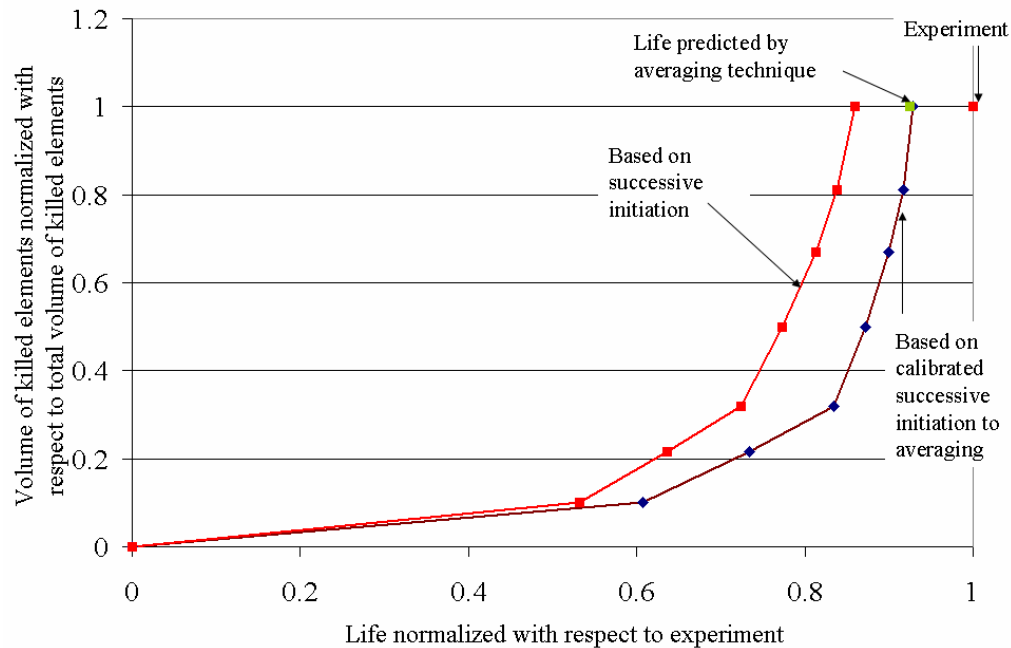


Figure 6-2: comparison of damage propagation calculated using successive initiation and calibrated successive initiation

## 6.2. Calibrating E-P constants for successive initiation including damage evolution

The same two models and procedures were used to calibrate the creep constants to experiment and averaging technique when damage evolution is taken into consideration. As mentioned earlier in chapter 5 the life is predicted to be longer relative to successive initiation when the damage evolution is taken into consideration due to softening in material and therefore decreasing the work densities after cycling. After applying the same procedure the calibrated constants are provided in Table 6-3

Table 6-3: E-P creep constants calibrated for successive initiation with damage evolution

Reference for $N_f$	d	$W_{c0}$ (mj/mm <sup>3</sup> )
Experiment [Osterman et al., 2006]	-1.07	1.851E4
Prediction by averaging technique	-0.86	2.85E2

To check the calibrated constants the critical ball of CTBAG132 was modeled again with successive initiation without damage. The durability was calculated using calibrated E-P constants to averaging technique. The result shows a good correlation to averaging technique.

### **6.3. Summary and Conclusions**

Conventionally E-P damage constants are generated for evaluating durability based on first few cycles of loading. They are not appropriate constants to be used when modeling the damage propagation explicitly. This chapter provides the calibrated E-P constants that can be used in modeling damage explicitly. It also provides E-P damage constants used in successive initiation when damage evolution and cyclic softening is considered.

## **7. Summary, contribution and future work**

Due to ambiguities, conflicting reports and controversies in the literature about effect of process induced voids on the reliability of electronic components; voids as one of the manufacturing defects are selected to be studied in depth in this thesis. An experiment was designed and implemented on printing and reflow processes of Pb-free solder interconnects in order to obtain error-seeded specimens. The specimens were characterized for voids and subjected to temperature cycling, in order to evaluate durability of specimens under thermo-mechanical loading. Statistical analysis of the void characterization as well as durability suggested that the detrimental effect of voids as a manufacturing defect may not be very strong. To verify this observation and in order to quantify the detailed influence of size, location, and volume fraction of voids, extensive modeling was conducted. A global-local modeling approach was used to model an error seeded solder ball with voids of different sizes and in different locations. An existing continuum damage model (Energy Partitioning model) was modified by successive initiation method and used to explicitly predict damage initiation and propagation in BGA solder joints. Two techniques were used to predict the life, averaging technique and successive initiation. In averaging technique that is conventionally used in literature, the energy densities used in energy partitioning damage model are averaged over 10% of the volume of the solder ball. The technique has been calibrated to experiment and predict the life fairly well. However, this technique cannot be used in order to study the damage initiation site and path in solder joint interconnect. To predict the damage initiation and propagation life and path in voided solder joints, successive initiation technique is suggested to be used. The creep and plastic energy densities of the elements are

monitored and elements are eliminated from the structure step by step as their damage exceeds the maximum tolerable damage threshold.

Modeling results show that damage starts around the joint and propagates circumferentially toward the center in thermo-mechanical cycling tests. Durability calculated by both techniques show non-monotonic interaction between void size and durability. If the voids are further away from damage path, their effect on durability is negligible and voids do not influence/alter the damage path. FEA results from successive initiation also suggests that voids in general are not detrimental to reliability except when a substantial portion of the damage path is covered with either a large void or many small voids with void area fraction of 20%. This is in consistency with IPC standards that classifies voids larger than 25% at the interface of solder and component or PWA as critical voids. It was observed that although small voids can slow down the propagation time of the crack front, but durability did not increase significantly because of either decrease in initiation time or because the damage propagation path deflects around the void to find alternate paths.

Another objective of this study was to use experimental data to identify the correct fatigue constants to be used when explicitly modeling fatigue damage propagation and evolution in Pb-free solders. Explicit modeling of damage propagation improves modeling accuracy when modeling solder joints of vastly different architectures, since the joint geometry may have a strong influence on the ratio of initiation-life to propagation-life. Most solder fatigue models in the literature do not provide this capability since they predict failure based only on the damage accumulation rates during the first few cycles in the undamaged joint.

In this study experimental results were used to identify the correct E-P damage constants to be used in successive initiation modeling for thermo-mechanical cycling.

Explicit modeling of damage propagation also raises the question of change in constitutive properties due to cyclic loading. As damage accumulates with successive cyclic loading, the constitutive properties of the material change. To account for changes in material properties when modeling lead free solder materials during thermo-mechanical cycling, a mechanism-based Energy Partitioning Damage Evolution (EPDE) model was developed using both experimental data and available micro-mechanics models. The model then was coupled into the successive initiation technique and the results were analyzed. The experimental results were used to identify the right E-P damage constants to be used in successive initiation with damage evolution.

Implementing EPDE in successive initiation showed that life predicted by successive initiation increases if softening of material is taken into consideration. The increase in life is caused by decrease in plastic and creep energies during thermo-mechanical cycling. Comparison between the lives predicted by successive initiation with and without damage evolution shows about 10% difference. Considering the small amount of effort that is required to include the cyclic change in constitutive properties, it is recommended that cyclic softening be included whenever the propagation-life is a significant portion of the total life under thermo-mechanical cycling.

### **7.1. Contribution of the dissertation**

The contributions of this study are divided into two parts. The first part gives an insight about effect of voids on durability due to its influence on damage initiation and propagation in BGA solder joints. In addition this dissertation establishes and documents

a systematic approach for studying damage initiation and propagation in any kind of interconnect, especially very long solder structures where the initiation to propagation ratio is much smaller than in BGA joints and averaging-based initiation models are not expected to provide a good correlation with experiment.

Furthermore, it introduces a new combined experimental/micromechanics based technique for considering damage evolution in modeling Pb-free solder materials, which is essential when modeling damage propagation explicitly. The main contributions of this dissertation are as follows:

1. The effect of process-induced voids on the durability of Sn-Pb and Pb-free solder interconnects in electronic products were under heavy controversy. This debate was more intensified in Pb-free solders; since voids are more common in Pb-free. The first contribution of this dissertation is to provide detailed insights about voids and their effect on durability, specifically on damage initiation and propagation.
2. The standards currently used by industry for voids, such as IPC standard, are established based on anecdotal and heuristic field experience and not on quantitative experiment and data. This dissertation provides insights about inspection and screening guidelines for voids in production of electronic assemblies. These insights are useful for developing criteria for acceptable void percentage and void location in interconnects. It also provides a source for evaluating the available standards. However, the point has to be taken into consideration that the model constants that are used in studying voids are obtained

from literature. If the model constants change or for different type of solder such as SnPb solders, the result may vary. Even though the trend is not likely to change with the type of solder, the critical void percentage might be sensitive to type of solder and damage model constants.

3. Durability of solder joints usually is calculated using averaging technique in FEA modeling. Although this technique has been used for many years in the area of fatigue, it does not provide a clear understanding of how damage initiates and propagates in solder joints. This study provides comprehensive documentation of successive initiation approach which is more applicable for prediction of damage initiation site and propagation path especially in long joints. The process has been automated and documented for 3-D FEA model for E-P damage model used in BGA solder joints. This procedure could easily be extended and used for other types of damage models and geometries.
4. When the solder undergoes cyclic loading the microstructure of the solder evolves. Cycling deteriorates material due to damage accumulation which causes material softening. This softening has not been considered in durability models developed for Pb-free solders so far. It is essential to consider this phenomenon in cases where damage propagation is modeled explicitly. This dissertation proposes an update to the energy partitioning model based on experimental data and micro-mechanics based technique that can predict the damage evolution in Pb-

- free solder materials. Damage evolution constants for plastic and creep have been obtained for SAC solder material in this study.
5. E-P damage constants conventionally used in modeling fatigue in lead free solder joint materials include both initiation and propagation and are based on damage accumulation in the first few cycles. These constants are not appropriate for use in methods where damage propagation is modeled explicitly. This dissertation provides a new set of E-P damage constants calibrated for methods that explicitly model the propagation explicitly such as successive initiation.
  6. This study also provides a set of calibrated E-P damage constants when the cyclic softening is included in explicit modeling of damage propagation to be used in geometries closed to BGA.
  7. This study also provides insight about different types of material containing small size or meso scale voids such as bone structure or other type of bio-material. The same approach might be applicable for studying the effect of meso scale voids on change in stress distribution, strength and durability of other types of material.

## **7.2.Suggestions for future work**

Based on insight obtained by this work, future works are suggested to improve the experiment, FEA modeling and analytical procedures conducted in this dissertation.

1. Parametric study conducted to evaluate the effect of voids only assesses the effect of voids on durability of BGA interconnects under thermo-mechanical loading. The effect of voids has not been

investigated in other types of interconnects and other types of loading such as shock, drop, or vibration and remains for future investigations.

2. The shape of the void has always been considered spherical. Some times this is not the case and voids are formed in different shapes that may influence the stress distribution inside the solder ball. This could be an area for future studies.
3. The stand off height of the solder joint has not been changed due to presence of voids. This might not be the case in some application. The change in stand off height should be considered in future work. In some application constraints in height of the solder joint might not result in increasing stand off height, instead it might increase the volume of the solder horizontally. This may have contradicting effect, including increasing the surface area of the solder, but resulting in a stiffer joint. These effects should be studied in future in more details.
4. In FEA modeling of voids the material properties in the solder is considered to be homogenous and isotropic. It was observed frequently in micro-structural analysis that solder balls had only a few grains. This makes the assumption of isotropic and homogeneity of material properties case dependent. Also the effect of intermetallic layers that caused non homogenous material properties has been ignored. In real applications these two factors have affect on thermo-mechanical durability and need to be taken into account in FEA modeling of solder joints.

5. In order to obtain better experimental verification about damage initiation and propagation, it is suggested that voided specimens cross sectioned and examined in different stages of life before failure and be compared with FEA analysis. This can provide a better insight of how damage initiates and propagates in voided solder joints.
6. Due to limitation in test data available in literature, in modeling damage evolution, the model constants were obtained from isothermal mechanical testing and were used to predict damage evolution in thermo-mechanical testing. Data provided in literature show that E-P damage constants are different in thermo-mechanical testing than isothermo-mechanical testing. This could also be true in E-P damage evolution constants. It is suggested that further studies be conducted to investigate the difference between damage evolution in isothermo-mechanical tests and thermo-mechanical tests. The damage evolution constants used in thermo-mechanical cycling need be obtained for thermo-mechanical loading.
7. In calibrating the E-P damage constants only the creep constants have been calibrated, since the plastic constants have much smaller effect on durability they have been assumed to remain the same. Plastic constants also need to be calibrated and is suggested to be done in future work.
8. In developing the damage evolution method, the load drop is considered to be completely due to change in material properties. In reality a macro crack may

have developed partially in the material after the cycling which also causes load drop. It is a better idea to separate the load drop caused by macro crack and cyclic softening in order to predict the change in material properties. Another solution which is suggested for future work is change in method of implementation in the modeling. Instead of killing elements, the elements can stay in the structure and material degradation can be applied only by including the damage predicted by EPDE method in material properties.

9. The model constants derived for damage evolution is obtained by average load drop over the bulk of solder in TMM machine. The damage however would in reality vary depending on where the elements are located; close to propagation path or away from propagation path. In locations that stress and strain is concentrated the damage would be higher. The more accurate method to calculate damage is to use FEA modeling to relate the damage propagation path and length to load drop which is suggested to be done in future.
10. Effect of kinematic hardening has not been considered in developing the damage model and in including the damage model in FEA. This effect could decrease the damage ratio predicted by EPDE model and should be included in future for more accurate prediction of damage evolution.

## **8. Appendices**

### **8.1. Appendix I: Pre-test micro-structural analysis**

As it was explained in previous sections, 6 variables have been varied in manufacturing process. These variation cause micro-structural variation. Study done by salam et all [Salam et al., 2004] on two different kinds of reflow profiles: Ramp-Soak-Spike and Ramp to Spike, for Sn-Ag-Cu solders showed that the most important factor that affects micro-structural refinement and thin layer of intermetallic is peak temperature. They also concluded that microstructure is sensitive to time above peak temperature. It is also seen in the literature that cooling rate has effect on grain size, intermetallic thickness and microstructure. In a study conducted by Lee [Lee, 1999] for optimizing the reflow profile for Sn-Pb solders, explained the effect of peak temperature and cooling ramp on grain refinement and intermetallic formation. Based on his proposed reflow profile, the slower cooling ramp results in courser grains and as the cooling ramp increases the grains are refined.

To study the effect of reflow variables three specimen were selected from three different boards that were reflowed under three different reflow condition. The first specimen was reflowed with all the reflow variables at the lowest level. The second board was reflowed with the reflow variables at the medium and third board was reflowed with all the reflow variables at the highest level. One component was selected from each board to be cross-sectioned before the temperature cycling test, to characterize the as-manufactured microstructure. The boards selected correspond to runs 1-3 in Table 2-1. The PWBs were correspondingly labeled A1, A2, and A3, as shown and discussed in Figure 8-1.

The cross sections were then analyzed under polarized light and the number of grains was counted as a function of the distance from the PWB bond pad. Pictures of these three samples are shown in Figure 8-1. As seen in specimens A1 and A2, the solder ball did not completely melt. The original solder ball contains only a few grains. It can be seen in Figure 8-2 for these two specimens that the number of grains decreases as the distance from the pad increases. This shows that solder ball did not completely melt during the reflow. The solder joint in these two cases responds anisotropically to thermo-mechanical loading. The picture also shows that A1 and A2 specimens suffer from insufficient wetting, insufficient intermetallic formation at the interface between the solder and PWA bond pad due to low peak temperature and short time above melting point. These joints are therefore not very strong. The solder ball in Specimen A3 however, has melted completely and the grains have re-crystallized and refined. Also sufficient intermetallic has formed at the interface with PWA bond pads to create a strong joint. Case A3 therefore has statistically homogeneous properties and responds isotropically to thermo-mechanical loading. Furthermore, the finer grain size is expected to cause better static and fatigue strength in specimen A3 than in specimens A1 & A2.

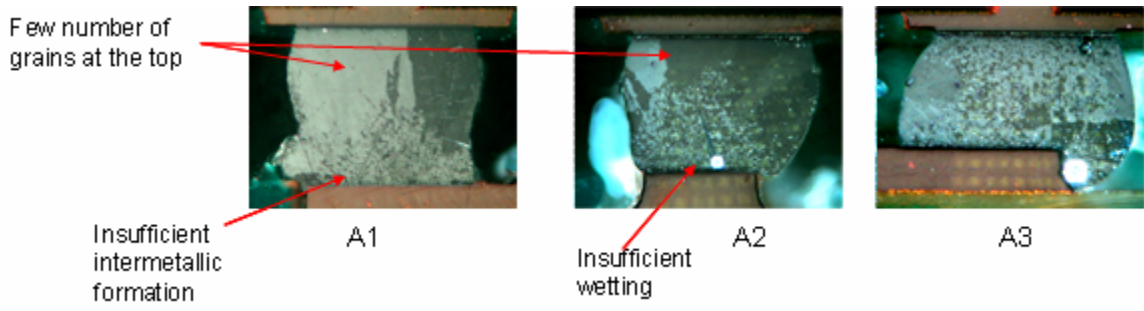


Figure 8-1: Specimens reflowed in three different levels of reflow variables (A1: all reflow variables at the lowest level, A2: all reflow variables at middle level, A3: all reflow variables at highest level)

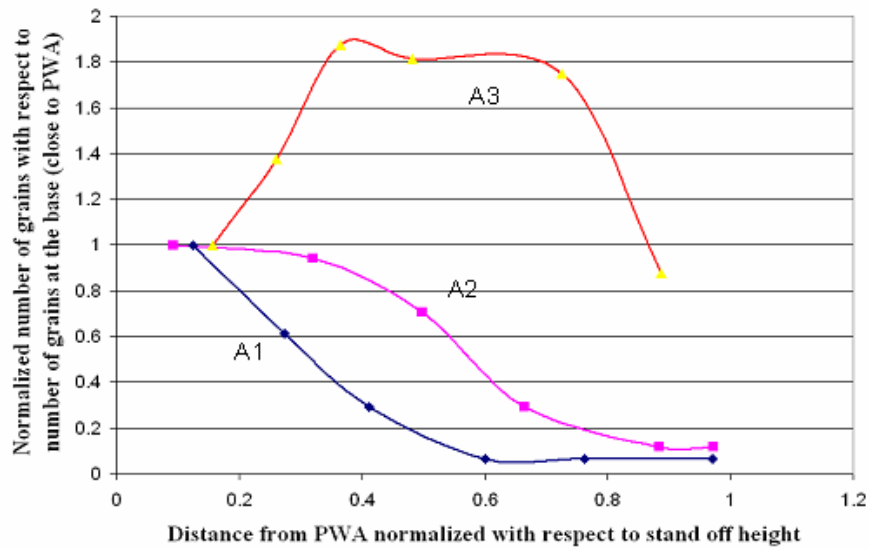


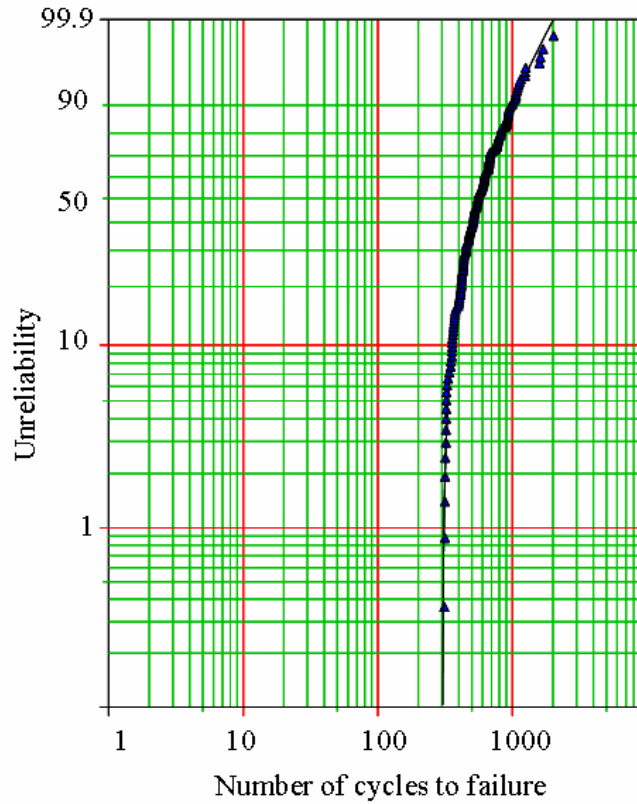
Figure 8-2: Number of grains as function of distance from board pad

## **8.2. Appendix II: Accelerated thermal cycling test results**

Accelerated thermal cycling test was conducted and the cycles to failure were recorded. The specimens are considered to have failed when the electrical resistance measured by the data acquisition system shows a sudden increase, “spike”, (several orders of magnitude relative to initial resistance) consistently through 10 successive cycles.

Weibull distributions were fit to the failure data using commercial software. Failures were found to have two distinct Weibull slopes ( $\beta$ ) and were accordingly divided into two populations: premature failure sub-population and main population of failures using a competing failure mode analysis. Both populations are shown in Figure 8-3 for CTBGA components. Competing failure mode analyses use two-parameter (2-P) Weibull distribution. The result of this analysis is provided in Appendix II. However, 2-P Weibull, might not be the best fit for the physics of fatigue failures. Therefore three-parameter (3-P) Weibull analysis was then used to analyze the failure populations. The 3-

P Weibull cumulative distribution functions (CDFs) for both premature and main failure



populations are shown in

Figure 2-11 for CTBGA interconnects. Comparison between the Weibull correlation coefficient of 2-P and 3-P analysis for both the premature and main failure populations shows a better fit of data to 3-P Weibull distribution. The corresponding characteristic life ( $\eta + \gamma$ ), is 641 cycles and Weibull slope ( $\beta$ ) is 1.28 for the main CTBGA population. The corresponding characteristic life for premature failures is 201 cycles and Weibull slope ( $\beta$ ) is 3.9. Figure 2-12 shows the corresponding probability density functions (PDFs) for both the premature failure population and the main population, for CTBGAs. The main population has a small overlap with the premature failure population. The premature failure population starts prior to zero cycles because it has a negative location parameter ( $\gamma$ ). This implies that there was damage introduced in the assembly and handling processes prior to the start of the thermal cycling test. Similar analysis was also

carried out for the MLFs and LCRs on the PWBs. This result shows that MLFs and LCRs are much more durable than CTBGAs (2-P Weibull characteristic life for the main population is 1332 cycles for MLFs, 1262 for LCRs and 671 for CTBGAs). A summary of the Weibull parameters and correlation coefficients is provided in Table 8-1, Table 8-2 and Table 8-3.

Table 8-1: Summary of the Weibull parameters for CTBGAs

	$\eta$	$\beta$	$\gamma$	$\rho$
CTBGA Main pop, 2-P	683	3.5		0.92
CTBGA Early pop, 2-P	191	1.5		0.97
CTBGA Main pop, 3-p	349	1.26	302	0.99
CTBGA Early pop, 3-p	360	3.9	-159	0.98

Table 8-2: Summary of the Weibull parameters for MLFs

	$\eta$	$\beta$	$\gamma$	$\rho$
MLFs Main pop, 2-P	1422	6.5		0.94
MLFs Early pop, 2-P	828	2.5		0.7
MLFs Main pop, 3-p	615	2	793	0.98
MLFs Early pop, 3-p	9957	51.88	-9117	0.89

Table 8-3: Summary of the Weibull parameters for LCRs

	$\eta$	$\beta$	$\gamma$	$\rho$
LCRs 2-P	1517	4.6		0.95
LCRs 3-P	806	1.65	703	0.99

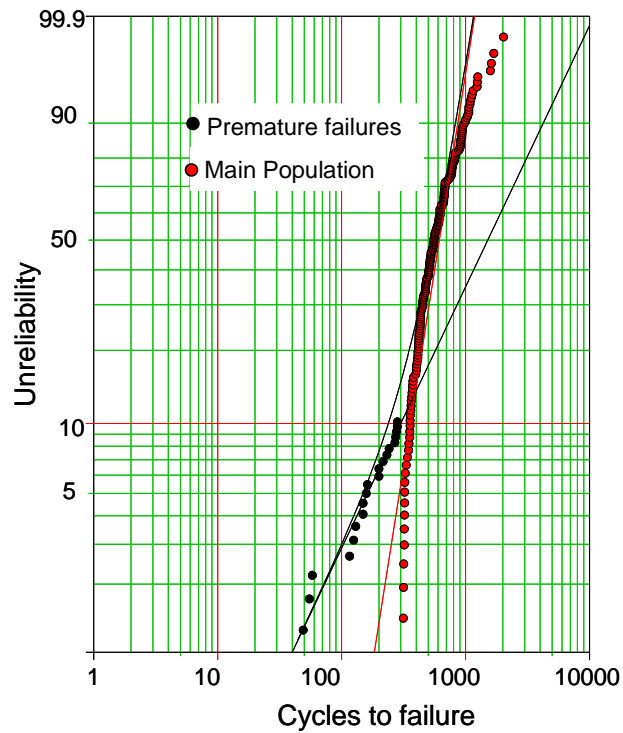


Figure 8-3: 2-P Competing failure modes Weibull diagram for CTBGA failures

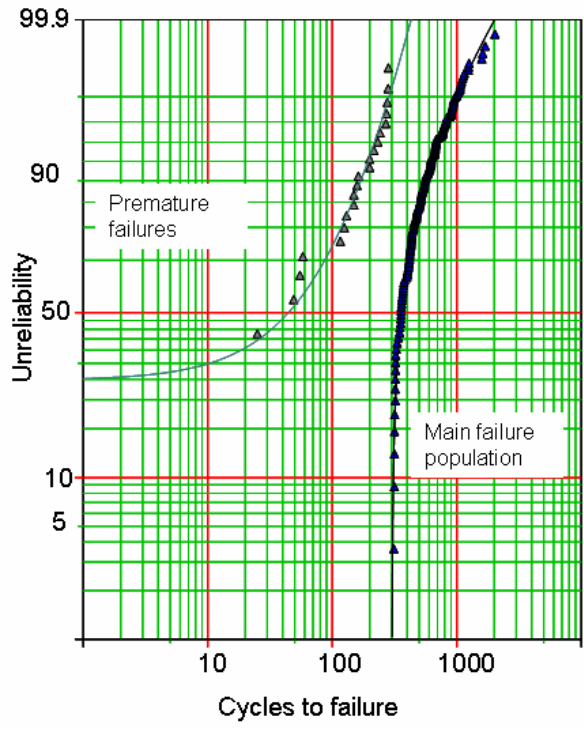


Figure 8-4: 3-P Weibull plots for premature failures and main population of failures of CTBGAs

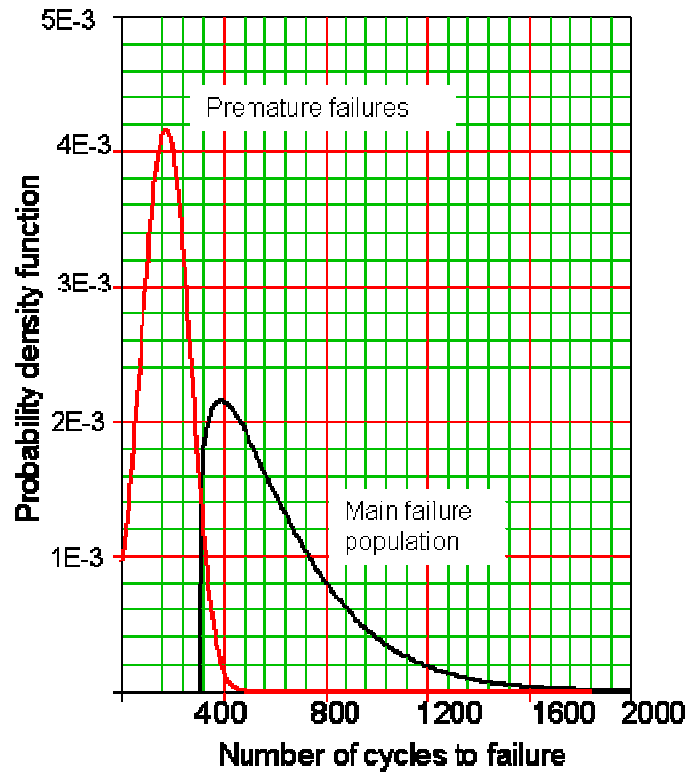


Figure 8-5: Probability density function for early and main population failures for CTBGA

## 9. References

1. Akay, H., H. Zhang, N. Paydar, "Experimental correlation of an energy based fatigue life prediction method for solder joints," Advances in Electronic Packaging, Proceeding of the Pacific Rim/ASME International Intersociety of Electronic and Photonic Packaging Conference, INTERpack, Vol. 2, pp. 1567-1574, 1997.
2. Antony J., "simultaneous optimization of multiple quality characteristics in manufacturing process using Taguchi quality loss function," The International Journal of Advanced Manufacturing Technology, Volume 17, Number 2 / January, 2001.
3. Apell, M.C., "Consideration for lead-free reflow soldering", Circuits Assembly, vol.15, no.3, March 2004. pp. 28-30.
4. Aspandiar, R., "Voids in solder joints", Intel Corporation, SMTA Northwest Chapter Meeting, September 2005.
5. Basaran, C., and Yan., C.Y., "A thermodynamic framework for damage mechanics of solder joints", ASME Journal of Electronic Packaging, Vol. 120, pp. 379-383, December 1998.
6. Chaw, C.L., Lau., K.J., Vianco, P., and Fang, H.E., "Behavior of Pb-free solder under thermo-mechanical loading", ASME Journal of Electronic Packaging, September 2004, Vol. 126, pp. 367-373
7. Coffin, L.F., "Fatigue at high temperature," Proceeding of ASTM, STP, 520, Philadelphia, PA, ASTM, 1973, PP. 5-34.
8. Coffin, L.F., "Fatigue at high temperature," Fourth International Conference on Fracture, 1978, I, pp. 263-92, xxviii+842 pp. UK, Oxford : Pergamon.
9. Coffin, L.F., 1954, Transactions of ASME, Vol. 76, pp. 931-950
10. "Competing failure mode analysis", Reliability Edge Newsletter, Quarter 4, Vol. 2, Issue3, 2001, <http://www.reliasoft.com/newsletter/4q2001/modes.htm>.
11. Darveaux, R, Benerji, K., Mawer, A, Dody, G., 1995, "Durability of Plastic Ball Grid Array assembly," Ball Grid Array Technology, Lau, J., Editor, McGraw Hill Inc, New York.
12. Dasgupta, A., Huang, B., and Lee, N.C., "Effect of lead-free alloys on voiding at microvias,"APEX, Anaheim, California, 2004
13. Deplanque, S.; Nuchter, W.; Wunderle, B.; Schacht, R.; Michel, B., "Lifetime prediction of SnPb and SnAgCu solder joints of chips on copper substrate based on crack propagation FE-analysis," Thermal, Mechanical and Multi-Physics

Simulation and Experiments in Micro-Electronics and Micro-Systems.  
Proceedings of EuroSimE 2006

14. Dickinson, M., "Mastering the dark art of screen printing", *Circuits Assembly*, vol.13, no.9, Sept. 2002. pp. 32-6.
15. Dutta, I., "A constitutive model for creep of lead free solders undergoing strain enhanced microstructural coarsening: a first report," *International Journal of Materials*, Vol. 32, No 4, pp. 201- 7, April 2003.
16. Dusek, M., and Hunt, C., "A novel measurement technique for stencil printed solder paste," *Soldering & Surface Mount Technology*, Vol. 15, No. 2, 2003. pp. 35-45.
17. Durairaj, R., Jackson, J.G., Ekere, N.N., Glinski, G., and Baily, C., "Correlation of solder Rheology with computational simulation of the stencil printing process," *Soldering and Surface Mount Technology*, v 14, n 1, 2002, pp. 11-17.
18. Echeverria, G., and Santos, D., "Effect of lead free assembly processing on solder joint voiding", 2004.
19. Engelmaier, W., "Fatigue life of leadless chip carrier solder joints during power cycling," *IEEE Transaction on Components, Hybrids, and Manufacturing Technology*, Vol. CHMT-6, No. 3, September 1983.
20. Erinc, M., Schreurs, P.J.G., Zhang, G.Q., and Geers, M.G.D., "Characterization and Fatigue Damage Simulation in SAC Solder Joints", *Journal of Microelectronic Reliability*, Vol. 44, 2004, pp. 1287-1292.
21. Fossum, A.F., Vianco, P.T., Neilson, M.K., and Pierce, D.M., "A Practical Visco-Plastic Damage Model for Lead-Free Solder", *Transaction of ASME Journal of Electronic Packaging*, Vol. 128, March 2006, pp. 71-81.
22. Frear, D.R., W.B. Jones, K.R. Kinsman, "Solder mechanics; A state of the art assessment", *Minerals, Metals &Material Society*, 1991.
23. Garofalo, B., "Fundamentals of creep and creep rapture," *McMillan Publications*, 1965, New York.
24. Gifkins, R.C., "Grain-Boundary Sliding and Its Accommodation During Creep and Superplasticity," *Metall. Trans. A*. Vol. 7A, no. 8, pp. 1225-1232. Aug. 1976.
25. Grivas, D., Murty, K.L., Morris, J.W., Jr., "Deformation of Sn-Pb alloys at relatively high strain rates," *Acta Metallurgica*, Vol. 27, pp.731-737, 1979.
26. Halford, G.R., Hirschberg, M.H., and Manson, S .S., "Temperature Effects on the Strain-Range Partitioning Approach for Creep Fatigue Analysis", *ASTM STP 520*, pp. 658-667, PA.

27. Halford, G.R., Hirschberg, M.H., and Manson, S .S., “Creep fatigue analysis by strain range partitioning”, ASME Journal of Electronic Packaging, Vol. 114, 1992, pp. 152-160
28. Harrison, M.R.; Vincent, J.H.; Steen, H.A.H, “Lead free reflow soldering for electronic assemblies”, Soldering & Surface Mount Technology, vol.13, no.3, 2001. p. 21-38.
29. Haswell, P., and Dasgupta, A., “Viscoplastic Characterization of Constitutive behavior of Two Solder Alloys”, ASME International Mechanical Engineering Congress and Exposition, November 14-19, 1999, Nashville, Tennessee.
30. Haswell, P., and Dasgupta, A., “ Durability Properties Characterization of Sn62Pb36Ag2 Solder Alloy”, Proceeding of ASME IMECE, EEP-Vol. 28, pp. 181-187, Orlando, Florida, 2000.
31. Haswell, P., and Dasgupta, A., “Viscoplastic Constitutive Properties of Lead-free Sn-3.9Ag-0.6Cu Alloy”, MRS Proceeding, San Francisco, CA, 2001.
32. Haswell, P., “Durability Assessment and Microstructural Observation of Selected Solder Alloys”, PhD Dissertation, University of Maryland, College Park, Md, 2001.
33. Herring, C., “Diffusional viscosity of polycrystalline solids,” Journal of Applied Physics, Vol. 21, pp-437-45, 1950.
34. History of SMT, Surface mount association website, [www.smts.org](http://www.smts.org), reviewed Jan 2006.
35. Hollomon, J.H., Lubahn, J.D., “Plastic flow of metals,” Phys. Rev. 70, 775 (1946) Issue 9-10 – 1 November 1946.
36. Huang, B., Dasgupta, A., and Lee, N.C., “Effect of SAC composition on soldering performance”, IEEE, SEMI Int’l Electronic Manufacturing Technology Symposium, 2004, Piscataway, NJ, USA: IEEE, 2004. P. 45-55.
37. Huang, J., Lia, H.Y., Qian, Y.Y., Jiang, Y.H., and Wang, Q.L., “A Dislocation Model of Shear Fatigue Damage and Life Prediction of SMT Solder Joints under Thermal Cycling”, IEEE Transactions on Components, Hybrid and Manufacturing Technology, Vol. 15, No. 4, August 1992, pp. 553-558
38. Jackson, G.J., Durairaj, R., and Ekere, N. N., “Characterization of Pb-free solder pastes for low cost flip-chip bumping”, Proceedings of the IEEE/CPMT International Electronics Manufacturing Technology (IEMT) Symposium, 2002, p 223-228.
39. JESD22-B111, JEDEC standard, “Board level drop test method of components for hand held electronic products”, July 2003.

40. Kachanov, L.M., "Introduction to continuum damage mechanics", Martin Nijhoff Publishers, 1986, Netherlands, Dordrecht
41. Kilinski, T.J., Lesniak, J.R., Sandor, B.I., "modern approaches to fatigue life prediction of SMT solder joints," In; Lau J.H Editor, Solder joint reliability theory and applications, New York, Van Nostrand Reinhold, 1991, Chapter 13.
42. Kim, D.S., Yu, Q., and Shibutani, T., "Effect of void formation on thermal fatigue reliability of lead-free solder joints", The Ninth Intersociety Conference on Thermal and Thermo-mechanical Phenomena in Electronic Systems. Las Vegas, NV, USA, 1-4 June 2004.
43. Lau, J., Chang, C., "Taguchi design of experiment for wafer bumping by stencil printing," IEEE Transactions on Electronic Packaging Manufacturing, Vol. 23, No. 3, July 2000.
44. Lau, J., Erasmus, S., "Effect of voids on Bump Chip Carrier (BCC++) solder joint reliability", IEEE Electronic Components and Technology Conference, 2002, pp. 992-1000.
45. "Lead-free solder reflow: Packaging", Application note 016101-0703, ZiLOG Inc, 2003.
46. Lee, N.C., "Reflow processing and troubleshooting SMT, BGA, CSP, and Flip chip technologies", Newnes Publication, 2002, U.S.A.
47. Lee, N.C., "Optimizing the reflow profile via defect mechanism analysis", Soldering and Surface Mount Technology , Vol. 11, Issue 1, pp. 13-20, 1999.
48. Li, L., Rao, Y., and Lin, J., "Pb free solder paste reflow window study for flip-chip wafer bumping", Proceedings of the International Symposium and Exhibition on Advanced Packaging Materials Processes, Properties and Interfaces, 2001, p 112-118.
49. Lee, W. W., Nguyen, L. T., Selvaduray, G.S. "Solder joint fatigue models: review and applicability to chip scale packages," Microelectronics Reliability, Vol. 40, pp. 231-244, 2000.
50. Maattanen, K., Happonen, J., Tuominen, A., "The effect of melting time on lead free solder strength", Advances in Electronic Materials and Packaging 2001, IEEE, 2001. p. 225-8.
51. Mangin, C.H., "Where quality is lost on SMT boards", Circuit Assembly, February 1991, p 63-64.
52. Manson, S.S., 1965, Experimental Mechanics, Vol. 5, No. 7, pp. 193-226

53. Manson, S.S., Halford, G.R., Hirschberg, M.H., "Creep fatigue analysis by strain range partitioning," ASME Symp. Design for Elevated Temperature Environments, 1971, pp. 12-28
54. McDowell, D.L., "A Nonlinear Kinematic Hardening Theory for Cyclic Thermoplasticity and Thermoviscoplasticity", International Journal of Plasticity, Vol. 8, pp. 695-728, 1992.
55. Melton, C., "Reflow soldering evaluation of lead free solder alloys", 1993 Proceedings. 43rd Electronic Components and Technology Conference, New York, NY, USA: IEEE, 1993. p. 1008-11.
56. "Micro-void resistant immersion silver for lead-free assembly," Cookson Electronics, <http://www.enthone.com/docs/AlphaSTARMicrovoidsBro.pdf>, Reviewed November 2006.
57. "Moisture/ reflow sensitivity classification for nonhermetic solid state surface mount devices", IPS/JEDEC, J-STD-020C, July 2004.
58. Mura, T., and Nakasone, Y., "A Theory of Fatigue Crack Initiation in Solids:, ASEM Transaction on Applied Mechanics, Vol. 57, pp. 1-6, March 1990.
59. Nabarro, F.R.N., "Steady-state diffusional creep (Steady state diffusional creep for materials with large grains and dislocations forming sinks for vacancies, obtaining strain rate)," Philosophical magazine, 8TH series. Vol. 16, pp. 231-237. Aug. 1967
60. Nguty, A.T., Salam, B., Durairaj, R., and Ekere, N.N., "Understanding the process window for printing lead free solder pastes", IEEE Transaction on Electronic Packaging Manufacturing, Vol. 24, No. 4, October 2001, pp. 249-254.
61. Nurmi, S. T., "The influence of multiple reflow cycles on solder joint voids for lead free PBGA", Soldering & Surface Mount Technology, vol.15, no.1, 2003. p. 31-8.
62. Okura, J.H., "Effect of temperature and moisture on durability of low cost flip chip on board (FCOB) assemblies", PhD Dissertation Defense, Department of Mechanical Engineering, University of Maryland, College park, 2001.
63. Okura, T.; Kanai, M.; Ogata, S.; Takei, T., " Optimization of solder paste printability with laser inspection technique", Seventeenth IEEE/CPMT International Electronics Manufacturing Technology Symposium 'Manufacturing Technologies - Present and Future, New York, NY, USA: IEEE. pp. 361-5, 1995.
64. Osterman, M, "CALCE lead free long term project", Calce consortium meeting, October 2006

65. Owen, M.; Hawthorne, J., "Process control for solder paste deposition", *Surface Mount Technology*, vol.14, no.1, Jan. 2000. p. 82, 84, 86.
66. Oyan, C., "Analysis of thermo-mechanical fatigue in solder joints", PhD dissertation, 1993, Department of Mechanical Engineering, University of Maryland, College Park.
67. Paris, P.C., Erdogan, F., "A critical analysis of crack propagation law," *Selected papers on Foundations of Linear Elastic Fracture Mechanics (A99-25742 06-39)*, Bethel, CT/Bellingham, WA, Society for Experimental Mechanics/Society of Photo-Optical Instrumentation Engineers (SEM Classic Papers. Vol. CP 1; SPIE Milestone Series. Vol. MS 137), 1997, p. 545-550; Discussion, p. 550, 551
68. Peck, D.J., "Solder paste in SMT: a training perspective", *Advanced Electronics Interconnects Center, Inc. IEEE, Electro 98. Professional Program Proceedings*, June 1998, pp. 1-14.
69. Qiu, L.Z., Zhong, G. W., Ai, P.Z., Shang, J.K., "Cyclic softening of Sn<sub>3.8</sub>Ag<sub>0.7</sub>Cu Lead Free Solder Alloy with Equiaxed Grain Structure", *Journal of Electronic Materials*, Vol. 34, No. 1, pp. 62-67. 2005.
70. Rajewski, K., "SMT process recommendations. Defect minimization methods for a no-clean SMT process", *IEEE Technical Applications Conference and Workshops. Northcon, 1995*, pp. 354-62, USA, New York, NY.
71. "Reflow soldering guidelines for lead-free packages", Application note 353, ALTERA Corporation, April 2004, Version 1.
72. Ryan, C., Oapos Neill, S., Donovan, J., Punch, J., Rodgers, B., and Murphy, E., "Investigation of the lead free surface mount soldering process: solder joint evaluation and process optimization", *ASME International Mechanical Engineering Congress and Exposition, IMECE 2004-60491*, Anaheim California.
73. Ryan, C., Oapos Neill, S., Donovan, J., Punch, J., Rodgers, B., and Murphy, E., "Optimizing lead free screen printing and reflow process parameters", *2004 9th IEEE Intersociety Conference on Thermal and Thermomechanical Phenomena in Electronic Systems*, June 2004, Las Vegas, NV.
74. Salam, B., Virseda, C., Da, H., Ekere, N.N., Durairaj, R., "Reflow profile study of Sn-Ag-Cu solder", *Soldering and Surface Mount Technology*, Vol. 16, no. 1, pp. 27- 34, 2004.
75. Schnider, D., "Reflow profile optimization", *Surface Mount Technology*, Vol 17, no. 9, pp. 60-62, Sep 2003.

76. Schubert, A., Walter, H., Dudek, R., Michel, B., "Thermo-mechanical Properties and creep deformation of Lead containing and Lead free solders," International Symposium on Advanced Packaging Materials, March 2001, Georgia, pp. 129-134.
77. Sharma, P., Ganti, S., Dasgupta, A., and Loman, J., "Prediction of rate independent constitutive behavior of Pb-free solders based on first principles", IEEE Transaction on Components and Packaging Technologies, Vol. 26, No. 3, September 2003.
78. Sharma, P., Dasgupta, A., "Micro-mechanics of creep-fatigue damage in Sn-Pb solder due to thermal cycling-Part I: formulation", Transaction of ASME Journal of Electronic Packaging, Vol. 124, pp. 292-297, September 2002.
79. Sharma, P., Dasgupta, A., "Micro-mechanics of creep-fatigue damage in Sn-Pb solder due to thermal cycling-Part II: mechanistic insights and cyclic durability predictions from monotonic data", Transaction of ASME Journal of Electronic Packaging, Vol. 124, pp. 298-303, September 2002.
80. Solomon, H., "Fatigue of 60/40 solder," IEEE Transactions on Component, Hybrids and Manufacturing Technology, Vol. CHMT-9, No. 9, December 1986, 423-432.
81. Solomon, H., "Low-Frequency, High-Temperature Low Cycle Fatigue of 60Sn--40Pb Solder," Low Cycle Fatigue; Bolton Landing, New York; USA; 30 Sept.-4 Oct. 1985. pp. 342-370. 1988
82. Stinson, B. K., "Micro-structural evolution in thermally cycled large area lead and lead free solder joints" Master thesis, Material science and engineering department, Virginia Polytechnic Institute and State University, June 2002.
83. Taguchi, G., "Taguchi methods: design of experiment", Quality Engineering series, American Supplier Institute, 1993.
84. "The Benefits of a Ramp-to-Spike Reflow Profile," [www.TKB-4U.COM](http://www.TKB-4U.COM).
85. "The latest in BGA implementation strategy," IPC-7095, Revision A, 2004.
86. Togethof, M.M.V., Chen, T.W., "Defects, fault coverage, yield and cost in board manufacturing", Proceedings. International Test Conference 1994. Altoona, PA, USA. p. 539-47.
87. Ubachs, R.L.J.M., Schreurs, P.J.G., and Geers, M.G.D., "Micro-structural behavior of solder alloys" Proceeding of 5<sup>th</sup> International Conference on Thermal and Mechanical Simulation and Experiments in Microelectronics and Microsystems, Eurosime, 2004, pp. 543- 547.

88. Upadhayayula, K., Dasgupta, A., "Physics of Failure guidelines for accelerated qualification of electronic systems", Quality and Reliability Engineering International, Vol. 14, pp. 433-447, 1998
89. Weertman, J., "Theory of steady state creep based on dislocation climb," Journal of Applied Physics, Vol. 26, 1213-17, 1955.
90. Wei, Y., Chow, L.C., Fang, H.E., Neilsen, M.K., "Characteristic of Creep Damage for 60Sn-40Pb Solder Material", Transactions of ASME Journal of Electronic Packaging, Vol. 123, September 2001, pp. 278-283.
91. Wen, S., Keer, L.M., Mavoori, H., "Constitutive and damage model for lead-free solder", Journal of Electronic Materials, Vol. 30, No. 9, 2001
92. Wen, S., "Damage Based Fatigue for Solder in Electronic Packaging", IEEE Transactions on Components and Packaging Technologies, Vol. 28, No. 3, September 2005, pp. 435-440
93. Wi, Y., Chow C.L., Lau, K.J., Vianco, P., Fang, H.E., "Behavior of lead free solders under thermo-mechanical loading", ASME, Journal of Electronic Packaging, Vol. 126, pp. 367-373, September 2004.
94. Willies, B., [www.leadfreesoldering.com](http://www.leadfreesoldering.com), January 2005.
95. Yang, X.J., Chow, C.L., and Lau, K.J., "A Unified Viscoplastic Description of 63Sn-37Pb Solder Alloy Under Cyclic Straining and Stressing", Proceedings of the Institution of Mechanical Engineers, Part C: Journal of Mechanical Engineering Science, Vol. 218, No. 9, 2004, pp. 909 – 920.
96. Yunus, M., Srihari, K., Pitarresi, J.M., and Primavera, A., "Effect of voids on the reliability of BGA/CSP solder joints", Microelectronics Reliability, vol.43, no.12, Dec. 2003. p. 2077-86
97. Zhang, Q., 2004 "Isothermal Mechanical and Thermo-Mechanical Durability Characterization of Selected Pb-free solders", Ph.D. Dissertation Defense, Department of Mechanical Engineering, University of Maryland, College Park
98. Zhang, Q., Dasgupta, A., and Haswll, P., "Viscoplastic constitutive properties and energy-partitioning model of lead-free Sn3.9Ag0.6Cu solder alloy", 53<sup>rd</sup> Proceeding of IEEE Electronic Components and Technology Conference, May 2003, pp. 1862-1868
99. Zhang, Q., Dasgupta, A., and Haswll, P., "Partitioned Viscoplastic-Constitutive Properties of the Pb-Free Sn3.9Ag0.6Cu Solder", Journal of Electronic Materials, Vol. 33, No. 11, November 2004, pp. 1338-1349.

100. Zhu, W.H., Stoeck, S., Pape, H., and Gan., S.L., “Comparative study on solder joint reliability using different FE models”, IEEE, Electronic Packaging Technology Conference, 2003.
101. [http://dictionary.laborlawtalk.com/Fatigue\\_\(material\)](http://dictionary.laborlawtalk.com/Fatigue_(material)), reviewed October 2006.